

---

Electronic Thesis and Dissertation Repository

---

12-11-2017 1:00 PM

# Syngenic Adipose-Derived Stem/Stromal Cells Delivered in Decellularized Adipose Tissue Scaffolds Enhance In Vivo Tissue Regeneration Through Host Cell Recruitment

Kevin P. Robb  
*The University of Western Ontario*

Supervisor  
Flynn, Lauren E.  
*The University of Western Ontario* Co-Supervisor  
Dekaban, Gregory A.  
*The University of Western Ontario*

Graduate Program in Biomedical Engineering  
A thesis submitted in partial fulfillment of the requirements for the degree in Master of Engineering Science  
© Kevin P. Robb 2017

Follow this and additional works at: <https://ir.lib.uwo.ca/etd>



Part of the [Molecular, Cellular, and Tissue Engineering Commons](#)

---

## Recommended Citation

Robb, Kevin P., "Syngenic Adipose-Derived Stem/Stromal Cells Delivered in Decellularized Adipose Tissue Scaffolds Enhance In Vivo Tissue Regeneration Through Host Cell Recruitment" (2017). *Electronic Thesis and Dissertation Repository*. 5075.  
<https://ir.lib.uwo.ca/etd/5075>

This Dissertation/Thesis is brought to you for free and open access by Scholarship@Western. It has been accepted for inclusion in Electronic Thesis and Dissertation Repository by an authorized administrator of Scholarship@Western. For more information, please contact [wlsadmin@uwo.ca](mailto:wlsadmin@uwo.ca).

## Abstract

Decellularized adipose tissue (DAT) represents a promising adipogenic bioscaffold for applications in soft tissue augmentation or reconstruction. With the goal of investigating the role of syngeneic donor adipose-derived stem/stromal cells (ASCs) and host myeloid cells during *in vivo* adipose tissue regeneration, transgenic reporter mouse strains were used to track these cell populations within ASC-seeded and unseeded DAT scaffolds. Donor ASCs were obtained from dsRed transgenic mice. These cells were shown to express characteristic cell surface markers, and multilineage differentiation capacity was confirmed. To facilitate cell tracking, DAT scaffolds were subcutaneously implanted into MacGreen mice in which myeloid cells express enhanced green fluorescent protein (EGFP). ASC-seeded DAT scaffolds augmented total cell recruitment as well as adipogenesis, and influenced EGFP<sup>+</sup> myeloid cell infiltration kinetics within the implants. The donor dsRed<sup>+</sup> ASCs were retained within the DAT scaffolds up to 8 weeks post-implantation, and did not contribute directly to the newly formed adipocytes.

## Keywords

Adipose-derived stem/stromal cells, extracellular matrix, macrophage, decellularized adipose tissue, adipose tissue, host response, biomaterials, cell-based therapy, tissue engineering, regenerative medicine.

## Co-Authorship Statement

Sections of Chapter 2 were included in the review article “Robb KP, Shridhar A, Flynn LE. *Decellularized matrices as cell-instructive scaffolds to guide tissue-specific regeneration*. ACS Biomaterials Science & Engineering. Accepted Nov. 13, 2017. DOI: 10.1021/acsbiomaterials.7b00619”. I conceptualized and wrote the manuscript in collaboration with Dr. Lauren Flynn, and prepared the original figures included in this thesis. Arthi Shridhar aided in figure design and was responsible for two summary tables not presented in this thesis.

## Acknowledgments

I would like to thank my supervisors Dr. Lauren Flynn and Dr. Greg Dekaban for their support and guidance over the course of my project. I would also like to express my gratitude to my advisory committee members Dr. Silvia Penuela and Dr. Sean Gill for their insightful feedback, as well as Dr. John Ronald for his collaboration with the *in vivo* optical imaging studies.

Thank you to all of the members of the Flynn lab who helped me over the course of my thesis. In particular, I would like to acknowledge Dr. Laura Juignet for her troubleshooting help and for assisting with the flow cytometry experiments. I would also like to thank Arthi Shridhar for her contributions toward my review article, and for her technical and emotional support in and out of the lab. In addition, special thanks goes to Cody Brown, Hisham Kamoun, and Gagandeep Singh for their technical assistance. I would also like to acknowledge Christy Barreira in the Dekaban lab for providing flow cytometry help, as well as Katie Parkins in the Ronald lab for her assistance with the *in vivo* optical imaging experiments.

I would like to extend a special thanks to my rock climbing pals, who provided much-needed comic relief and a healthy distraction from my studies. To my wonderful feline friend, Frances, thank you for sharing the ups and downs with me – your companionship means more to me than you will ever know.

Lastly, to my parents, Sylvia and Mike Robb, and my sister, Melanie: thank you for being there for me and for your endless support. This would not have been possible without you.

# Table of Contents

Abstract .....	i
Co-Authorship Statement.....	ii
Acknowledgments.....	iii
Table of Contents .....	iv
List of Tables .....	viii
List of Figures .....	ix
List of Appendices .....	xii
List of Abbreviations .....	xiii
Chapter 1 .....	1
1 Introduction .....	1
1.1 Project motivation and rationale .....	1
1.2 Hypothesis and specific aims.....	3
Chapter 2.....	5
2 Literature Review.....	5
2.1 Adipose tissue engineering .....	5
2.1.1 Adipose tissue composition, structure, and function .....	5
2.1.2 Current strategies for adipose tissue engineering .....	7
2.2 ASCs as a regenerative cell source .....	8
2.2.1 ASC isolation procedures .....	9
2.2.2 ASC immunophenotype.....	10
2.2.3 ASC differentiation capacity.....	12
2.2.4 ASC paracrine functions .....	13
2.3 The ECM and tissue decellularization .....	15

2.3.1	The ECM.....	15
2.3.2	Tissue decellularization .....	17
2.3.3	Decellularized adipose tissue scaffolds .....	17
2.4	Stem/progenitor cells and ECM-derived scaffolds for tissue engineering .....	19
2.4.1	Stem/progenitor cell sources and seeding strategies for ECM-derived scaffolds .....	19
2.4.2	Stem/progenitor cell-instructive effects of decellularized scaffolds.....	20
2.4.3	Mechanisms of stem/progenitor cell modulation by ECM-derived scaffolds .....	23
2.5	Host response to biomaterials in tissue engineering .....	28
2.5.1	Overview of the host response to biomaterials .....	28
2.5.2	Macrophage response to biomaterials and role in tissue engineering.....	31
2.6	Summary .....	34
Chapter 3.....		35
3	Materials and Methods.....	35
3.1	Materials .....	35
3.2	Animals.....	35
3.3	ASC isolation and culture .....	35
3.4	ASC characterization .....	36
3.4.1	Immunophenotyping.....	36
3.4.2	Adipogenic differentiation .....	37
3.4.3	Osteogenic differentiation.....	39
3.4.4	Chondrogenic differentiation .....	40
3.5	DAT scaffold fabrication and seeding .....	41
3.5.1	Adipose tissue procurement and decellularization .....	41
3.5.2	Scaffold preparation and seeding.....	42

3.6 Scaffold implantation, tissue harvest, and Masson’s trichrome staining.....	43
3.6.1 Masson’s trichrome staining.....	44
3.7 Immunohistochemical detection of dsRed <sup>+</sup> donor cells.....	44
3.8 <i>In vivo</i> optical imaging.....	45
3.9 Immunohistochemical assessment of macrophage infiltration and macrophage phenotypic markers.....	46
3.10 Statistical Analysis.....	47
Chapter 4.....	48
4 Results.....	48
4.1 ASC characterization.....	48
4.1.1 Cell surface marker expression.....	48
4.1.2 Trilineage differentiation.....	50
4.2 ASC seeding and attachment to DAT scaffolds.....	53
4.3 Cell recruitment and tissue remodeling within implanted DAT scaffolds.....	55
4.3.1 Qualitative assessment of cell infiltration and tissue remodeling.....	55
4.3.2 Cell recruitment.....	59
4.3.3 Adipose tissue remodeling.....	60
4.4 Histological detection and optical tracking of syngeneic donor dsRed <sup>+</sup> ASCs within implanted DAT scaffolds.....	61
4.4.1 Immunohistochemical detection of donor dsRed <sup>+</sup> cells.....	61
4.4.2 <i>In vitro</i> fluorescent detection of transgenic ASCs and macrophages seeded onto DAT scaffolds.....	65
4.4.3 <i>In vivo</i> tracking of dsRed <sup>+</sup> donor cells.....	68
4.5 Immunohistochemical analysis of infiltrating myeloid cells.....	70
4.5.1 Iba1 <sup>+</sup> myeloid cell infiltration in DAT implants.....	70
4.5.2 Macrophage phenotypic markers in DAT scaffolds.....	76

Chapter 5.....	79
5 Discussion .....	79
Chapter 6.....	87
6 Conclusions and Future Directions .....	87
6.1 Summary of findings.....	87
6.2 Conclusions.....	89
6.3 Future recommendations.....	90
References.....	94
Appendix 1.....	123
Appendix 2.....	132
Curriculum Vitae .....	134



## List of Tables

Table 3.1. Summary of differentiation media formulations .....	37
Table 3.2. Specifications for immunohistochemistry protocols. ....	47
Table 4.1. Adipose tissue remodeling in ASC-seeded and unseeded DAT implants .....	61

## List of Figures

Figure 2.1. Stem/progenitor cell-instructive effects mediated by ECM-derived scaffolds .....	21
Figure 2.2. Proposed mechanisms by which compositional, biomechanical, and structural properties of ECM-derived scaffolds direct stem/progenitor cell behaviour and responses .....	25
Figure 3.1. Scaffold implantation and excision .....	44
Figure 4.1. dsRed <sup>+</sup> mouse ASCs express characteristic cell surface markers .....	49
Figure 4.2. ASCs differentiate toward the adipogenic lineage .....	51
Figure 4.3. ASCs differentiate toward the osteogenic lineage.....	52
Figure 4.4. ASCs differentiate toward the chondrogenic lineage.....	53
Figure 4.5. ASCs attach to DAT scaffolds under <i>in vitro</i> dynamic seeding conditions ...	54
Figure 4.6. ASC-seeded DAT scaffolds enhance cell recruitment, adipogenesis, and angiogenesis .....	57
Figure 4.7. Low levels of cell recruitment, adipogenesis, and angiogenesis were observed in unseeded DAT scaffolds.....	58
Figure 4.8. ASC-seeding enhances cell recruitment within DAT scaffolds .....	60
Figure 4.9. Syngeneic dsRed <sup>+</sup> donor cells are observed in ASC-seeded DAT scaffolds up to 8 weeks post-implantation and are not localized to newly formed adipocytes .....	63
Figure 4.10. dsRed <sup>+</sup> cells are not observed in unseeded DAT implant controls .....	64
Figure 4.11. Quantitative analysis of immunohistochemical staining confirmed positive dsRed staining within the ASC-seeded but not unseeded implants .....	65

Figure 4.12. dsRed <sup>+</sup> ASCs seeded onto DAT scaffolds <i>in vitro</i> can be detected by optical imaging .....	67
Figure 4.13. Donor dsRed <sup>+</sup> cells are detected through optical imaging of ASC-seeded implant regions of mice at 24 h, 72 h, 3, and 5 weeks post-implantation.....	69
Figure 4.14. Representative images of the scaffold periphery of EGFP and Iba1 co-staining in ASC-seeded DAT implants.....	71
Figure 4.15. Representative images of the scaffold periphery of EGFP and Iba1 co-staining in unseeded DAT implants.....	72
Figure 4.16. Quantitative analysis of EGFP and Iba1 co-staining along the implant periphery .....	74
Figure 4.17. Myeloid cell expression patterns of iNOS appear similar between seeded and unseeded DAT scaffolds .....	77
Figure 4.18. Myeloid cell expression patterns of Arg-1 appear similar between seeded and unseeded DAT scaffolds .....	78
Supplementary Figure 1. Representative scatter plots depicting fluorescence minus one (FMO) flow cytometry controls.....	123
Supplementary Figure 2. Immunohistochemistry of tissue-positive (left panels) and no primary (right panels) controls for collagen I (top panels) and collagen II (bottom panels) .....	124
Supplementary Figure 3. Immunohistochemistry of tissue-positive, no primary, and tissue-negative controls for dsRed staining .....	125
Supplementary Figure 4. Immunohistochemistry of mouse spleen tissue-positive, no primary, and tissue-negative controls for EGFP staining .....	126

Supplementary Figure 5. Immunohistochemistry of mouse spleen tissue-positive (left panels) and no primary (right panels) controls for Iba1 (top panels), iNOS (middle panels), and Arg-1 (bottom panels) .....	127
Supplementary Figure 6. Single channel and merged images of ASC-seeded DAT scaffolds co-stained for EGFP and iNOS .....	128
Supplementary Figure 7. Single channel and merged images of unseeded DAT scaffolds co-stained for EGFP and iNOS.....	129
Supplementary Figure 8. Single channel and merged images of ASC-seeded DAT scaffolds co-stained for EGFP and Arg-1.....	130
Supplementary Figure 9. Single channel and merged images of unseeded DAT scaffolds co-stained for EGFP and Arg-1. ....	131

## List of Appendices

Appendix 1. Supplementary Figures.....	123
Appendix 2. Regulatory Approvals. ....	132

## List of Abbreviations

μL	microliter
μm	micrometer
μmole	micromole
2D	2-dimensional
3D	3-dimensional
ADAMs	a disintegrin and metalloproteinase
ALP	alkaline phosphatase
ANG-1	angiopoietin-1
APC	allophycocyanin
Arg-1	arginase-1
ASCs	adipose-derived stem/stromal cells
ATM	adipose tissue macrophages
ATP	adenosine triphosphate
BAT	brown adipose tissue
bFGF	basic fibroblast growth factor
BMI	body mass index
bmMSCs	bone marrow-derived mesenchymal stem/stromal cells
BMP	bone morphogenetic protein
BSA	bovine serum albumin
C/EBP	CCAAT/enhancer-binding protein
CCAC	Canadian Council on Animal Care
CCL	chemokine (C-C motif) ligand
CCR	C-C chemokine receptor
CD	cluster of differentiation
cm	centimeter
CMP	common myeloid progenitor
CMV	cytomegalovirus
Csf1r	colony stimulating factor 1 receptor
CXCL-12	chemokine (C-X-C) motif ligand 12
CXCR	C-X-C chemokine receptor

DAB	3,3'-diaminobenzidine
DAT	decellularized adipose tissue
DCB	decellularized cancellous bone
DMEM:Ham's	Dulbecco's Modified Eagle's Medium:Ham's F12
dsRed	<i>Discosoma</i> red fluorescent protein
ECM	extracellular matrix
EDTA	ethylenediaminetetraacetic acid
EGFP	enhanced green fluorescent protein
FAK	focal adhesion kinase
FBS	fetal bovine serum
FSC	forward scatter
g/L	gram/liter
GAGs	glycosaminoglycans
G-CSF	granulocyte colony stimulating factor
GFP	green fluorescent protein
GLUT-4	glucose transporter-4
GM-CSF	granulocyte-macrophage colony stimulating factor
GPDH	glycerol-3-phosphate dehydrogenase
h	hour
HGF	hepatocyte growth factor
HLA-DR	human leukocyte antigen-antigen D related
Iba1	ionized calcium-binding adapter molecule 1
IBMX	3-isobutyl-1-methylxanthine
IDO	indoleamine 2,3-dioxygenase
IFATS	International Federation for Adipose Therapeutics and Science
IFN- $\gamma$	interferon-gamma
IL	interleukin
iNOS	inducible nitric oxide synthase
ISCT	International Society for Cellular Therapy
kPa	kilopascal
L/min	liter/minute

LCA	leukocyte common antigen
LIF	leukemia inhibitory factor
LPL	lipoprotein lipase
M-CSF	macrophage colony stimulating factor
MCAM	melanoma cell adhesion molecule
mg	milligram
mg/kg	milligram/kilogram
mg/L	milligram/liter
min	minute
mL	milliliter
mm	millimeter
mM	millimolar
MMPs	matrix metalloproteinases
MSCs	mesenchymal stem/stromal cells
NETs	neutrophil extracellular traps
NK cell	natural killer cell
nm	nanometer
NO	nitric oxide
PAI-1	plasminogen activator inhibitor-1
PBS	phosphate-buffered saline
PDGF	platelet-derived growth factor
PECAM	platelet endothelial cell adhesion molecule
pen-strep	penicillin-streptomycin
PGA	polyglycolic acid
PLA	polylactic acid
PLGA	poly(lactic-co-glycolic acid)
PMSF	phenylmethylsulfonyl fluoride
PODXL	podocalyxin-like
PPAR $\gamma$	peroxisome proliferator-activated receptor-gamma
RGD	arginine-glycine-aspartic acid
ROI	region-of-interest



rpm	revolutions per minute
RUNX2	runt-related transcription factor 2
SIS	small intestinal submucosa
SMAD	signaling mothers against decapentaplegic
SOX9	sex-determining region Y-related high motility group box 9
SPB	Sorenson's phosphate buffer
SSC	side scatter
SVF	stromal vascular fraction
TBS	tris-buffered saline
TGF- $\beta$	transforming growth factor-beta
TIMPs	tissue inhibitors of metalloproteinases
TNF $\alpha$	tumour necrosis factor-alpha
trypsin/EDTA	trypsin/ethylenediaminetetraacetic acid
v/v	volume/volume
VCAM-1	vascular cell adhesion molecule 1
VEGF	vascular endothelial growth factor
WAT	white adipose tissue

# Chapter 1

## 1 Introduction

### 1.1 Project motivation and rationale

Subcutaneous adipose tissue (fat) is an integral component of the integumentary system, functioning to store energy and provide insulation. However, adipose tissue has a limited capacity for self-renewal; damage can lead to scar tissue formation and contracture, for example in cases of trauma, lipodystrophies, and oncologic resection [1, 2]. Current reconstructive and cosmetic procedures for soft tissue augmentation include the use of dermal fillers and fat grafts; however, these are associated with poor long-term retention, high costs, and the potential for surgical complications [3]. To address the clinical need for stable and effective soft tissue replacements, previous work from the Flynn laboratory has demonstrated that decellularized adipose tissue (DAT) scaffolds represent a promising tissue-specific platform for the delivery of adipose-derived stem/stromal cells (ASCs) as an adipose tissue engineering strategy [4, 5]. In particular, subcutaneous implantation of the DAT into an immunocompetent Wistar rat model demonstrated that ASC-seeded scaffolds helped to stimulate angiogenesis and host-derived fat formation [4]. Importantly, the allogeneic donor ASCs were shown to support a pro-regenerative microenvironment associated with increased expression of the anti-inflammatory cytokine interleukin (IL)-10, and a shift toward a more constructive M2 macrophage phenotype [4].

ASCs can secrete a wide array of angiogenic and chemotactic factors, as well as immunomodulatory cytokines including IL-10, IL-13, hepatocyte growth factor (HGF), and leukemia inhibitory factor (LIF), depending on the local microenvironment [6]. Supporting that transplanted ASCs may promote regeneration through indirect paracrine mechanisms by modulating the immune response, *in vitro* co-culture studies have confirmed that ASCs can promote the expression of M2 macrophage markers through contact-independent mechanisms [7-10]. Furthermore, Dong *et al.* demonstrated that donor ASCs incorporated into human fat grafts increased the fraction of M2-like

macrophages and improved implant survival within an athymic mouse model [11]. Other mesenchymal stem/stromal cell (MSC) populations have also been shown to enhance the recruitment of monocytes and macrophages through chemotactic factor production [12, 13], indicating another key mechanism through which the ASCs could modulate the inflammatory response.

The immunomodulatory activity of ASCs is an attractive feature supporting their use in adipose tissue engineering since macrophages and inflammation have been shown to play an integral role in fat formation. Using a silicone-encased Matrigel chamber as an engineering model for neo-adipogenesis, Thomas *et al.* demonstrated that the addition of the sterile inflammation agent Zymosan into the chamber significantly augmented fat formation [14]. Moreover, incorporation of the agent aminoguanidine to attenuate inflammation was shown to reverse these effects [14]. The same group showed that adipose tissue regeneration was associated with an initial infiltration of bone marrow-derived macrophages thought to be important for recruiting adipocyte precursors originating from the bone marrow as well as neighbouring tissues [15]. A follow-up study revealed that macrophages played an integral role in the regenerative process. Local depletion of macrophages using Clodronate liposomes incorporated into the Matrigel chamber resulted in a dramatic reduction in angiogenesis and adipogenesis within the system [16]. Interestingly, a similar role for inflammation has been implicated in the pathophysiology of obesity. More specifically, the degree of adipose tissue macrophage infiltration has been correlated to adiposity [17], with macrophages being a significant source of pro-inflammatory cytokines that contribute to the chronic inflammatory state associated with this condition [18-20]. Collectively, these findings support a key role for macrophages in adipogenesis.

The pro-adipogenic DAT scaffolds have been shown to retain features of the complex adipose tissue extracellular matrix (ECM) [21], and display similar biomechanical properties to native human fat [22, 23]. As such, the DAT represents a rational cell-instructive delivery vehicle for ASCs in an adipose tissue engineering strategy [4]. Building on a promising foundation of previous *in vitro* and *in vivo* data, there is a need to develop a deeper understanding of regenerative mechanisms mediated by DAT

scaffolds and ASCs. As such, the primary goal of the current study was to track and characterize infiltrating myeloid cells, including macrophages, as well as donor ASCs in tandem through the use of dual transgenic reporter mouse models. The results of this work support the rationale for a tissue-specific approach for cell delivery and tissue engineering, and suggest the need for further investigation of the role of inflammation in adipose tissue regeneration.

## 1.2 Hypothesis and specific aims

The hypothesis for this work was that *syngeneic donor ASCs will influence myeloid cell infiltration kinetics, and will enhance cell recruitment and adipogenesis within DAT scaffolds implanted subcutaneously in mice*. To facilitate donor ASC cell tracking, ASCs were isolated from transgenic *Discosoma* red fluorescent protein (dsRed) mice (B6.Cg-Tg(CAG-DsRed\*MST)1Nagy/J; C57BL/6J background; Jackson Laboratory, Bar Harbor, ME) in which all cells express dsRed under the control of the chicken beta actin promoter coupled with the cytomegalovirus (CMV) immediate early enhancer [24]. DAT scaffolds seeded with dsRed<sup>+</sup> ASCs were implanted subcutaneously along with unseeded controls into MacGreen transgenic reporter mice (B6N.Cg-Tg(Csf1r-EGFP)1Hume/J; C57BL/6J background; Jackson Laboratory, Bar Harbor, ME) in which cells of the myeloid lineage (including macrophages, monocytes and neutrophils) express enhanced green fluorescent protein (EGFP) under the control of the mouse colony stimulating factor 1 receptor (*Csf1r*) promoter [25, 26]. To address the central hypothesis, the specific aims of this Master's thesis were:

- 1) To characterize the cell surface phenotype and multilineage differentiation capacity (adipogenic, chondrogenic, and osteogenic) of ASCs isolated from the inguinal fat pad of dsRed mice, and to establish methods for seeding the murine ASCs onto the DAT scaffolds.
- 2) To assess total cell infiltration and adipogenesis within ASC-seeded and unseeded DAT scaffolds implanted subcutaneously into the MacGreen mouse model over 8 weeks.
- 3) To perform ASC tracking studies to assess donor ASC retention within the implanted DAT scaffolds.

- 4) To characterize the myeloid cell population infiltrating the DAT implants through immunohistochemical staining for macrophage markers.

## Chapter 2

### 2 Literature Review

Sections of this chapter were included in the review article “Robb KP, Shridhar A, Flynn LE. *Decellularized matrices as cell-instructive scaffolds to guide tissue-specific regeneration*. ACS Biomaterials Science & Engineering. Accepted Nov. 13, 2017. DOI: 10.1021/acsbiomaterials.7b00619”

#### 2.1 Adipose tissue engineering

##### 2.1.1 Adipose tissue composition, structure, and function

Adipose tissue is a specialized form of loose connective tissue that functions primarily as a regulator of energy homeostasis. Fat is distributed within subcutaneous and visceral depots, including in the epicardial and intramuscular regions, as well as in the bone marrow [27]. In mammals, adipose tissue exists in two forms: brown adipose tissue (BAT) and white adipose tissue (WAT) [28]. BAT is predominantly found in neonates and in hibernating mammals, and functions as a mechanism of heat generation via non-shivering thermogenesis [29]. Brown adipocytes represent a small fraction of adipocytes in adult humans; however, BAT is thought to play a potential metabolic role in obesity, as low levels of BAT have been correlated to increased body mass index (BMI) and fat accumulation in humans and animal models [30, 31]. WAT comprises the majority of adipose tissue in adults and functions to store energy in the form of triglycerides and other lipids [32]. In response to energy demands and hormonal stimuli, triglycerides are hydrolyzed forming free fatty acids and glycerol that are released by adipocytes into the circulation, allowing subsequent cellular uptake and conversion to energy sources via downstream biochemical pathways [33]. Given that WAT is a major component of subcutaneous tissues, it has been of predominant interest in adipose tissue engineering strategies. In developing these strategies, WAT also represents a convenient source of both cells and scaffolding material [5, 34, 35], as discussed in detail in Sections 2.2 and 2.3.

A wide variety of cell types are found in adipose tissue, with adipocytes representing the largest proportion [36]. Adipocytes are terminally-differentiated cells specialized to store and release lipids contained within a lipid droplet, which comprises >90% of the total cell volume [37]. Other cell types found in adipose tissue include adipose-derived stem/stromal cells (ASCs; discussed in Section 2.2) as well as more committed pre-adipocytes that give rise to adipocytes [38]. Adipose tissue is highly vascularized, with each adipocyte supplied by an extensive capillary network, allowing for uptake and release of nutrients and waste products [39]. Further, adipose tissue also receives significant innervation from both sympathetic and parasympathetic inputs that act in concert to regulate lipid metabolism [40]. Adding to the complexity of this tissue is the presence of immune cells including macrophages, neutrophils, and lymphocytes, which are found at low levels within healthy adipose tissue [28]. In the pathophysiology of obesity, increased levels of adipose tissue macrophages (ATMs) are associated with adiposity [17], and the pro-inflammatory cytokines released by ATMs are a key contributor to chronic inflammation in obese patients [18-20].

As mentioned, the main function of WAT is energy storage, but it also provides mechanical cushioning and insulates the body to prevent heat loss [41]. Moreover, WAT is an essential endocrine organ, secreting adipose tissue cytokines, known as adipokines, which are involved in a variety of processes including nutritional control, angiogenesis, vascular homeostasis, blood pressure control, and inflammation [42, 43]. Of these, leptin was the first-discovered adipokine recognized for its role in mediating energy balance and metabolism by regulating appetite [44]. Adiponectin is another well-studied adipokine known to display pleiotropic actions including regulation of gluconeogenesis, glucose uptake, and lipid catabolism [45]. In addition, adiponectin displays anti-inflammatory functions associated with reduced tumour necrosis-factor-alpha (TNF $\alpha$ ) and interleukin (IL)-6 production in adipose tissue and other tissues, as well as increased IL-10 secretion [46]. Other known adipokines include plasminogen activator inhibitor-1 (PAI-1) involved in fibrinolysis and regulation of insulin sensitivity [47], and the pro-angiogenic protein, vascular endothelial growth factor (VEGF) [48].

## 2.1.2 Current strategies for adipose tissue engineering

Adipose tissue has a limited capacity for self-repair; thus, damage or deficits can lead to scar tissue formation and contracture [1, 2]. A range of conditions are associated with subcutaneous adipose tissue deficits including congenital defects, lipodystrophies, aging, trauma, and cancer [49, 50]. Plastic and reconstructive surgeries to treat such abnormalities are highly prevalent, with 290,000 breast augmentations, 2.6 million soft tissue filler procedures, and 4.5 million oncologic resections performed in the United States in 2016 [51]. For small volume deficits, current treatment options include autologous fat transfer and dermal fillers such as hyaluronic acid-based materials [52, 53]. However, these treatments are associated with poor long-term retention necessitating regular follow-up treatments, and in the case of fat grafting, there is the potential for oil cyst formation [53-56]. The preferred treatment option for larger volume deficits involves autologous tissue transfer of vascularized flaps of skin, fat, and muscle [57] but these procedures are costly, and have high complication rates, including donor site morbidity [3].

Synthetic implants have been explored as an alternative treatment for adipose tissue deficits. These include biocompatible absorbable polymers such as poly(lactic-co-glycolic acid) (PLGA), polyglycolic acid (PGA), and polylactic acid (PLA) [2, 58, 59]. Synthetic polymers offer the advantage of controlled tuning of the biomechanical properties and degradation rate via cross-linking, enabling the design of a material that matches the mechanical properties of the tissue of interest, as well as the potential for controlled release of growth factors or cytokines [60]. However, the long-term retention of synthetic materials *in vivo* remains a significant hurdle [61, 62], along with issues related to fibrous encapsulation of the implants which can cause severe pain, as well as implant migration and rupture [63].

Naturally-derived materials represent an additional avenue of exploration for the treatment of adipose tissue abnormalities. For example, collagen scaffolds have been shown to support angiogenesis and adipogenesis *in vivo* [64, 65]. Bellas *et al.* demonstrated that porous silk sponges seeded with lipoaspirate retained their volume



over the course of an 18 month study in a subcutaneous nude rat model [66]. Additionally, injectable alginate-based scaffolds have been shown to support adipogenesis *in vitro* and *in vivo* [67, 68]. In the category of naturally-derived materials, decellularized scaffolds have been investigated with the goal of retaining instructive extracellular matrix (ECM) components to guide tissue regeneration [3]. Given that this is a primary focus of this work, ECM-derived scaffolds will be discussed in detail in Section 2.3.

While ECM-derived scaffolds have shown promise in tissue engineering applications, there is emerging evidence to support that combination strategies involving the dual use of cell-instructive scaffolds with stem/progenitor cells may be more effective than either cells or scaffolds alone [63, 69]. In particular, donor stem/progenitor cells can help to stimulate regeneration within implanted ECM-derived scaffolds, and can be conveniently sourced from adult tissues. Stem/progenitor cell sourcing and regenerative mechanisms are discussed in greater detail below, with an emphasis on the utility of ASCs in adipose tissue engineering.

## 2.2 ASCs as a regenerative cell source

Mesenchymal stem/stromal cells (MSCs) are a cell population capable of *in vitro* clonal expansion and multipotent differentiation [70, 71]. MSCs are a commonly studied regenerative cell source first discovered in the adult bone marrow [70, 71]; however, MSC populations have since been identified and isolated from a variety of other adult tissues, including adipose tissue and peripheral blood, as well as from the dermis, heart, and lungs [72-76]. In particular, MSCs sourced from adipose tissue (ASCs) have received growing interest due to their ease of access through minimally invasive procedures, and the ability to obtain higher yields of these cells relative to bone marrow-derived MSCs (bmMSCs) [77]. Immunohistochemical analysis has suggested that in native tissues, ASCs reside in the perivascular niche adjacent to neighbouring endothelial cells and pericytes [78]; however, their exact localization remains controversial due to the lack of unique markers to identify the population [79, 80]. With the aim of standardizing approaches for ASC characterization, the International Federation for Adipose

Therapeutics and Science (IFATS) in conjunction with the International Society for Cellular Therapy (ISCT) have defined ASCs as having the following minimum criteria: 1) ASCs are plastic-adherent cells, 2) ASCs should express a standard cell surface phenotypic profile (described in more detail below), and 3) ASCs should maintain *in vitro* multipotency toward the adipogenic, osteogenic, and chondrogenic lineages [81].

### 2.2.1 ASC isolation procedures

A variety of methods have been developed for the isolation of ASCs from adipose tissue, including from lipoaspirate [82-84]. In general, these protocols involve enzymatic digestion and separation steps via centrifugation to yield the stromal vascular fraction (SVF), a heterogeneous population of cells consisting of MSCs, pre-adipocytes, endothelial progenitor cells, fibroblasts, pericytes, circulating blood cells, macrophages, and smooth muscle cells [85, 86]. The ASC population can then be further purified from the SVF through selection and expansion of the adherent cell population on tissue culture plastic. However, this plastic-adherent population remains heterogeneous in terms of cell morphology (including small rapidly self-renewing cells, spindle-like cells, and large flattened cells), as well as the presence of variable ratios of uni-, bi-, and tri-potent cells, progenitors, and more differentiated subpopulations [87-90]. Importantly, the wide array of ASC isolation procedures and growth conditions can influence the yield, expansion rates, and differentiation capacity of these cells [91, 92]. Attempts to standardize these procedures are ongoing in order to improve the consistency and reproducibility of the therapeutic efficacy of ASCs for clinical applications.

ASCs can be isolated from both visceral and subcutaneous depots in a variety of anatomical locations, and there is increasing evidence that ASCs sourced from different locations display functional differences *in vitro* [93, 94]. For example, a previous study from our laboratory comparing ASCs isolated from subcutaneous, omental, pericardial, and thymic remnant depots, showed that levels of osteogenic differentiation were enhanced in ASCs harvested from the omentum, while adipogenic differentiation was augmented in ASCs derived from the subcutaneous and pericardial depots [95]. Moreover, ASCs isolated from lipoaspirate sourced from the upper arm and medial thigh

have been reported to display higher proliferative and differentiation capacities relative to fat from the trochanteric and superficial or deep abdominal regions [96]. This depot-dependency could potentially be exploited in the application of ASCs in cell-based therapies by extracting specific populations that may be predisposed toward a desired cellular fate. In addition to the influence of adipose tissue depots, donor health status, BMI, age, sex, and other factors contribute to donor variability in terms of the yield and functionality of ASCs [97-100]. However, the influence of these factors is difficult to study due to their complexity and interdependency, and further work involving large-scale studies is required in order to better understand the impact of these different factors on the therapeutic potential of ASCs.

While the study of human ASCs is important for clinical translation, investigation of ASCs from other mammalian sources is important for pre-clinical model studies to develop a deeper understanding of the mechanisms of ASC-mediated tissue regeneration. In contrast to human ASCs, mouse ASCs have been far less well-characterized. These cells can be isolated from the gonadal and inguinal fat pads of mice using extraction protocols similar to those for human tissue [101]. The multilineage differentiation potential of mouse ASCs has been confirmed by a number of groups [102-106]. While detailed comparison studies have yet to be reported in the literature, factors such as mouse strain, age, sex, and the selected fat depot for extraction are likely to influence murine ASC differentiation capacity and functionality.

### 2.2.2 ASC immunophenotype

As previously mentioned, a panel of markers has been defined by IFATS and the ISCT as a means to standardize the characterization of human ASCs through cell surface phenotyping (Table 2.1). In general, the ASC cell surface phenotype is similar to bmMSCs with the exception of CD34, which is highly expressed on human ASCs at early culture passages, as well as positive expression of CD36 (fatty acid translocase) [72, 107, 108]. A joint statement from IFATS and the ISCT recommended that flow cytometric analyses of ASCs include at least two primary positive and two primary

negative markers, along with secondary positive and negative markers to strengthen the characterization [81].

**Table 2.1. Human ASC cell surface phenotype** [81, 108]

	<b>Antigen</b>
<b>Primary positive markers (&gt;80%)</b>	CD90 (Thy-1) CD105 (endoglin) CD73 (ecto-5'-nucleotidase) CD44 (hyaluronic acid receptor) CD29 ( $\beta$ 1-integrin) CD13 (aminopeptidase-N) CD34 (progenitor associated marker)* CD146 (melanoma cell adhesion molecule, MCAM)*
<b>Secondary positive markers</b>	CD10 (neprilysin) CD26 (dipeptidyl peptidase-4) CD49d ( $\alpha$ 4-integrin)* CD49e ( $\alpha$ 5-integrin) CD36 (fatty acid translocase)
<b>Primary negative markers (&lt;2%)</b>	CD31 (platelet endothelial cell adhesion molecule, PECAM) CD45 (leukocyte-common antigen, LCA) CD235a (glycophorin A) HLA-DR (human leukocyte antigen-antigen D related)
<b>Secondary negative markers</b>	CD3 (T-cell co-receptor) CD11b ( $\alpha$ M-integrin) CD49f ( $\alpha$ 6-integrin) CD106 (vascular cell adhesion molecule 1, VCAM-1) PODXL (podocalyxin-like)

\*variable levels of expression

Cell surface phenotyping of murine ASCs revealed that human ASCs had a similar cell surface marker expression profile with some exceptions [102, 106, 109-111]. While considered positive markers in human ASCs, murine ASCs have been reported negative for CD34 [106, 109, 110] and CD146 [102], with more variable expression levels of CD105 [106, 109-111].

### 2.2.3 ASC differentiation capacity

ASCs are capable of differentiation along the adipogenic, osteogenic, and chondrogenic lineages [81]. Adipogenic differentiation protocols typically involve the culture of ASCs at cellular confluence, since close cell-cell contact promotes growth arrest required for subsequent differentiation [38]. In addition, a cocktail of chemical agents, cytokines, and hormones are added to the culture media to stimulate adipogenic differentiation. These supplements include glucocorticoid agonists such as dexamethasone and hydrocortisone, as well as supra-physiologic concentrations of insulin, which is important for initiating the induction of ASCs toward the adipogenic lineage [112]. Activation of the early transcription factors CCAAT/enhancer-binding protein (C/EBP)- $\beta$  and C/EBP $\delta$  stimulates expression of the primary transcription factors of adipogenesis: C/EBP $\alpha$  and peroxisome proliferator-activated receptor-gamma (PPAR $\gamma$ ) [113]. This in turn upregulates adipocyte-specific genes, including expression of lipoprotein lipase (*LPL*), glucose transporter-4 (*GLUT-4*), and glycerol-3-phosphate dehydrogenase (*GPDH*) associated with lipid accumulation and terminal differentiation [114, 115]. Additionally, adipogenic media formulations often include synthetic PPAR $\gamma$  ligands such as rosiglitazone and troglitazone, which can directly stimulate adipogenic gene expression [116, 117].

Osteogenic differentiation of ASCs can be induced using a variety of media supplements including beta-glycerophosphate, insulin, vitamin D, dexamethasone, and ascorbate-2-phosphate in order to stimulate matrix deposition and mineralization [35, 104, 118]. The process of osteogenic differentiation begins with a proliferative phase and the formation of dense cell nodules, followed by ECM production and secretion that is linked to osteocyte maturation and matrix mineralization [119]. A variety of biochemical signaling pathways are implicated in osteogenic differentiation, including the canonical Wnt and bone morphogenic protein (BMP) signaling pathways, as well as the signaling mothers against decapentaplegic (SMAD) phosphorylation pathway [120, 121].

To stimulate chondrogenic differentiation, ASCs are cultured in 3D aggregates in order to enhance cell-cell and cell-ECM interactions and to mimic the mesenchymal condensation

process during embryogenesis [122]. Chondrogenic media formulations often include factors such as insulin, transforming growth factor-beta (TGF- $\beta$ ), dexamethasone, and ascorbate-2-phosphate in order to further stimulate the process of chondrogenic differentiation [104, 123]. Differentiation is initiated with the upregulation of the transcription factor sex-determining region Y-related high motility group box 9 (SOX9) transcription factor, the master regulator of chondrogenesis [122]. The combined SOX9 activation and cellular condensation prompts the formation of pre-chondrocytes, followed by further maturation toward proliferating chondrocytes, linked to a shift from collagen I to collagen II expression along with the production of other cartilage ECM proteins including aggrecan, collagen IX, and collagen XI [124]. Late stages of chondrogenic differentiation are associated with increased expression of runt-related transcription factor 2 (RUNX2) and formation of pre-hypertrophic chondrocytes, followed by terminal differentiation into hypertrophic chondrocytes [125].

#### 2.2.4 ASC paracrine functions

In addition to their capacity to differentiate along multiple cell lineages, ASCs can secrete beneficial paracrine factors to stimulate host-derived tissue regeneration [126, 127]. These include a wide array of cytokines and growth factors that can modulate the immune response, as well as promote cell survival and angiogenesis [101]. In particular, the immunomodulatory effects of MSCs have received growing interest, and while these effects have been better characterized in bmMSCs, several studies have indicated that bmMSCs and ASCs may display similar immunomodulatory functions [128-131]. The immunoregulatory capacity of ASCs has mainly been studied in association with monocytes/macrophages and T cells, and is primarily mediated by the secretion of cytokines that include IL-10, IL-13, prostaglandin E2, indoleamine 2,3-dioxygenase (IDO), hepatocyte growth factor (HGF), and leukemia inhibitory factor (LIF) [132, 133].

In assessing the influence of ASCs on the macrophage response, studies typically examine the effects of ASCs on macrophage phenotype. In a classification system analogous to the Th1/Th2 system for T lymphocytes, macrophage phenotypes have been broadly classified along a spectrum that includes M1-polarized “pro-inflammatory”

macrophages, and M2-polarized “anti-inflammatory” or “pro-regenerative” macrophages [134]. As such, several *in vitro* co-culture studies have indicated that ASCs may modulate inflammation by promoting a shift toward an M2-like macrophage phenotype through contact-independent mechanisms [7-10]. These findings have been confirmed in animal models [9, 135], including a study in which ASCs incorporated into human fat grafts implanted in an athymic mouse model augmented the expression of the M2 macrophage markers CD163 and CD206 after 14 days [11]. A potential role for exosomes and microRNAs released by MSCs has also been implicated in regulating macrophage phenotype [136]. Wang *et al.* reported that miR-223 release by mouse bmMSCs was important for suppressing pro-inflammatory cytokine secretion by lipopolysaccharide-stimulated macrophages, and was crucial to the cardioprotective effects of bmMSC-derived exosomes in a polymicrobial sepsis mouse model [136]. In addition to modulating macrophage phenotype, MSCs have been shown to recruit monocytes/macrophages through secretion of chemokines, including chemokine (C-C motif) ligand (CCL)-2,3,4,7 and -12 within the tumour microenvironment as well as in wound healing [12, 13].

The immunomodulatory role of ASCs has also been demonstrated through cross-talk with T cell populations. In particular, ASCs have been shown to inhibit T cell activation and pro-inflammatory cytokine production, as well as augment levels of regulatory T cells [137]. Pro-inflammatory cytokines have been associated with increased expression of immunosuppressive factors by MSCs [137, 138]. For example, interferon-gamma (IFN $\gamma$ ) stimulation of human ASCs has been shown to augment their expression of IDO [139] and prostaglandin-E2 [140], which in turn suppress T cell proliferation in direct and indirect co-culture models. Interestingly, the immunosuppressive functions of ASCs have enabled their use in both allogeneic and xenogeneic animal models without the need for immunosuppressants [141]. Moreover, these properties have prompted the use of allogeneic ASCs for the treatment of acute graft-versus-host disease, showing beneficial outcomes as a salvage therapy in steroid-refractory patients [142-144]. Importantly, Lai *et al.* demonstrated that human ASCs at passage 3 inhibited proliferation of IL-17-producing CD4<sup>+</sup> T cells from patients with systemic lupus erythematosus, while passage

8 cells had the opposite effect [145], suggesting that *in vitro* expansion of ASCs may influence their immunomodulatory capacity.

Anti-apoptotic and angiogenic factor secretion by ASCs has also been reported, including factors such as VEGF, HGF, TGF- $\beta$ , and platelet-derived growth factor (PDGF) [146, 147]. In support of this, the administration of allogeneic ASCs lead to improved neovascularization in mouse models for hindlimb ischemia through indirect paracrine mechanisms involving the secretion of pro-angiogenic factors [148-151]. These observations have been corroborated in a variety of other models for ischemic diseases (recently reviewed by Zhao *et al.* [152]). An important role for HGF in mediating these responses has also been identified. Downregulation of HGF expression through RNA interference impaired the ability of human ASCs to promote the survival, proliferation, and migration of mature and progenitor endothelial cells *in vitro*, as well as their ability to promote reperfusion in a nude mouse hindlimb ischemia model [153].

## 2.3 The ECM and tissue decellularization

### 2.3.1 The ECM

The ECM is a complex network of proteins and polysaccharides with tissue-specific composition and architecture, consisting of cell-secreted structural and functional molecules that are essential for providing physical support and modulating cell signaling within tissues [154]. There are two main types of ECM: the basal lamina and the interstitial matrix. The basal lamina is a highly bioactive mesh-like network that functions as a base for cell-attachment and as a mechanical barrier in epithelial tissues [155]. The interstitial matrix helps to define the 3D structure of a tissue and consists of structural and bioactive components that are secreted by resident cells [156]. The ECM is a crucial component of the cellular microenvironment as it dynamically mediates cellular functions [156].

In general, the ECM is comprised of fibrous proteins, glycoproteins, glycosaminoglycans (GAGs), and proteoglycans; however, the proportion of these components, their organization and/or the presence of specialized macromolecules varies across tissues



[154]. Fibrous proteins in the ECM include collagen and elastin, which provide structural support to the tissue. Collagen is the most abundant protein in mammals and includes 28 subtypes that function to provide structural integrity, strength, and stability to the ECM [157]. Elastin is another key structural protein that contributes to the elastic properties of soft tissues, particularly within the skin, lungs, and blood vessels [158]. Glycoproteins are another important component of the ECM; these proteins are covalently bound to mono-, di-, or oligosaccharides and function to promote cell attachment and link ECM components [159]. Additionally, GAGs and proteoglycans serve critical roles within the ECM. GAGs are long unbranched polysaccharides consisting of a repeating disaccharide unit, while proteoglycans are a subclass of glycoprotein defined by their covalent linkage to one or more sulphated GAG chains [158]. The highly charged nature of GAGs and proteoglycans functions to attract and bind water molecules within the ECM, as well as to sequester growth factors [160].

Further specialization of the ECM is demonstrated by the ability of cells to dynamically alter ECM components in order to meet the metabolic and mechanical demands of the tissue [161]. Within the context of tissue repair, ECM dynamics are similarly important as the ECM is known to regulate the diverse array of cell types involved at all stages of wound healing [162]. Turnover of ECM components is mediated by a balance of ECM synthesis by the cells within the tissue, and matrix degradation through cell-secreted enzymes such as matrix metalloproteinases (MMPs) and ADAMs (a disintegrin and metalloproteinase) family members, which degrade ECM components [163]. Moreover, secretion of tissue inhibitors of metalloproteinases (TIMPs) serves as an additional level of control by inhibiting MMP function, allowing for tight regulation of matrix dynamics [164]. This complex interrelationship between cells and the ECM is essential for maintaining normal tissue homeostasis, as dysregulation has been associated with a variety of pathologies including liver cirrhosis, pulmonary fibrosis, and cancer [165, 166].

### 2.3.2 Tissue decellularization

Recognizing the importance of the 3D microenvironment in mediating cell function both *in vitro* and *in vivo*, there has been growing interest in the design of cell-instructive biomaterials platforms to help direct cell behavior and promote tissue regeneration [167-170]. As the complexity of the native ECM cannot be easily replicated using synthetic materials, a growing body of work has examined the use of scaffolds derived from decellularized tissues as cell culture and delivery vehicles [171, 172]. Decellularized scaffolds are fabricated using customized protocols designed to extract antigenic cellular components – including organelles, lipids, nucleic acids, and membrane-associated/cytosolic proteins – to obtain a complex ECM enriched in structural proteins. These scaffolds are bioactive and inherently biodegradable, allowing for matrix remodelling and integration into host tissues. Thus, decellularized materials are an attractive platform for tissue engineering strategies due to their potential to stimulate *in situ* tissue regeneration. Several decellularized ECM products are currently in clinical use, including those derived from human or animal small intestinal submucosa (SIS), bladder, dermis, and heart valves [173].

### 2.3.3 Decellularized adipose tissue scaffolds

DAT scaffold fabrication was first reported by the Flynn laboratory in 2010 as a biomaterial platform for soft tissue engineering strategies [5]. Human adipose tissue is a rich source of ECM, and is frequently discarded as surgical waste; therefore, fat represents an abundant and economical alternative to xenogeneic-sourced tissues for decellularized materials [5]. Since the original 2010 report, decellularization protocols for human adipose tissue have been developed by a number of other groups [34, 174-177]. In general, these protocols involve initial freeze/thaw cycles in hypotonic salt solutions to promote cell lysis, coupled with isopropanol or other polar solvents to solubilize cellular components and lipids within the tissue [177]. Further, enzymatic treatment with trypsin/ethylenediaminetetraacetic acid (trypsin/EDTA), DNase, and RNase serves to release cells and degrade nuclear components. While the majority of adipose tissue decellularization protocols involve the use of detergents to extract lipids and cellular components, the Flynn laboratory protocol is uniquely detergent-free [5]. The lack of

detergents in the Flynn protocol is an effort to better preserve ECM composition [5], since these agents can cause marked reductions in more soluble ECM components such as GAGs [178, 179] and growth factors [180], and residual detergents may have cytotoxic effects.

DAT scaffolds fabricated using the Flynn methods provide an inductive microenvironment for the adipogenic differentiation of ASCs *in vitro* [181], as well as for *in vivo* fat formation [4]. More specifically, ASCs cultured on the scaffolds upregulated the expression of the adipogenic genes *PPAR $\gamma$*  and *C/EBP $\alpha$*  in the absence of exogenous growth factors [181]. When cultured in adipogenic differentiation media, ASCs seeded on DAT scaffolds displayed high levels of GPDH enzyme activity and adipogenic gene expression relative to 3D cell aggregate and 2D monolayer culture controls [181]. Moreover, DAT scaffolds have been shown to support angiogenesis and adipogenesis within an immunocompetent subcutaneous Wistar rat model, and pre-seeding of the scaffolds with allogeneic ASCs further enhanced tissue remodeling [4]. Using a different DAT preparation protocol, Wang *et al.* showed that unseeded DAT scaffolds also supported adipogenesis and neovascularization in a subcutaneous Fischer rat model [174].

In addition to the use of DAT in its intact form, the Flynn laboratory has developed methods to incorporate the DAT as a cell-instructive component in a variety of scaffold formats suited to different tissue engineering applications. For example, microporous foams derived from  $\alpha$ -amylase-digested DAT have demonstrated a potent angiogenic response along with gradual resorption in a subcutaneous immunocompetent Wistar rat model, which would be favourable for use in wound healing applications [182]. The Flynn laboratory also developed DAT-based microcarriers as a stem cell expansion platform and injectable biomaterial [183-185], as well as injectable hydrogel composites for localized cell delivery and treatment of small volume adipose tissue deficits [186-188]. In assessing the adipogenic differentiation of ASCs, the pro-adipogenic properties of the DAT-based biomaterials were conserved across the full range of scaffold formats [5, 182-184, 187, 188], supporting the importance of scaffold composition in directing tissue-specific differentiation. DAT-based hydrogel composites have also been developed

by a number of other groups [176, 189, 190], including a protocol incorporating decellularized human lipoaspirate [177].

## 2.4 Stem/progenitor cells and ECM-derived scaffolds for tissue engineering

Stem/progenitor cells are of great interest in the fields of tissue engineering and regenerative medicine due to their innate ability to self-renew and differentiate along multiple lineages. From a translational perspective, the poor localization, retention and survival of cells delivered in suspension points to the need for rationally-designed cell delivery systems with properties tuned to the target site for regeneration [191-193]. As such, decellularized materials may act as promising cell delivery vehicles to guide stem/progenitor cell-mediated regeneration [63]. In the following section, the use of stem/progenitor cells and ECM-derived scaffolds for tissue engineering strategies is discussed, with emphasis on the potential for decellularized materials to modulate stem/progenitor cell behaviour.

### 2.4.1 Stem/progenitor cell sources and seeding strategies for ECM-derived scaffolds

A variety of stem/progenitor cell types have been explored for use in tissue engineering strategies. Depending on the stem/progenitor cell source and the tissue of interest, the recellularization of ECM-derived scaffolds with stem/progenitor cells may enable repopulation with a range of cell types through engraftment and differentiation or enhancement of tissue regeneration through indirect paracrine mechanisms [126, 127]. In the following discussion, emphasis will be placed on studies investigating MSCs, as these have been most commonly studied for regenerative applications [194], are readily accessible, and have the potential to be used autologously or allogeneically [195-197].

The goal in recellularization of ECM-derived scaffolds is to repopulate the ECM with appropriate cell numbers and distribution in order to recapitulate the spatial organization and density of cells in the native tissues, while taking into account the variety of cell types that may be required. Methods for recellularization are designed based on the tissue type and selected application (reviewed in [198, 199]). In general, recellularization can be

completed in culture prior to implantation or can rely on the infiltration of host cells. In the simplest approach, cell seeding can be achieved statically, by allowing cells to passively settle onto the scaffold. Alternatively, dynamic seeding involving the infusion of cells into the scaffold through mechanical agitation or perfusion can be applied. In addition, some seeding strategies take advantage of residual vessel lumens within the scaffold as a means of cell delivery [199].

#### 2.4.2 Stem/progenitor cell-instructive effects of decellularized scaffolds

In this section, “stem/progenitor cell-instructive effects” of ECM-derived scaffolds are defined as any cellular response to the material that may ultimately aid in tissue regeneration. By this definition, decellularized ECM can instruct stem or progenitor cell behaviour through a variety of direct and indirect means, such as by mediating stem/progenitor cell adhesion, migration, proliferation, paracrine factor production, and/or differentiation (Figure 2.1). A common challenge that has been encountered in strategies attempting to deliver stem cells in suspension is that of poor long-term cell viability, which may be related to the loss of cell adhesion leading to anoikis, or to harsh conditions within the target microenvironment [200, 201]. Consequently, ECM-derived scaffolds have been explored as potential cell delivery platforms to enhance stem/progenitor cell adhesion, viability, and proliferation. Indeed, Sharma *et al.*, have shown in a baboon bladder regeneration model that autologous green fluorescent protein (GFP)-labelled bmMSCs seeded on decellularized porcine SIS scaffolds displayed high expression levels of the proliferation marker Ki-67 within the implant region at 10 weeks post-implantation [202]. Similarly, decellularized porcine SIS scaffolds showed significantly improved survival and proliferation relative to cell delivery alone, as evidenced by bioluminescence imaging of donor syngeneic luciferase<sup>+</sup> murine ASCs seeded onto the scaffolds in a murine excisional wound model [203]. By promoting stem/progenitor cell retention and survival, ECM-derived scaffolds may allow these cells to have increased therapeutic efficacy, while providing an inductive substrate that could potentially direct differentiation and/or paracrine factor production, as discussed in greater detail below.

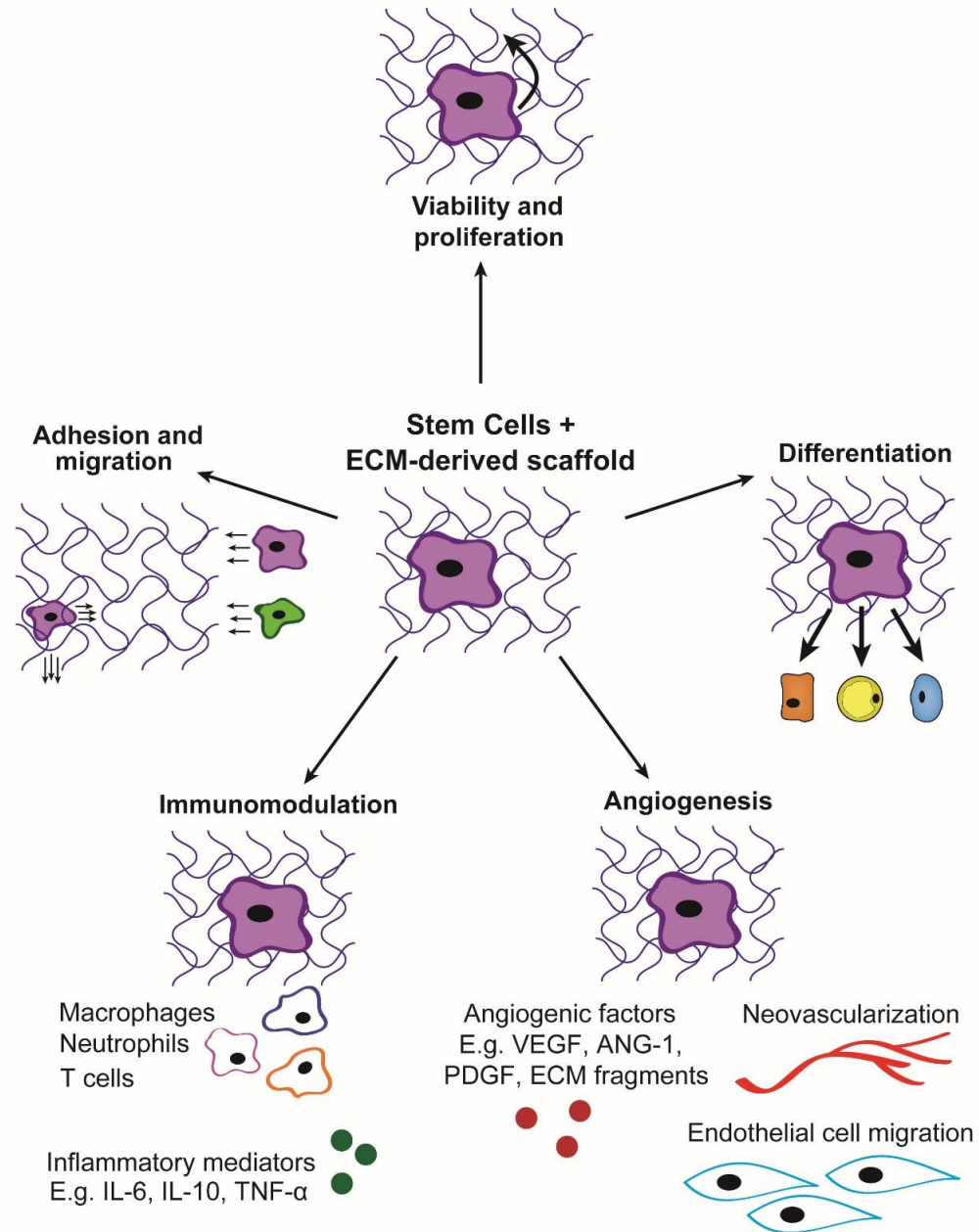


**Figure 2.1. Stem/progenitor cell-instructive effects mediated by ECM-derived scaffolds.** ECM-derived scaffolds can influence stem/progenitor cell adhesion, migration, viability, proliferation, and differentiation along multiple lineages. Moreover, these scaffolds can influence stem/progenitor cell secretion of paracrine factors to promote angiogenesis, and modulate the immune response. VEGF: vascular endothelial growth factor; ANG-1: angiopoietin-1; PDGF: platelet derived growth factor; IL-6: interleukin 6; IL-10: interleukin 10; TNF- $\alpha$ : tumor necrosis factor-alpha.

A wide array of studies have reported that donor stem/progenitor cells can enhance tissue regeneration in ECM-derived scaffolds. In addition, there is a growing body of literature that supports the use of seeded stem or progenitor cell populations as potentially directly contributing to tissue regeneration through engraftment and differentiation. In particular, tissue-specific ECM has been widely postulated to promote lineage-specific differentiation *in vitro*. This has been supported through work of the Flynn laboratory using DAT scaffolds and ASCs [5, 182-184, 187, 188]. Similar results have been demonstrated by a number of other groups comparing a variety of ECM sources, showing tissue- and region-specific differentiation of stem or progenitor cells [204-207].

While stem/progenitor cells have the potential to contribute to new tissue development through differentiation, there is evidence to suggest that the predominant mechanism of regeneration for MSC populations is indirect through the secretion of beneficial paracrine factors that promote the establishment of a more conducive milieu for host tissue regeneration [126, 127]. Key studies demonstrating the immunomodulatory and pro-angiogenic functions of MSC populations seeded within decellularized tissue bioscaffolds are discussed below. In all cases, it is important to note that the overall response of stem/progenitor cells to ECM-derived scaffolds *in vivo* will also be mediated by reciprocal signaling and action of host cells that infiltrate the scaffolds following implantation, including immune cells such as macrophages, and host-derived progenitors.

As previously discussed, MSC populations, including those derived from adipose tissue, secrete a variety of angiogenic, immunomodulatory, and cytoprotective factors, and these can play a central role in mediating tissue regeneration [126, 127]; however, few studies have systematically examined the impact of ECM-derived scaffolds on the stem/progenitor cell secretory profile. There is emerging evidence to suggest that ECM-derived scaffolds may help to provide a supportive microenvironment for stem/progenitor cell paracrine factor production. In support of this, the Flynn laboratory demonstrated in an immune-competent rat subcutaneous implantation model that seeding human DAT with allogeneic rat ASCs modulated the macrophage phenotype, increasing the relative fraction of infiltrating macrophages that expressed the pro-regenerative M2 macrophage marker CD163 [4]. The study also reported enhanced angiogenesis and host-derived

adipose tissue formation within the ASC-seeded bioscaffolds suggesting that the ASCs contributed to tissue regeneration through indirect paracrine mechanisms [4]. Moreover, using a rat bladder reconstruction model, Pokrywczynska *et al.* demonstrated differential cytokine production in the implant region of decellularized rat bladder matrix seeded with allogeneic bmMSCs as compared to unseeded implants or MSCs delivered alone [208]. The authors reported a qualitative increase in anti-inflammatory cytokine production observed by immunohistochemistry in parallel with improved tissue regeneration within the seeded versus unseeded scaffolds [208]. Other groups have demonstrated that seeding decellularized porcine SIS [209] or decellularized rat spinal cord [210] with allogeneic bmMSCs decreased macrophage and/or T cell infiltration in comparison to unseeded controls in a porcine epicardial patch model and rat spinal cord injury model, respectively.

In terms of angiogenic factor production, Nie *et al.* demonstrated that rat ASCs cultured on decellularized human dermal ECM sheets (AlloDerm<sup>®</sup>) secreted significant quantities of VEGF, HGF, TGF- $\beta$ , and basic fibroblast growth factor (bFGF) *in vitro* [211]. Using a diabetic rat excisional wound model, the same study reported increased CD31<sup>+</sup> blood vessel density and augmented protein levels of these angiogenic factors within seeded scaffolds as compared to unseeded controls. A number of other groups have also provided histological and immunohistochemical evidence that seeding decellularized scaffolds with MSCs improves neovascularization *in vivo* as compared to unseeded controls [4, 208, 212-215].

### 2.4.3 Mechanisms of stem/progenitor cell modulation by ECM-derived scaffolds

The compositional, biomechanical, and structural properties of the ECM are unique to a given tissue and each can play an integral role in mediating cell behaviour. Decellularized bioscaffolds can be designed to retain some of these properties and modulate the behaviour of stem/progenitor cells by re-capitulating properties of the native stem cell niche (summarized in Figure 2.2). However, it is important to recognize that it can be extremely challenging to decouple the individual effects of the compositional, biomechanical, and structural properties of the scaffold, as they are closely linked and the



scaffolds have innate heterogeneity. In addition, there is a dynamic interrelationship between the stem/progenitor cells and these engineered cellular microenvironments. Seeded or infiltrating regenerative cell populations will sense and respond to the ECM within the decellularized tissues, and in turn remodel the scaffolds via the action of MMP and ADAM family members, as well as through the synthesis of new matrix components [216]. The properties of the remodeled ECM may be extensively altered through these cell-ECM interactions, which can subsequently impact the downstream cellular response [162, 163].

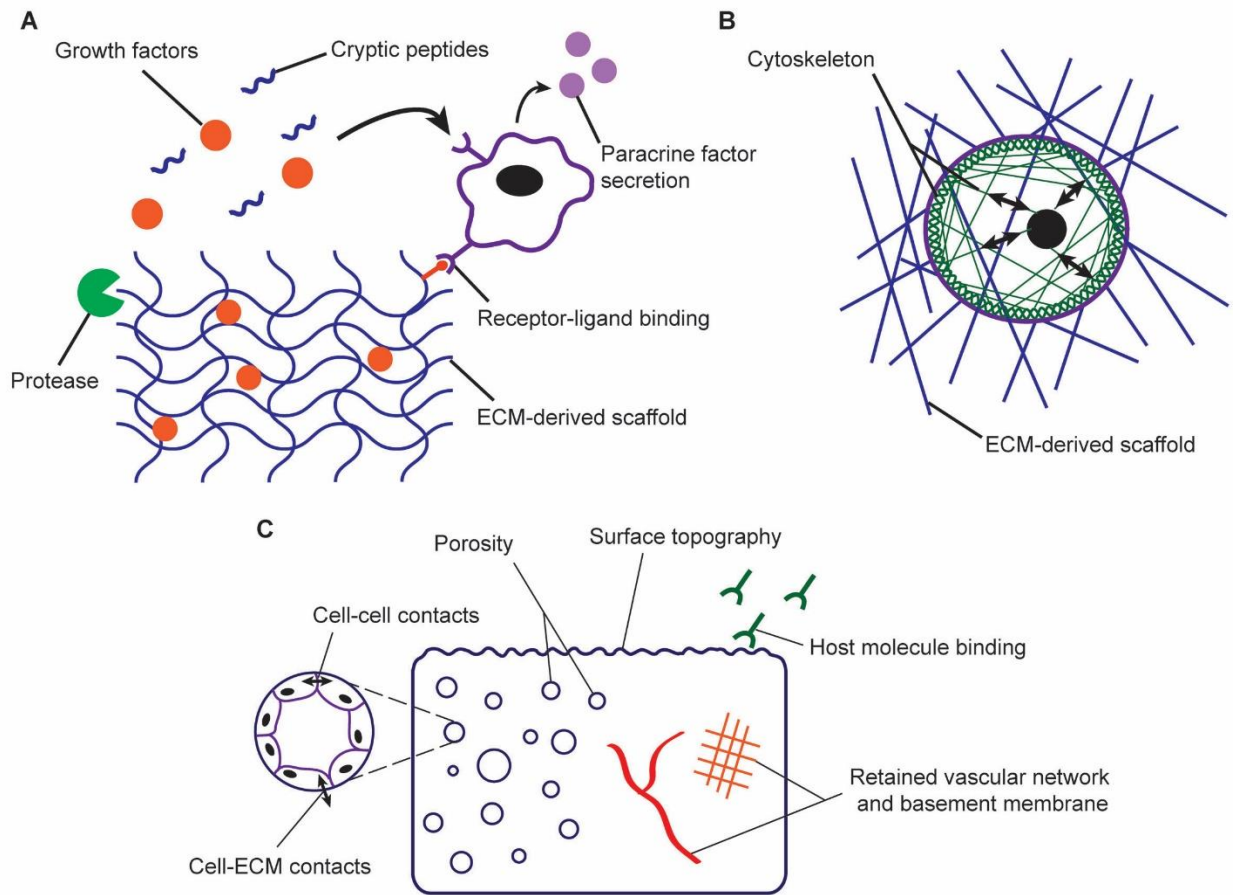


**Figure 2.2. Proposed mechanisms by which compositional, biomechanical, and structural properties of ECM-derived scaffolds direct stem/progenitor cell behaviour and responses.** A) Stem/progenitor cells may interact with the scaffold directly through receptor-ligand binding or indirectly through binding of growth factors and/or cryptic peptides released by proteases that degrade the ECM. These cell-ECM interactions may in turn influence paracrine factor secretion by the cells. B) Biomechanical properties of the scaffold influence mechanical forces transmitted via the cytoskeleton to alter cell responses through mechanotransduction pathways. C) Scaffold porosity governs the surface area available for cell-ECM contacts, as well as the degree of cell-cell contact. Surface topography and molecular functionality influence host cell and protein binding. Vascular networks and basement membranes may be conserved after decellularization, and may play a role in cellular organization.

Similar to the importance of ECM components in directing cellular processes within the native stem cell niche [217], during regeneration [218] and in pathological conditions [219], the complex ECM composition within decellularized scaffolds likely plays a key role in influencing stem/progenitor cell behaviour. Indeed, the retention of structural and functional proteins in decellularized tissues has been demonstrated by a number of research groups [220-223]. For example, a recent study from the Flynn laboratory employed mass spectrometry-based screening to compare the protein content of the DAT with human decellularized cancellous bone (DCB) [21]. Through the use of a novel processing method involving treatment of protein extracts with purified collagenase to deplete highly-abundant collagen and enable detection of lower abundance proteins, the study demonstrated that the DAT and DCB extracts were compositionally distinct, identifying 804 and 1210 proteins, respectively, in the collagenase-treated samples [21]. The DAT was shown to include a diverse range of non-structural bioactive ECM components and a variety of adipogenic proteins that were consistently more highly expressed in the DAT compared to the DCB [21].

While scaffold composition may influence stem/progenitor cell behaviour via direct binding of the cells to bioactive ECM components, another potential mechanism could involve the action of ECM degradation products, termed matrikines [224]. In native tissues, matrikines are generated through the proteolytic action of MMP and ADAM family members [216], and are known to recruit stem/progenitor cells, as well as modulate cell adhesion, migration and differentiation [225-227]. Examples of these “cryptic peptides” include the Arg-Gly-Asp (RGD) peptide derived from fibronectin and collagen, which promotes cell adhesion [216], as well as the hydrophobic sequences VGVPG and VGVAPG derived from elastin, which stimulate smooth muscle cell proliferation [228] and fibroblast, monocyte, and macrophage chemotaxis [229] respectively. Fragments of other ECM products such as hyaluronic acid generated during tissue injury and inflammation have been shown to stimulate angiogenesis and MMP production [216], as well as modulate macrophage phenotype [230]. Further, retained glycosaminoglycans (GAGs) within the decellularized tissues can bind and sequester soluble growth factors, regulating their availability and activity [231]; MMP degradation

of the ECM may trigger their release, allowing for dynamic regulation of stem/progenitor cell behaviour [217].

In addition to scaffold composition, the biomechanical properties of ECM-derived scaffolds can influence cell behaviour. The biomechanical properties of native ECM vary greatly across tissues [232] and are known to influence stem cell adhesion, proliferation, migration and differentiation [217, 233]. Cells are able to sense mechanical forces through cell adhesion complexes that can activate signaling cascades to influence cell behaviour [234]. For example, mechanotransduction through integrin binding to the ECM can activate downstream focal adhesion kinase (FAK) and phosphoinositide 3-kinase (PI3K) pathways, which regulate stem cell self-renewal [235, 236]. While the effects of ECM-derived scaffold biomechanical properties on stem/progenitor cell function have not been well-studied to date, previous work with synthetic hydrogel platforms suggests that mimicking the biomechanical properties of the native tissues may help to direct lineage specification. In 2D culture studies on collagen-containing polyacrylamide gels, human bmMSCs demonstrated enhanced expression of neurogenic markers on soft matrices simulating the stiffness of brain (0.1 – 1 kPa), myogenic markers on intermediate matrices simulating the stiffness of muscle (8 – 17 kPa), and osteogenic markers on the stiffest substrates studied (25 – 40 kPa) [237]. In further support of this, the pro-adipogenic properties of the DAT may be related to its biomechanical properties, as previous characterization studies from our laboratory have shown that DAT sourced from a range of human fat depots displayed elastic, hyperelastic, and deformation patterns similar to that of native breast adipose tissue [22, 23].

The molecular and three-dimensional architecture of decellularized scaffolds is likely another key mediator of stem/progenitor cell behaviour. Notably, Brown *et al.* showed that decellularized scaffolds derived from a variety of tissue types displayed distinct structural and morphological differences, demonstrating the tissue-specificity of these features [238]. Certain structural features, such as the basement membrane, which can be conserved following decellularization, have been shown to guide cell migration and growth patterns [239]. Other parameters such as scaffold porosity could impact the cellular response by facilitating nutrient and oxygen diffusion, as well as by modulating

cell-cell and cell-ECM interactions that can influence cell adhesion, migration, proliferation, and differentiation [240, 241]. In particular, cell density and shape are well-recognized mediators of stem cell lineage commitment [242], and may be important factors in modulating the response of stem/progenitor cells seeded on decellularized bioscaffolds. For example, in comparing the adipogenic differentiation of human ASCs in composite hydrogels incorporating DAT particles of varying sizes ( $278 \pm 3 \mu\text{m}$  vs.  $38 \pm 6 \mu\text{m}$ ), the Flynn laboratory showed that adipogenic differentiation was enhanced in the scaffolds containing small particles and a higher cell density, which was postulated to be due to enhanced cell-cell interactions in the ASCs clustered around the smaller particles [187].

## 2.5 Host response to biomaterials in tissue engineering

There has been growing interest in the role of the host response and specific immune cell populations in tissue engineering applications. Historically, the development of implanted biomaterials has focused on the use of “inert” materials to minimize the interaction of the material with host cell populations [243]. However, a major limitation of these materials is their tendency to promote fibrous encapsulation of the implant through excessive matrix deposition by fibroblasts, macrophages, and other cell types involved in the foreign body reaction [244]. For example, biologically inert titanium implants used in orthopedic and oral/maxillofacial surgeries can pose issues of fibrous encapsulation which can negatively impact the long-term stability of the implant and lead to peri-implant bone resorption [245, 246]. Recognizing the complex physiological response involved in tissue injury and healing, there has been a shift toward the design of bioactive materials that selectively interact with host immune cell populations in order to promote the integration and remodeling of these materials with the surrounding tissues.

### 2.5.1 Overview of the host response to biomaterials

The implantation of a biomaterial triggers a cascade of events involving a wide array of cell types and secreted factors. Adsorption of coagulation factors and complement proteins to the material begins immediately within seconds of implantation [247]. Coagulation factors include components of both the intrinsic and extrinsic coagulation

cascades, initiated by factor XII and tissue factor, respectively [248, 249]. Binding of these factors leads to downstream platelet activation and thrombin formation on the implant surface [249, 250]. At the same time, activation of the complement cascade occurs upon contact with the biomaterial via the classical, alternative, and lectin pathways [251, 252]. Together, the coagulation and complement systems interact with and regulate each other synergistically, leading to the recruitment and activation of inflammatory cells [253]. Moreover, endogenous danger signals known as alarmins are released by the nearby tissues that are inevitably damaged upon surgical implantation of the material [247, 254]. Alarmins include molecules such as adenosine triphosphate (ATP), uric acid, and fibrinogen, as well as cleaved ECM components such as collagen peptides, hyaluronic acid, and fibrinogen [254]. These factors interact with pattern recognition receptors that contribute to leukocyte recruitment and inflammation [254, 255]. Given that ECM proteins can directly mediate leukocyte binding via integrins [256], this represents another likely mechanism whereby immune cell recruitment occurs in ECM-derived scaffolds. In support of this, Uzarski *et al.* demonstrated the adhesion of platelets, leukocytes, and endothelial cells to decellularized human umbilical vein scaffolds *in vitro* with differential levels of adhesion to scaffolds prepared using four different decellularization protocols [257].

The combined events related to the coagulation and complement cascades and release of alarmins are followed by recruitment of circulating granulocytes including neutrophils and mast cells to the biomaterial implant [258]. In particular, neutrophils are central to the initial host response, functioning to phagocytose debris, produce cytotoxic reactive oxygen species, and release granules containing proteases and other factors [259].

Through a process termed NETosis, neutrophils are also known to release neutrophil extracellular traps (NETs), decondensed chromatin enriched in antimicrobial agents that act to trap and kill microbes while minimizing damage to host cells [260]. Neutrophils are thought to persist for very short time points less than three days following injury; longer durations are typically associated with an adverse immune response and increased severity of inflammation [261]. However, in mouse models, neutrophils have also been shown to persist for several weeks within models of tissue repair [262].

In addition, there is increasing evidence that neutrophil phenotypes can be adapted based on the microenvironment and that these cells can modulate the downstream response of macrophages, dendritic cells, and T cells [263]. For example, mouse neutrophils have been shown to produce IL-10, an anti-inflammatory cytokine associated with modulating macrophage phenotype and suppressing the pro-inflammatory functions of other immune cells [264, 265]; however, IL-10 production by human neutrophils is controversial [263, 266, 267]. Neutrophils have also been shown to be capable of suppressing T cell activation and proliferation through the production of hydrogen peroxide, arginase, and nitric oxide synthase 2 [268-270]. Little is known regarding which biomaterial characteristics may induce a favourable neutrophil response; however, this represents an active area of research due to increased recognition of their functional heterogeneity [271]. In addition to neutrophils, mast cells have been identified as another key granulocyte involved in the initial response to polymer-based biomaterials, with degranulation and histamine release linked to the foreign body reaction through recruitment of fibroblasts, macrophages, and other granulocytes in mice and humans [272-275].

Following the recruitment of granulocytes, other immune cells begin to infiltrate the biomaterial. Among these, macrophages are of predominant interest in tissue engineering due to their high degree of plasticity and their diverse roles at multiple stages of tissue repair (discussed in greater detail in the following section). T cells have also been shown to infiltrate ECM-derived scaffolds in animal models by a number of groups [209, 210, 276]. Wang *et al.* recently reported on the use of humanized mice to investigate the T cell response to subcutaneously injected hydrogels derived from porcine or human cadaveric decellularized myocardium [277]. The authors demonstrated that both the xenogeneic and allogeneic ECM elicited a shift from cytotoxic CD8<sup>+</sup> T cell infiltration on day 3 post-implantation, to predominantly CD4<sup>+</sup> T helper cells on day 7. While increased T cell recruitment was observed in the xenogeneic porcine ECM-derived scaffold, both materials promoted a shift toward a constructive pro-remodeling Th2 phenotype.

Other infiltrating immune cells include dendritic cells and myeloid-derived suppressor cells. These cells have not been well-studied with respect to the host response to

biomaterials, but are likely to play a role. Dendritic cells are antigen presenting cells that activate T cells and natural killer (NK) cells and display immunoregulatory functions by inducing T cell anergy, antigen-specific tolerance, as well as activation of regulatory T cells [278]. Naturally-derived biomaterials including alginate, chitosan, and agarose have been shown to induce differential effects on dendritic cell maturation and activation, with some studies reporting pro-inflammatory responses, and others demonstrating pro-tolerogenic effects [279, 280]. Myeloid-derived suppressor cells are a heterogeneous population of myeloid cells and are also known to act as potent suppressors of T cell activation [281]. The contribution of these cells in the context of tissue engineering has not been studied, but both are implicated as key players in the resolution of inflammation and subsequent tissue repair [282, 283].

## 2.5.2 Macrophage response to biomaterials and role in tissue engineering

Macrophages have recently gained considerable attention in the field of tissue engineering. Macrophages are phagocytic innate immune cells derived from a common myeloid progenitor (CMP) in the bone marrow [284]. Stimulation of CMPs through a cytokine cascade that includes granulocyte-macrophage colony stimulating factor (GM-CSF), granulocyte colony stimulating factor (G-CSF), and macrophage colony stimulating factor (M-CSF) leads to their eventual differentiation into monocytes which enter the circulation [284]. Circulating monocytes are a heterogeneous group of cells with at least three existing subset populations [285]. CD14<sup>hi</sup>CD16<sup>-</sup> monocytes in humans (Ly6c<sup>high</sup>Gr1<sup>+</sup> cells in mice) are considered “classical inflammatory monocytes” that rapidly migrate to tissues upon injury or infection in response to receptor/ligand interactions involving C-C chemokine receptor (CCR)-2 on monocytes and the chemokine CCL2 [285]. In contrast, CD14<sup>+</sup>CD16<sup>+</sup> monocytes in humans (Ly6c<sup>low</sup>Gr1<sup>-</sup> in mice) are “nonclassical monocytes”; these cells lack CCR2 expression and function to patrol the vasculature and clear damaged endothelial cells [285]. Humans also have a third subset of monocytes, the intermediate subset defined as CD14<sup>-/low</sup>CD16<sup>+</sup> that are also involved in inflammatory responses [285]. It is unclear whether there is an equivalent subset in mice [285].



Upon extravasation into tissues, monocytes differentiate into macrophages [284]. These cells display distinct phenotypic profiles based on the tissue type and surrounding microenvironment. Macrophage phenotypes have been broadly classified along a spectrum that includes M1-polarized classically-activated macrophages, and M2-polarized alternatively-activated macrophages [134]. These definitions are largely based on *in vitro* studies and they continue to evolve with further investigation into the roles and function of these cells *in vivo* [286]. Nonetheless, the M1/M2 classification system represents a useful construct for discussing the diversity of macrophage functions *in vivo*. In general, M1-polarized macrophages can be induced by IFN $\gamma$ , lipopolysaccharide, and TNF $\alpha$ , and are considered pro-inflammatory cells that secrete reactive oxygen species and cytokines that include IL-1 $\beta$ , IL-6, and TNF $\alpha$  [134]. In contrast, M2-polarized macrophages are induced by IL-4, IL-10, and IL-13, as well as glucocorticoids, and are associated with the resolution of inflammation, as well as tissue repair [134]. M2 macrophages have been further categorized into M2a, M2b, and M2c subtypes based on their stimuli for differentiation and molecular marker expression profiles [287, 288]. Each of these subtypes are associated with immunoregulatory functions through secretion of IL-10 and other subtype-specific cytokines, and may be present in varying numbers based on the time course of tissue repair, and the interstitial cytokine milieu [287]. For example, M2c macrophages are induced by IL-10 and glucocorticoids, and express the receptors CD163 and CD206 [287, 289]. This subpopulation is involved in matrix deposition and tissue remodeling through MMP secretion, as well as regulating inflammation through IL-10 and TGF- $\beta$  secretion [287, 289]. The plasticity of macrophages has been demonstrated *in vitro* through experiments in which M1- or M2-polarized macrophages have been induced to express markers of the opposing phenotype [290, 291]. However, whether or not macrophages display similar phenotypic changes *in vivo* is controversial, with some studies supporting this concept [292-294], while others suggest that the macrophage subsets arise from different populations of infiltrating monocytes [295-297].

Within the context of tissue repair, both M1 and M2 macrophages are thought to play an integral role at multiple stages of healing. In cutaneous wound healing, initial infiltration

of M1-like macrophages is thought to be important for clearance of pathogens and debris, followed by a shift toward M2 macrophages that regulate the inflammatory response and promote tissue formation and remodeling [286, 298, 299]. Involvement of both M1 and M2 cells is thought to be crucial; for example, in the process of angiogenesis, M1 macrophages have been shown to initiate vessel sprouting, while M2 macrophages mediated vascular remodeling, anastomosis, and recruitment of pericytes [300].

In tissue engineering, the macrophage response to biomaterials is central to the regenerative process. As mentioned, a major issue that has been encountered in the use of synthetic implants is the tendency for the material to become encapsulated in an almost avascular sheath of connective tissue [301]. Macrophages are implicated in this foreign body response through a process known as “frustrated phagocytosis”, in which the inability of the macrophages to phagocytose the material due to limited biodegradability and size restrictions leads to cell fusion and formation of multinucleate bodies along the implant periphery [301]. In contrast, the response to ECM-derived scaffolds is markedly different, allowing for cell infiltration and interaction with bioactive ECM components. Similar to the native repair process, several groups have indicated through *in vivo* studies that ECM-derived scaffolds promote a shift from the expression of M1 macrophage markers at early time points, to expression of M2 markers over time [302-304]. Indeed, Brown *et al.* have shown through the comparison of 14 ECM-derived surgical mesh materials implanted in the rat abdominal wall that increased numbers of M2-like macrophages and a higher ratio of M2:M1 macrophage markers at 14 days post-implantation served as a statistical predictor of constructive tissue remodeling assessed by histomorphometry at 14 and 35 days post-implantation [305]. A possible mechanism through which decellularized scaffolds may modulate the immune response could involve ECM degradation products, as treatment of bone marrow-derived mouse macrophages with pepsin-digested porcine decellularized SIS promoted an M2 macrophage phenotype [306]. A recent study by Londono *et al.* pointed to the influence of incomplete decellularization on macrophage phenotype demonstrating that collagen scaffolds supplemented with varying concentrations of DNA, mitochondria, or cell membrane remnants stimulated expression of M1 macrophage markers in a dose-dependent manner

after implantation in an abdominal wall defect rat model [307], emphasizing the importance of careful characterization of decellularized scaffolds.

## 2.6 Summary

Adipose-derived stem/stromal cells have been investigated as a regenerative cell source capable of multilineage differentiation *in vitro*, as well as the secretion of beneficial paracrine factors that may aid in tissue repair. Recognizing the importance of delivery strategies in cell-based therapies, decellularized scaffolds have been shown to retain properties of the native ECM and can instruct cell behaviour to guide tissue regeneration. With this in mind, the Flynn laboratory is developing DAT scaffolds as a pro-adipogenic cell delivery platform for ASCs in adipose tissue engineering applications [4]. However, further investigation of the ASC-mediated regenerative mechanisms would be beneficial for the development of clinically-translational approaches to enable stable and predictable adipose tissue regeneration. In particular, the host response is crucial to tissue repair, and increasingly, studies have demonstrated that macrophages play a central role in this process. Further, ASCs have been demonstrated to have the capacity to modulate the macrophage response to implanted biomaterials and may help to promote constructive tissue remodeling. Therefore, the objective of the current study was to examine donor ASCs and infiltrating myeloid cells within ASC-seeded and unseeded DAT scaffolds using transgenic mouse models to facilitate tracking and characterization of these cell populations.

## Chapter 3

### 3 Materials and Methods

#### 3.1 Materials

Chemicals and reagents were purchased from Sigma Aldrich (Oakville, ON) unless otherwise stated.

#### 3.2 Animals

All animal studies were performed in accordance with the Canadian Council on Animal Care (CCAC) guidelines and were approved by the Animal Care Committee at Western University (Protocol # 2015-049; Appendix 2). Mice were housed in clean barrier facilities under humidity- and light-controlled conditions, and fed *ad libitum* with free access to water. Murine adipose-derived stem/stromal cells (ASCs) were obtained from 8-12 week old male dsRed mice (B6.Cg-Tg(CAG-DsRed\*MST)1Nagy/J; C57BL/6J background; Jackson Laboratory, Bar Harbor, ME). Scaffold implantation studies were performed using a total of thirty hemizygous 8-12 week old female MacGreen transgenic mice (B6N.Cg-Tg(Csf1r-EGFP)1Hume/J; C57BL/6J background; Jackson Laboratory, Bar Harbor, ME).

#### 3.3 ASC isolation and culture

ASCs were isolated from the inguinal fat pads of dsRed mice according to previously published methods [308]. Briefly, fat pads from 4-7 mice were minced with sharp surgical scissors and added to 15 mL of collagenase digest solution consisting of 0.1% Type I Collagenase (Worthington Biochemical Corp., Lakewood, NJ), 1% bovine serum albumin (BSA), and 2 mM calcium chloride in cation-free phosphate-buffered saline (PBS). The tissue suspension was agitated (75 rpm) at 37°C for 1 hour and then centrifuged at 300 x g for 5 min to obtain the stromal vascular fraction. The cell pellet was then re-suspended in PBS + 1% BSA and passed through a 100 µm filter (Corning Inc., Corning, NY). The cells were centrifuged again (300 x g for 5 min) and re-suspended in proliferation medium composed of Dulbecco's Modified Eagle's

Medium:Ham's F12 (DMEM:Ham's F12) with 10% fetal bovine serum (FBS; Gibco<sup>®</sup>, Invitrogen, Burlington, ON) and 1% penicillin-streptomycin (pen-strep; Gibco<sup>®</sup>, Invitrogen, Burlington, ON) prior to plating on Primaria<sup>™</sup> flasks (Corning Inc., Corning, NY). After 24 h incubation (37°C, 5% CO<sub>2</sub>), the flasks were rinsed with sterile PBS to remove cellular debris and unattached cells, and the proliferation medium was then replaced. The cells were passaged at confluence using 0.25% trypsin/0.1% ethylenediaminetetraacetic acid (trypsin/EDTA; Gibco<sup>®</sup>, Invitrogen, Burlington, ON) and re-plated at 6,000-7,000 cells/cm<sup>2</sup> on standard tissue culture polystyrene flasks (Corning Inc., Corning, NY) beyond passage zero (P0). Media changes were performed every 2-3 days and P3 cells were used in all studies.

## 3.4 ASC characterization

### 3.4.1 Immunophenotyping

Flow cytometry was performed in conjunction with Mrs. Christy Barreira (Research Assistant, Dekaban laboratory), and Dr. Laura Juignet (Post-doctoral Fellow, Flynn laboratory). P3 dsRed<sup>+</sup> murine ASCs were incubated with 5 mL of 0.48 mM Versene Solution (Gibco<sup>®</sup>, Invitrogen, Burlington, ON) for 10 min at 37°C to detach the cells, followed by addition of 5 mL of complete media and centrifugation (1200 x g, 5 min). The cell pellet was re-suspended in PBS supplemented with 5% FBS, and hemocytometer counts with trypan blue-stained cell suspensions were performed to aliquot 250,000 cells each in 5 mL polystyrene round-bottom tubes (Falcon<sup>®</sup>, Corning, NY). After centrifugation (450 x g, 7 min), the cell pellets were re-suspended in 250 µL of PBS containing the LIVE/DEAD<sup>™</sup> Fixable Aqua Dead Cell Stain (Fisher Scientific, Ottawa, ON) prepared according to the manufacturer's instructions. After 30 min of incubation in the dark at room temperature, cells were pelleted (450 x g, 7 min) and re-suspended in 100 µL of PBS + 5% FBS and the following monoclonal APC-conjugated antibodies from eBioscience (Ottawa, ON) were added to separate tubes: anti-CD29 (1 µg/mL; cat. 17-0291), anti-CD31 (2 µg/mL; cat. 17-0311), anti-CD44 (0.24 µg/mL; cat. 17-0441), anti-CD45 (0.5 µg/mL; cat. 17-0451), and anti-CD90.2 (0.24 µg/mL; cat. 17-0902). The cells were then incubated for 25 min at 4°C in the dark and centrifuged at 450 x g for 7 min). An additional wash step was performed in PBS, and the cells were then re-

suspended in 200  $\mu\text{L}$  of PBS + 5% FBS. The stained cells were fixed through the addition of 100  $\mu\text{L}$  of PBS + 0.5% paraformaldehyde, and stored at 4°C in the dark. Flow cytometry was performed within 24 h of staining using an LSRII analytical cytometer (Becton Dickinson) at the London Regional Flow Cytometry Facility. Live singlets were gated on the basis of the forward and side scatter properties, with further gating performed using fluorescence minus one (FMO) controls, including wild-type (dsRed<sup>-</sup>) P3 murine ASCs isolated from non-transgenic 8-12 week old male C57BL/6J mice that were cultured in parallel to the dsRed<sup>+</sup> cells. Data analysis was performed using FlowJo software (version 10.0.8; Tree Star, Ashland, OR).

### 3.4.2 Adipogenic differentiation

ASCs were plated at 50,000 cells/cm<sup>2</sup> on 12-well TPP<sup>®</sup> plates and incubated in proliferation media for 24 h. The cells were then induced to differentiate using an adipogenic differentiation medium (Table 3.1) adapted from the literature [308]. Media was changed every 2-3 days and adipogenic differentiation was characterized through oil red O staining and measurement of glycerol-3-phosphate dehydrogenase (GPDH) enzyme activity at 14 days in comparison to non-induced controls maintained in proliferation medium.

**Table 3.1. Summary of differentiation media formulations.** All formulations were prepared in DMEM:Ham’s F12 with 10% FBS and 1% pen-strep. IBMX: 3-isobutyl-1-methylxanthine, TGF- $\beta$ 1: transforming growth factor beta-1.

<b>Adipogenic differentiation media [308]</b>	<b>Osteogenic differentiation media [105]</b>	<b>Chondrogenic differentiation media</b>
10 mg/mL troglitazone*	345 $\mu\text{M}$ ascorbic acid	50 $\mu\text{g}/\text{mL}$ ascorbic acid
0.25 mM IBMX*	10 mM $\beta$ -glycerol phosphate	100 nM dexamethasone
33 $\mu\text{M}$ biotin	1 $\mu\text{M}$ retinoic acid	6.25 $\mu\text{g}/\text{mL}$ TGF- $\beta$ 1 (R&D Systems, cat. 100-B-001)
17 $\mu\text{M}$ D-pantothenic acid		
10 mg/mL human insulin		
1 $\mu\text{M}$ dexamethasone		

\*Included only for the first 72 h of differentiation

### 3.4.2.1 Oil red O staining

Oil red O histological staining was performed as previously described [184] to visualize intracellular lipid accumulation. Following 30 min fixation at room temperature in 10% neutral buffered formalin, the cells were rinsed three times with deionized water and incubated in oil red O working solution (3 parts oil red O stock consisting of 3 g/L oil red O in 99.9% isopropanol to 2 parts deionized water) for 8 min under gentle agitation. Cells were then rinsed with deionized water to remove excess stain, and counterstained with hematoxylin for 2 min. Staining was performed in technical triplicates for each trial and the experiment was repeated for a total of 4 biological replicates (n=3 induced, 3 non-induced technical replicates, N=4 experiments from separate ASC isolations). The samples were imaged using the EVOS<sup>®</sup> XL Core imaging system (Fisher Scientific, Ottawa, ON).

In order to semi-quantitatively analyze the levels of intracellular lipid accumulation in the oil red O-stained samples, dye elution was performed after imaging the samples, followed by spectrophotometric analysis of the extracted dye (n=3, N=3). After thorough rinsing of the plates with deionized water to remove non-specific background, 350  $\mu$ L of absolute isopropanol was added to each well and incubated for 15 min under gentle agitation at room temperature. Following this, 100  $\mu$ L of the supernatant was then transferred from each replicate sample into triplicate wells of a 96-well plate. Absorbance was read at 492 nm using a CLARIOstar<sup>®</sup> spectrophotometer (BMG LabTech, Ortenberg, Germany). Wells with isopropanol alone were included to measure the background absorbance levels. The average absorbance was calculated for each sample, with the background subtracted.

### 3.4.2.2 GPDH Enzyme Activity

Quantitative assessment of adipogenic differentiation was performed by measuring the activity of the lipid biosynthetic enzyme GPDH (N=4, n=3), following previously described protocols [184]. A commercially available spectrophotometric assay (cat. KT-010; Kamiya Biomedical Company, Seattle, WA) was used to measure intracellular GPDH activity with levels normalized to total cytosolic protein using the Bio-Rad protein

assay (Bio-Rad Laboratories Inc., Hercules, CA) with an albumin standard. All samples were measured at an absorbance of 340 nm using a CLARIOstar® spectrophotometer (BMG LabTech, Ortenberg, Germany). One unit of GPDH activity was defined as the activity required to oxidize 1  $\mu$ mole of NADH in 1 minute.

### 3.4.3 Osteogenic differentiation

For osteogenic differentiation, ASCs were plated at 15,000 cells/cm<sup>2</sup> in 12-well plates pre-coated with laminin (cat. L2020, 1.6  $\mu$ g/cm<sup>2</sup>) and incubated in proliferation medium for 24 h. Differentiation was induced using osteogenic medium (Table 3.1) [105], with media changes performed every 2-3 days. Osteogenic differentiation was assessed via von Kossa staining of matrix mineralization, as well as assessment of alkaline phosphatase (ALP) enzyme activity in comparison to non-induced controls maintained in proliferation medium.

#### 3.4.3.1 Von Kossa staining

Matrix mineralization was visualized after 28 days of differentiation by von Kossa staining as described previously (n=2-3, N=3) [309]. The cells were fixed in 10% neutral buffered formalin for 30 min and rinsed with deionized water. Following this, the plates were incubated in 1% silver nitrate solution under ultraviolet light for 90 minutes. After rinsing, 5% sodium thiosulfate solution was added to the wells and incubated for 2 min. Counterstaining with hematoxylin was performed for 2 min, and the plates were imaged using the EVOS® XL Core imaging system (Fisher Scientific, Ottawa, ON).

#### 3.4.3.2 ALP enzyme activity

After 7 days of culture in differentiation media, measurement of ALP enzyme activity was performed as previously described (n=3, N=4) [309]. Extraction of intracellular protein was performed by sonicating the cells in enzyme extraction buffer (5 mM tris, 20 mM tricine, 1 mM EDTA, pH 7.4), followed by centrifugation (13,000 x g, 10 min) and collection of the cell supernatant. Next, 100  $\mu$ L of the extracted sample was incubated with an equal volume of *p*-nitrophenyl liquid substrate (cat. N7653) in a 96-well plate for 30 min at 37°C. The reaction was then quenched with 100  $\mu$ L of 3 N NaOH and the



absorbance was measured at 405 nm using a CLARIOstar<sup>®</sup> spectrophotometer (BMG LabTech, Ortenberg, Germany). Absorbance values were referenced to a *p*-nitrophenol standard curve, with normalization to total intracellular protein using the Bio-Rad protein assay (Bio-Rad Laboratories Inc., Hercules, CA) with an albumin standard. One unit of ALP activity was defined as the amount of enzyme required to catalyze the production of 1  $\mu$ mole of *p*-nitrophenol per minute.

### 3.4.4 Chondrogenic differentiation

ASC chondrogenic differentiation was induced in 3D cell aggregate cultures based on methods previously described [183]. In brief, 1 mL of proliferation medium containing 250,000 ASCs was transferred into a 15 mL vented cap conical tube and centrifuged at 300 x g for 5 min. ASCs were cultured in proliferation medium for 3 days to allow the cells to self-assemble into 3D aggregates. The medium was then replaced with chondrogenic medium (Table 3.1), with half media changes performed every second day. On day 28, the cell pellets were rinsed in PBS and frozen on dry ice in Tissue-Tek<sup>®</sup> O.C.T.<sup>™</sup> Compound (Sakura<sup>®</sup> Finetek, Torrance, CA). Differentiation was qualitatively assessed by immunohistochemical staining for collagen I and II relative to non-induced controls maintained in proliferation medium (n=3, N=3).

#### 3.4.4.1 Immunohistochemical staining for collagen I and II

The cell aggregates were cryosectioned (5-7  $\mu$ m) and stored at -80°C. Prior to staining, the sections were washed with PBS, followed by blocking for 1 h at room temperature in PBS containing 10% goat serum and 0.2% Tween-20. The sections were then incubated with primary antibodies to collagen I (1:200 dilution; cat. ab34710; Abcam, Toronto, ON) or collagen II (1:200 dilution; cat. ab34712; Abcam, Toronto, ON) overnight at 4°C. After washing with PBS, a goat anti-rabbit secondary antibody (1:500; cat. ab96902; Abcam, Toronto, ON) was then applied to the tissue sections for 1 h at room temperature. The sections were then washed, followed by mounting using DAPI mounting medium (Abcam, Toronto, ON) and imaging with the EVOS<sup>®</sup> FL Imaging System. Tissue-positive porcine auricular cartilage samples and no primary controls were used to confirm staining specificity.

## 3.5 DAT scaffold fabrication and seeding

### 3.5.1 Adipose tissue procurement and decellularization

Subcutaneous human adipose tissue was obtained with informed consent from elective breast reduction or abdominoplasty surgeries at Cumberland Laser Clinic, St. Joseph's Hospital, or University Hospital in London, Ontario with approval from the Research Ethics Board at Western University (HREB# 105426; Appendix 2). The tissues were transported to the lab on ice in sterile PBS supplemented with 20 mg/mL BSA, and processed within 2 hours of excision. Cauterized tissue was removed and the remaining sample was transferred into hypotonic 10 mM Tris-EDTA buffer (pH 8.0), and frozen at -80°C. Tissue decellularization was performed using an established 5-day detergent-free protocol [5]. A working volume of 100 mL solution/50 g of tissue was used for all decellularization solutions. The solutions were supplemented with 1% (v/v) antibiotic-antimycotic (ABAM; Gibco®, Invitrogen, Burlington, ON) and 0.27 mM phenylmethylsulfonyl fluoride (PMSF), with the exception of steps including 0.25% trypsin/0.1% EDTA where PMSF was excluded. All incubations were performed at 37°C under constant agitation at 120 rpm.

In brief, the adipose tissue samples were thawed at 37°C under agitation, and the tissue was placed in fresh 10 mM Tris-EDTA buffer. The samples were then frozen at -80°C and this processing step was repeated for a total of three freeze-thaw cycles. After the final freeze-thaw, the tissue was subjected to enzymatic digestion in 0.25% trypsin/0.1% EDTA (Gibco®, Invitrogen, Burlington, ON) overnight. Polar solvent extraction was then performed by transferring the samples into absolute isopropanol for a total of 48 h, with gentle mechanical manipulation and solution changes to promote lipid extraction every 8 h. The samples were then rinsed three times (30 min each) in Sorenson's phosphate buffer (SPB) rinsing solution (8 g/L NaCl, 200 mg/L KCl, 1 g/L Na<sub>2</sub>HPO<sub>4</sub>, and 200 mg/L KH<sub>2</sub>PO<sub>4</sub>, at pH 8.0), and incubated in 0.25% trypsin/0.1% EDTA for 6 h. Following three additional 30 min washes in SPB rinsing solution, the samples were transferred to a second enzymatic digestion solution (55 mM Na<sub>2</sub>HPO<sub>4</sub>, and 17 mM KH<sub>2</sub>PO<sub>4</sub>, 4.9 mM MgSO<sub>4</sub>·7H<sub>2</sub>O) containing 15,000 U DNase Type II (from bovine pancreas), 12 mg RNase Type III A (from bovine pancreas), and 2000 U lipase Type VI-S (from porcine

pancreas). Three 30 min washes were then performed in SPB rinsing solution prior to incubation in absolute isopropanol for 8 h, followed by an additional three 30 min rinses in the same rinsing solution. The decellularized adipose tissue (DAT) was then frozen at -80°C and lyophilized.

### 3.5.2 Scaffold preparation and seeding

Lyophilized DAT was cut into ( $7.0 \pm 0.5$ ) mg scaffolds and re-hydrated in deionized water overnight. Three 30 min washes in 70% ethanol were performed, followed by overnight incubation in 70% ethanol to decontaminate the scaffolds. The scaffolds were then transferred under aseptic conditions into sterile PBS and incubated for 3 h at room temperature, followed by an additional two 30 min rinses in fresh sterile PBS. The PBS was then replaced with ASC proliferation medium (89% DMEM:Ham's F12, 10% FBS, 1% pen-strep) and the scaffolds were incubated overnight at 37 °C and 5% CO<sub>2</sub>.

Prior to scaffold seeding, P2 ASCs were trypsinized and counted using a hemocytometer. Each DAT scaffold was transferred into a 15 mL vented cap conical tube containing 3 mL of proliferation medium and  $2 \times 10^6$  ASCs. The scaffolds were dynamically seeded for 24 h using a BenchWaver<sup>TM</sup> 3D rocker (Mandel, Guelph, ON) at 90 rpm (37 °C, 5% CO<sub>2</sub>).

For the initial seeding pilot studies, three different seeding densities were examined:  $0.5 \times 10^6$  ASCs/scaffold,  $1.0 \times 10^6$  ASCs/scaffold, and  $2.0 \times 10^6$  ASCs/scaffold (n=3 technical replicates; N=2 experiments with separate batches of isolated ASCs). After 24 h of seeding, the scaffolds were frozen over dry ice in Tissue-Tek<sup>®</sup> O.C.T.<sup>T.M.</sup> Compound (Sakura<sup>®</sup> Finetek, Torrance, CA). The scaffolds were then stored at -80°C for subsequent sectioning (5-7 µm sections) and mounting with DAPI mounting medium (Abcam, Toronto, ON) in order to visualize cells. Images were taken using the EVOS<sup>®</sup> FL Imaging System (Invitrogen, Ottawa, ON). All subsequent studies were performed using a seeding density of  $2 \times 10^6$  ASCs/scaffold.

### 3.6 Scaffold implantation, tissue harvest, and Masson's trichrome staining

As stated previously, implantation studies were performed using 8-12 week old female MacGreen transgenic mice. All surgeries were performed under sterile conditions using sterile surgical tools. Animals were anesthetized with 1.5% isoflurane in oxygen at 1 L/min throughout the surgical procedure, and administered subcutaneous injections of meloxicam (2 mg/kg loading dose; 1 mg/kg follow up dose at 24 h) as an analgesic, as well as bupivacaine (2 mg/kg) as a local anaesthetic. Two small incisions (~1 cm) were made on the dorsa of each mouse below each scapula, and subcutaneous pockets were created below the panniculus carnosus using blunt-ended forceps. One ASC-seeded and one unseeded DAT scaffold were placed into the separate pockets created in each mouse and the incisions were closed using 11 mm Michel wound clips (Fig. 3.1A).

At time points of 72 h, 1, 3, 5, and 8 weeks post-implantation, cohorts (n=6 mice per time point) were euthanized by isoflurane overdose and the scaffolds were excised within their surrounding tissues (Fig. 3.1B). The excised scaffolds were bisected using a scalpel and half of each implant was fixed in 10% neutral buffered formalin for 24 h prior to being transferred to 70% ethanol for paraffin-embedding. The remaining half of each scaffold was frozen over dry ice in Tissue-Tek<sup>®</sup> O.C.T.<sup>T.M.</sup> Compound (Sakura<sup>®</sup> Finetek, Torrance, CA) for immunohistochemical analysis.

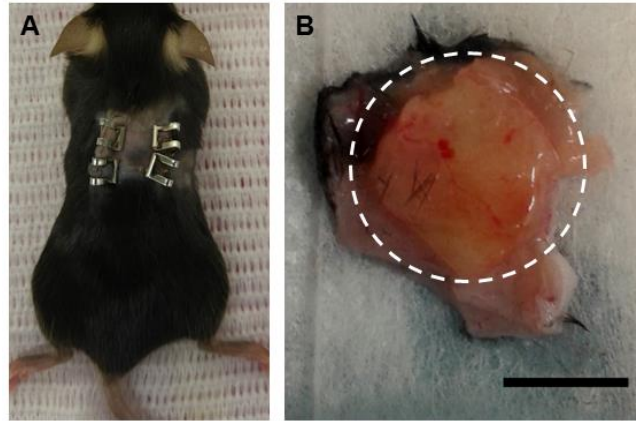


**Figure 3.1. Scaffold implantation and excision.** A) Each mouse was implanted with one seeded and one unseeded scaffold inserted into separate subcutaneous pockets on the dorsa below each scapula. Incisions were closed with surgical staples. B) The basal surface of an excised DAT scaffold. Dotted line delineates scaffold region; scale bar: 0.5 cm.

### 3.6.1 Masson's trichrome staining

Sections of 5-8  $\mu\text{m}$  thickness from paraffin-embedded tissues were deparaffinized in xylene, and rehydrated in a graded ethanol series prior to Masson's trichrome staining. The tissue sections were then dehydrated in a graded ethanol series and mounted with Permount® (Fisher Scientific, Ottawa, ON). Slides were scanned at 20X magnification using an Aperio ImageScope system and software (Vista, CA). The fraction of the implants infiltrated by cells or remodeled into adipose tissue was quantified relative to the total implant area using the Spectrum ImageScope software.

### 3.7 Immunohistochemical detection of dsRed<sup>+</sup> donor cells

For dsRed staining, 5  $\mu\text{m}$  sections from paraffin-embedded tissues were deparaffinized and re-hydrated in a graded ethanol series, followed by heat-mediated antigen retrieval in citrate solution (pH 6.0) at 95°C for 30 min. This was followed by blocking (10% goat serum + 0.1% Tween-20 in Tris-buffered saline (TBS)) for 1 h at room temperature. The tissue sections were then incubated overnight at 4°C with a rabbit polyclonal anti-RFP primary antibody (1:200 in TBS + 5% goat serum + 0.1 % Tween-20, cat. 600-401-379;

Rockland Immunochemicals, Limerick, PA). Following this, the tissue sections were washed in TBS, and endogenous peroxidases were quenched in 3% H<sub>2</sub>O<sub>2</sub> for 15 min at room temperature. After applying a goat anti-rabbit HRP-conjugated secondary antibody (1:300 in TBS, Abcam cat. Ab6721), sections were washed in TBS and incubated with 3,3'-diaminobenzidine (DAB) for 5 min at room temperature followed by counter-staining with Harris hematoxylin and lithium carbonate, dehydration in a graded ethanol series, and mounting with Permount<sup>®</sup> (Fisher Scientific, Ottawa, ON). Slides were scanned at 20X magnification using an Aperio ImageScope system and software (Vista, CA), and quantitative analysis of positively stained pixels was performed using the Fiji software [310]. DAT scaffolds implanted into dsRed<sup>+</sup> mice and wild-type mice were used as positive and negative controls respectively, along with no primary controls to confirm staining specificity.

### 3.8 *In vivo* optical imaging

Optical imaging studies were performed in collaboration with Dr. John Ronald (Department of Medical Biophysics, Western University) with technical assistance from Ms. Katie Parkins (PhD Candidate, Ronald laboratory) using the IVIS<sup>®</sup> Lumina XRMS *In Vivo* imaging system (PerkinElmer, Waltham, MA). In an initial pilot study, DAT scaffolds were seeded with dsRed<sup>+</sup> donor ASCs or EGFP<sup>+</sup> macrophages derived from MacGreen mice isolated and cultured by Mr. Hisham Kamoun (MESc Candidate, Flynn lab). Scaffolds were seeded using the methods outlined in Section 3.5.2; for ASC-seeding, densities of 0.5 x 10<sup>6</sup> ASCs/scaffold, 1.0 x 10<sup>6</sup> ASCs/scaffold, and 2.0 x 10<sup>6</sup> ASCs/scaffold were used, and for macrophage-seeding, densities of 0.25 x 10<sup>6</sup> ASCs/scaffold, 0.5 x 10<sup>6</sup> ASCs/scaffold, and 1.0 x 10<sup>6</sup> ASCs/scaffold were used, with unseeded controls included to assess levels of autofluorescence in the DAT (n=3 technical replicates/seeding density). These seeding densities were selected based on previously noted differences between these cell populations in terms of cell attachment to the DAT scaffolds. The total radiant efficiency for either dsRed or EGFP fluorescence was measured within the different seeded scaffolds using region-of-interest (ROI) analysis in the Living Image<sup>®</sup> 4.5.2 Software (PerkinElmer, Waltham, MA).

Subsequent *in vivo* studies were performed to track dsRed<sup>+</sup> donor ASCs within the implants in living mice. A longitudinal study was performed with eight mice (N=8) imaged at a baseline of 24 h pre-implantation, as well as at 24 h, 1, 3, 5, and 8 weeks post-implantation. At 24 h prior to each imaging time point, the hair on the dorsal region in the implant area was removed with shaving and Nair<sup>TM</sup> hair removal cream. At all time points, the mice were anesthetized using 2% isoflurane in oxygen at 1 L/min and the lateral surface of each animal was imaged. The total radiant efficiency was measured within the region of the implanted scaffolds using ROI analysis in the same software described above. At some time points, darkening of the skin within the implant region was noted, due to changes in the hair growth cycle over time. This appeared to greatly interfere with signaling acquisition for some mice, and as a result, these mice were excluded such that data from 3-8 mice was collected at each of the time points.

### 3.9 Immunohistochemical assessment of macrophage infiltration and macrophage phenotypic markers

To examine infiltrating macrophages, immunohistochemical staining was performed using the specifications outlined in Table 3.1. Co-staining was performed for the following combinations of markers: EGFP with Iba1, EGFP with arginase-1 (Arg-1), and EGFP with inducible nitric oxide synthase (iNOS). Five micron sections from fresh-frozen tissues were fixed in acetone at -20°C for 10 min. After washing in TBS, the sections were blocked for 1 h at room temperature. The primary antibody for Iba1, iNOS, or Arg-1 was then applied at a dilution of 1:100 in the blocking solution and incubated overnight at 4°C. The tissue sections were then washed in TBS and the secondary antibody was applied at a dilution of 1:500 in TBS for 30 min at room temperature. EGFP staining was then performed using the same procedures, but with no secondary antibody required since the primary antibody used was directly conjugated to the Alexa Fluor 647 fluorophore. After the EGFP antibody incubation, the tissue sections were washed and stained with Hoescht (Fisher Scientific, Ottawa, ON) followed by mounting with Fluoroshield<sup>TM</sup> Mounting Medium (Abcam, Toronto, ON). For EGFP/Iba1 co-staining, blinded quantitative analysis was performed in ImageJ through manual counting of DAPI<sup>+</sup> cells positive for both markers and cells positive only for EGFP. Average

counts from 5-6 20X images taken along the implant periphery (2-3 along the basal border, 2-3 along the apical border) were recorded for each section. EGFP/iNOS and EGFP/Arginase-1 co-staining was performed on adjacent sections and assessed qualitatively. All images were taken at 20X magnification with the EVOS® FL Imaging System (Invitrogen, Ottawa, ON). Tissue-positive mouse spleen controls and no primary controls were used to confirm staining specificity for each of these markers.

**Table 3.2. Specifications for immunohistochemistry protocols.**

	<b>EGFP</b>	<b>Iba1</b>	<b>iNOS</b>	<b>Arg-1</b>
Blocking solution	TBS + 10% rabbit serum + 0.1% tween-20	TBS + 10% goat serum + 0.1% tween-20	TBS + 5% BSA + 0.1% tween-20	TBS + 5% BSA + 0.1% tween-20
Primary antibody	Rabbit polyclonal, Alexa 647 (cat. A-31852 <sup>a</sup> )	Rabbit monoclonal (cat. ab178846 <sup>b</sup> )	Rabbit polyclonal (cat. ab15323 <sup>b</sup> )	Chicken polyclonal (cat. ABS535 <sup>c</sup> )
Secondary antibody	-	Goat anti-rabbit, Alexa 594 (cat. ab150080 <sup>b</sup> )	Goat anti-rabbit, Alexa 594 (cat. ab150080 <sup>b</sup> )	Goat anti-chicken, Alexa 568 (cat. A11041 <sup>a</sup> )

<sup>a</sup>Fisher Scientific, Ottawa, ON; <sup>b</sup>Abcam, Toronto, ON; <sup>c</sup>Millipore, Etobicoke, ON

### 3.10 Statistical Analysis

Data were analyzed using GraphPad Prism 6.0 software (GraphPad Software, San Diego, CA) and are reported as the mean  $\pm$  standard deviation. Differences were considered statistically significant at  $p < 0.05$ . Grubb's test was used to identify statistical outliers.



## Chapter 4

### 4 Results

#### 4.1 ASC characterization

##### 4.1.1 Cell surface marker expression

Immunophenotyping of dsRed<sup>+</sup> murine adipose-derived stem/stromal cells (ASCs) at passage 3 (P3) showed cell surface marker expression consistent with previous findings [106, 311]. Analysis of the viable cell population demonstrated that the ASCs were positive for the stromal cell markers CD29 ( $99.3 \pm 0.8\%$ ), CD44 ( $99.0 \pm 0.8\%$ ), and CD90 ( $98.6 \pm 0.9\%$ ). Further, the cells were negative for the endothelial cell marker CD31 ( $0.1 \pm 0.1\%$ ) and the hematopoietic pan-leukocyte marker CD45 ( $0.6 \pm 0.3\%$ ) (N=3 separate ASC isolations; Figure 4.1, fluorescence minus one (FMO) controls shown in Supplementary Figure 1).

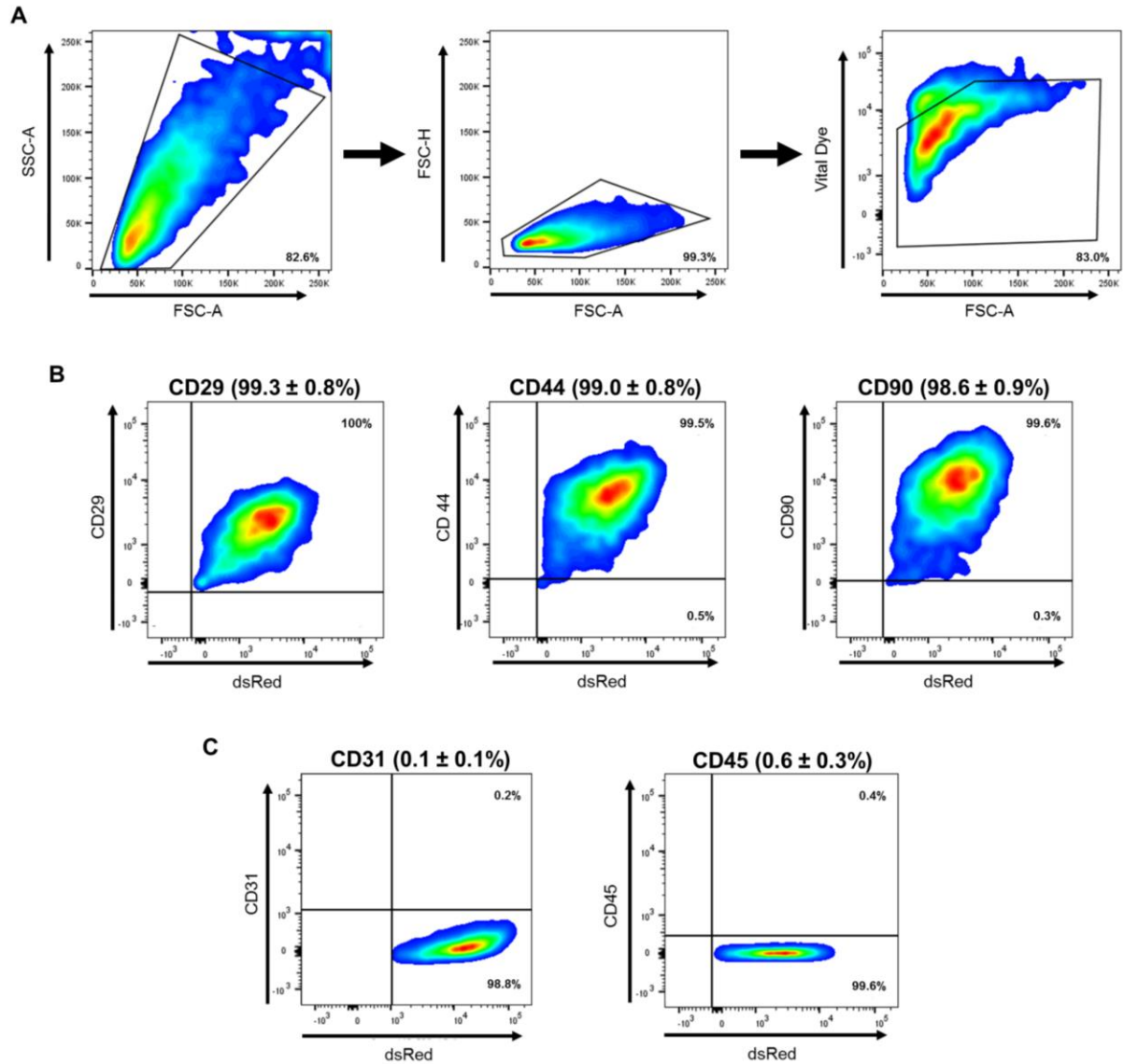


**Figure 4.1. dsRed<sup>+</sup> mouse ASCs express characteristic cell surface markers.** A) Cells were gated based on their forward scatter (FSC) and side scatter (SSC) distribution (82.6%) followed by selection of FSC singlets (99.3%), and selection of the viable cell population (83.0%). B) Representative scatter plots from one biological replicate demonstrating dsRed<sup>+</sup> cell expression of CD29 (100% positive), CD44 (99.5% positive), and CD90 (99.6% positive). Mean ± standard deviation from N=3 separate experiments displayed above each plot. C) dsRed<sup>+</sup> cells were negative for CD45 (0.2% positive) and CD31 (0.4% positive). Mean ± standard deviation from N=3 separate experiments displayed above each plot.

#### 4.1.2 Trilineage differentiation

To verify that the ASCs used in these studies displayed multipotent differentiation potential, the capacity of the cells to differentiate in culture toward the adipogenic, osteogenic, and chondrogenic lineages was confirmed.

ASCs cultured under adipogenic conditions exhibited intracellular lipid accumulation characteristic of developing adipocytes after 14 days of culture, whereas non-induced controls showed minimal lipid droplet formation as assessed by qualitative oil red O staining (n=3 induced, 3 non-induced wells, N=3 experiments from different ASC isolations; Figure 4.2A). Quantitative absorbance measurements of the dye eluted from oil red O-stained plates by spectrophotometry showed significantly greater levels of staining in induced relative to non-induced controls (Figure 4.2B). In addition, significantly enhanced activity of the enzyme glycerol 3-phosphate dehydrogenase (GPDH) involved in lipid biosynthesis was observed relative to non-induced controls after 14 days of culture (n=3, N=4; Figure 4.2C).

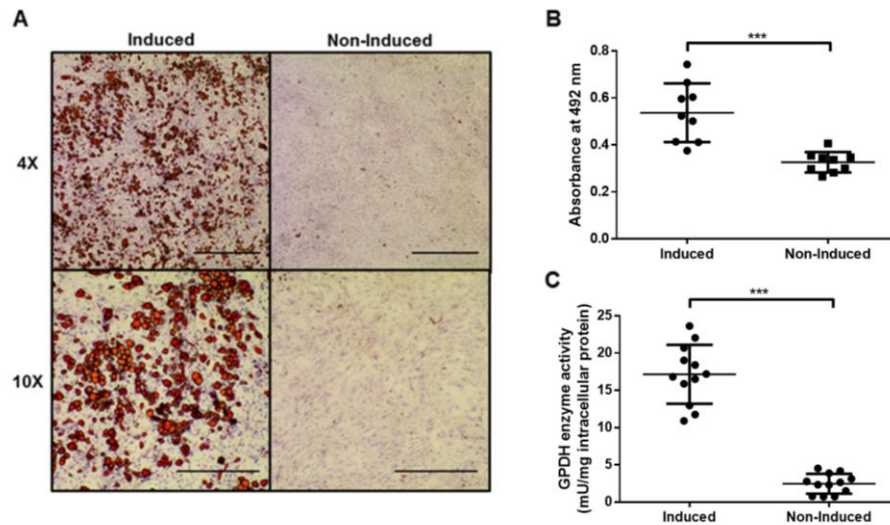


**Figure 4.2. ASCs differentiate toward the adipogenic lineage.** A) ASCs induced toward the adipogenic lineage displayed enhanced intracellular lipid accumulation (red stain) relative to non-induced controls after 14 days of culture (n=3, N=3). 4X scale: 1000  $\mu\text{m}$ , 10X scale: 500  $\mu\text{m}$ . B) Absorbance measurements of dye eluted from oil red O-stained plates revealed increased oil red O staining in induced cultures by spectrophotometry (n=3, N=3). C) Greater GPDH enzyme activity was observed in induced cell cultures at 14 days (n=3, N=4). Student's t-test. \*\*\*p<0.001.

In cells grown under osteogenic conditions, induced cells displayed significantly higher activity levels of the enzyme alkaline phosphatase (ALP) – an early marker of osteogenesis involved in the mineralization process – relative to non-induced controls (n=3, N=4; Figure 4.3A). After 28 days of culture, small mineral deposits could be visualized by von Kossa staining within induced cells, but not in non-induced controls (n=2-3, N=3; Figure 4.3B).

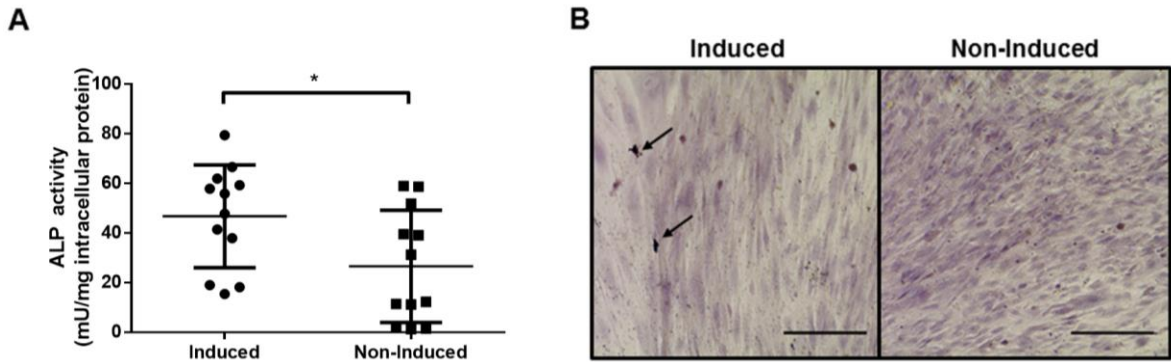


**Figure 4.3. ASCs differentiate toward the osteogenic lineage.** A) Increased ALP enzyme activity was observed after 7 days in culture in induced cells relative to non-induced controls (n=3, N=4). B) Mineralization (arrows) was detected in ASCs cultured under osteogenic conditions for 28 days (n=2-3, N=3; scale: 200  $\mu$ m). Student's t-test. \*p<0.05.

Lastly, to assess chondrogenic differentiation, collagen I and II expression was qualitatively evaluated by immunohistochemistry within 3D cell aggregates. Collagen II is the predominant form of collagen found in the extracellular matrix (ECM) of healthy articular cartilage and the chondrogenic differentiation of mesenchymal stem/stromal cells (MSCs) is associated with a shift from collagen I to collagen II expression [312]. A qualitatively higher collagen II to collagen I ratio was observed within induced cell aggregates compared to non-induced controls suggestive of chondrogenic differentiation (n=2-4, N=3; Figure 4.4, staining controls shown in Supplementary Figure 2).

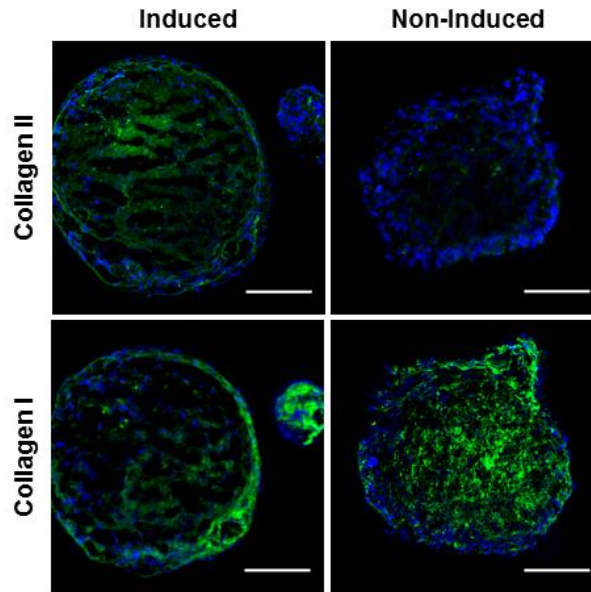


**Figure 4.4. ASCs differentiate toward the chondrogenic lineage.** Induced cell aggregates displayed a qualitatively higher ratio of collagen II to collagen I expression compared to non-induced controls after 28 days of culture.  $n=2-4$ ,  $N=3$ . Green: positive staining for collagen I or II (as indicated), blue: cell nuclei. Scale: 200  $\mu\text{m}$ .

## 4.2 ASC seeding and attachment to DAT scaffolds

Initial pilot studies were performed in order to verify the attachment of ASCs to the DAT scaffolds with dynamic seeding on a 3D rocker for 24 h. Staining results confirmed cell attachment for each of the three seeding densities examined ( $0.5 \times 10^6$  ASCs/scaffold,  $1 \times 10^6$  ASCs/scaffold,  $2 \times 10^6$  ASCs/scaffold;  $n=3$  technical replicates,  $N=2$  separate batches of ASC isolations; Figure 4.5). The majority of attached cells were observed along the scaffold periphery, with fewer cells distributed heterogeneously toward the interior. Qualitative comparisons showed greater numbers of attached cells in the scaffolds seeded at the higher densities. A seeding density of  $2 \times 10^6$  ASCs/DAT scaffold was selected for all subsequent *in vivo* experiments, as there was a more homogeneous distribution of ASCs along the scaffold periphery in this group.

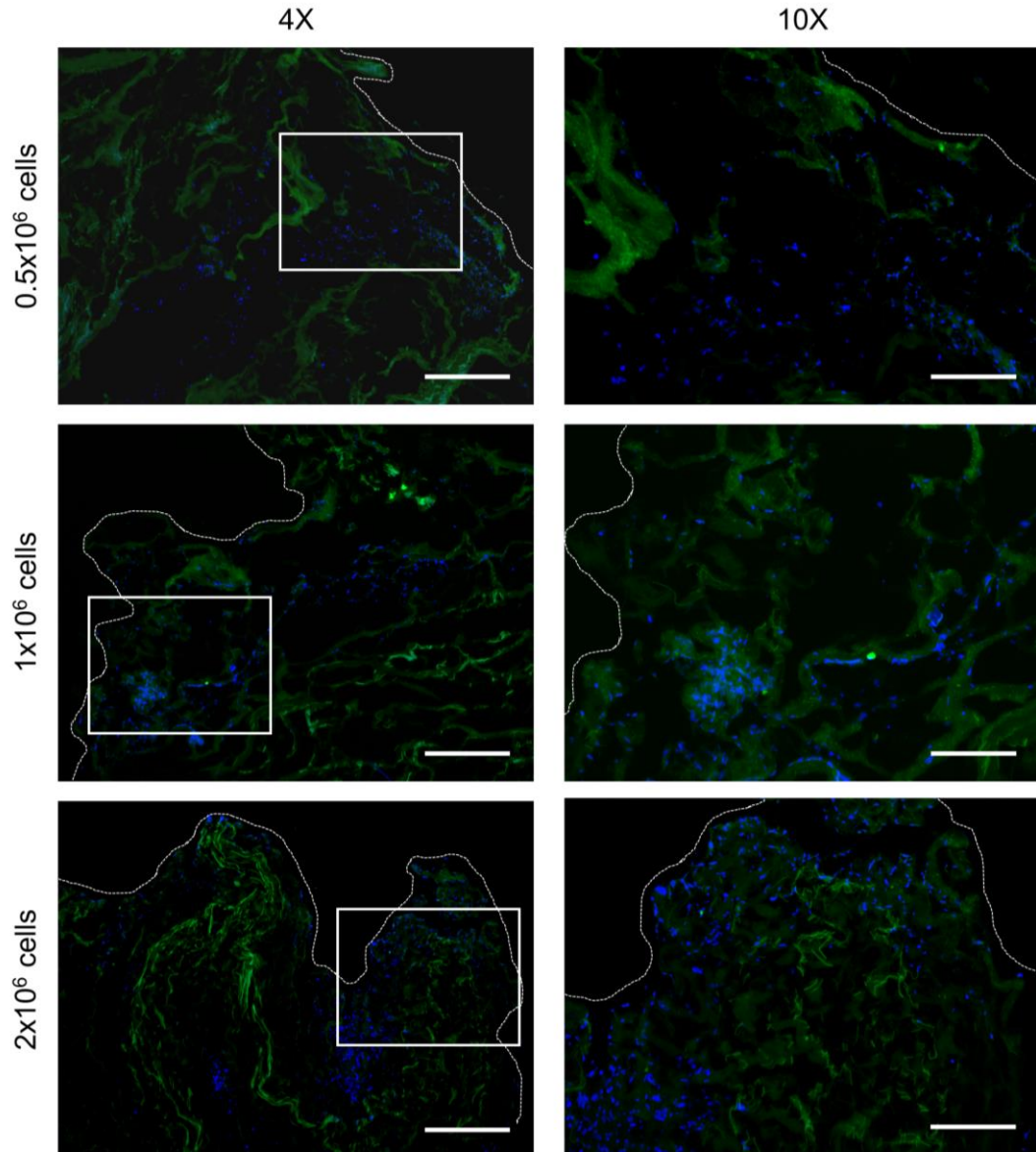


**Figure 4.5. ASCs attach to DAT scaffolds under *in vitro* dynamic seeding conditions.** Representative images along the scaffold periphery of DAT scaffolds seeded at three different cell densities ( $0.5 \times 10^6$  ASCs/scaffold,  $1 \times 10^6$  ASCs/scaffold,  $2 \times 10^6$  ASCs/scaffold) demonstrate ASC attachment. Insets in 4X images (left panels) are magnified at 10X (right panels). Dotted line: scaffold periphery. Blue: cell nuclei, green: scaffold autofluorescence. 4X scale: 500  $\mu\text{m}$ , 10X scale: 250  $\mu\text{m}$ .  $n=3$ ,  $N=2$ .

## 4.3 Cell recruitment and tissue remodeling within implanted DAT scaffolds

ASC-seeded and unseeded DAT scaffolds were well tolerated after subcutaneous implantation into MacGreen mice. The incision sites healed within the course of the first week and there were no detectable signs of inflammation or irritation in any of the animals. Macroscopically, the implants appeared to retain their shape and volume over the course of the 8 week period.

Masson's trichrome stained sections of ASC-seeded and unseeded DAT implants were used to qualitatively assess cell recruitment, angiogenesis, and adipogenesis at 72 h, 1, 3, 5, and 8 weeks post-implantation. Follow-up quantitative analysis of cell infiltration and adipogenesis was performed to examine differences between the seeded and unseeded scaffold groups.

### 4.3.1 Qualitative assessment of cell infiltration and tissue remodeling

In Masson's trichrome stained sections, a thin fibrous capsule was visualized along the scaffold periphery starting at the 1 week time point, persisting over the course of the study. All adipocytes and blood vessels contained within this fibrous capsule were considered newly formed tissues. Within the seeded implants, the DAT appeared to be denser and slightly contracted at the 8 week time point relative to the unseeded implants in which the scaffold shape and structure appeared to be relatively consistent over time.

Qualitatively, there appeared to be increased cell recruitment within the ASC-seeded implants at the later time points relative to 72 h (Figure 4.6). In contrast, low levels of cell infiltration were observed in the unseeded DAT controls (Figure 4.7). Erythrocyte-containing blood vessels were detected in both the ASC-seeded and unseeded DAT scaffolds along the implant periphery. Qualitatively, greater numbers of vessels were visualized in the seeded versus unseeded scaffolds as early as 1 week post-implantation. Newly formed adipose tissue was also observed within the seeded and unseeded scaffold groups, and was predominantly localized along the apical border; however, in a small



fraction of the implants, mature adipocytes were also observed on the lateral surfaces toward the periphery.

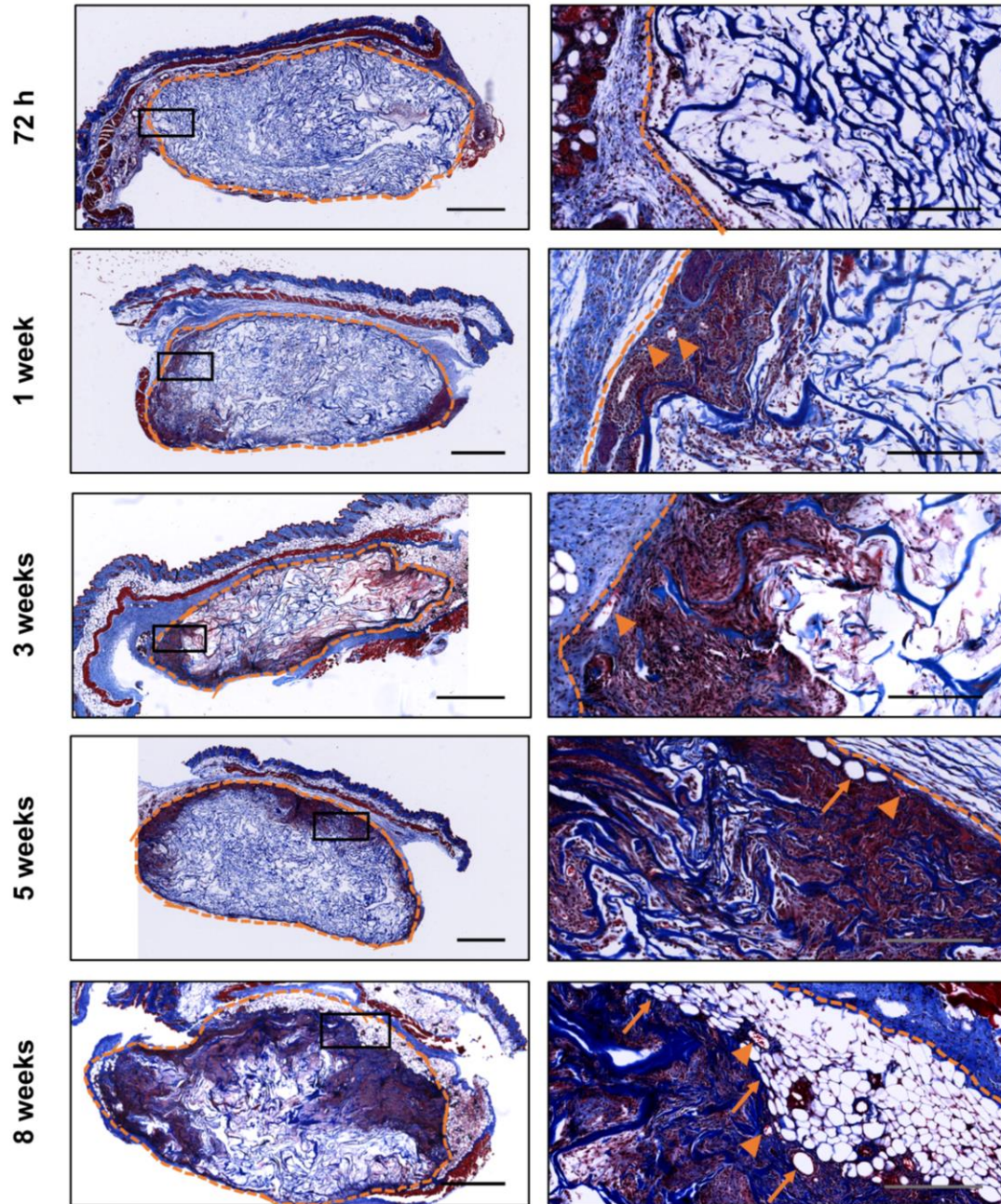


**Figure 4.6. ASC-seeded DAT scaffolds enhance cell recruitment, adipogenesis, and angiogenesis.** Representative images of seeded DAT implants excised at each time point are shown. Insets in left panels are magnified in right panels. Dotted line: scaffold periphery; arrows: adipocytes; arrow heads: erythrocyte-containing blood vessels. Left panels scale: 1 mm, right panels scale: 200  $\mu$ m.

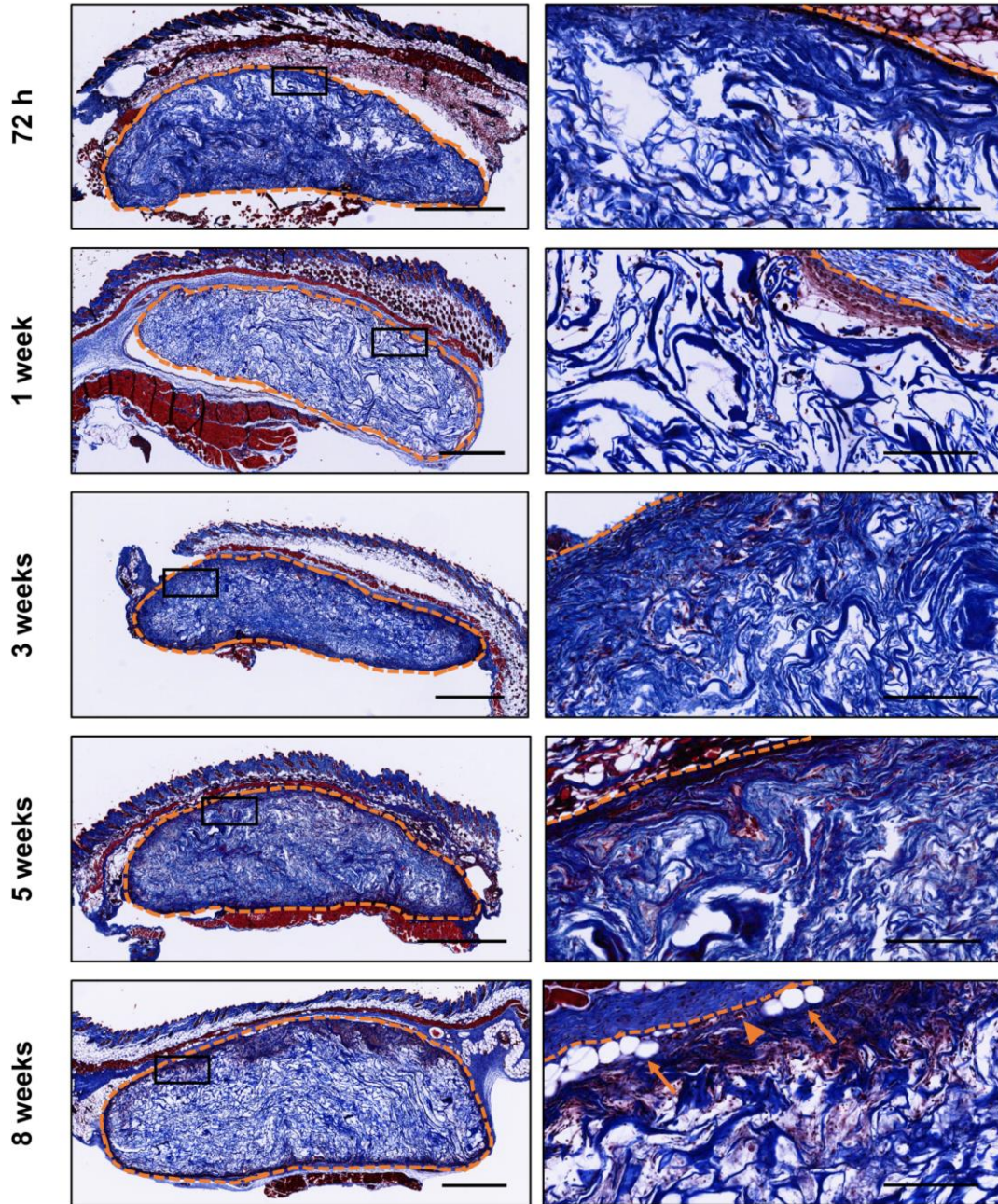


**Figure 4.7. Low levels of cell recruitment, adipogenesis, and angiogenesis were observed in unseeded DAT scaffolds.** Representative images of unseeded DAT implants excised at each time point are shown. Insets in left panels are magnified in right panels. Dotted line: scaffold periphery; arrows: adipocytes; arrow heads: erythrocyte-containing blood vessels. Left panels scale: 1 mm, right panels scale: 200  $\mu$ m.

### 4.3.2 Cell recruitment

Measurement of the degree of cell infiltration in ASC-seeded and unseeded implants was performed on Masson's trichrome stained sections (Figure 4.8A). Within seeded scaffolds, there was significantly greater cell recruitment at 1 and 5 weeks compared to 72 h post-implantation (N=5-6 implants/treatment group/time point; Figure 4.8B). At 8 weeks post-implantation, cell recruitment within the seeded scaffold group was significantly greater compared to the previous time points, and was significantly different from the unseeded controls. Within the unseeded scaffolds, there was increased cell infiltration at 8 weeks post-implantation relative to the unseeded controls at 72 h.

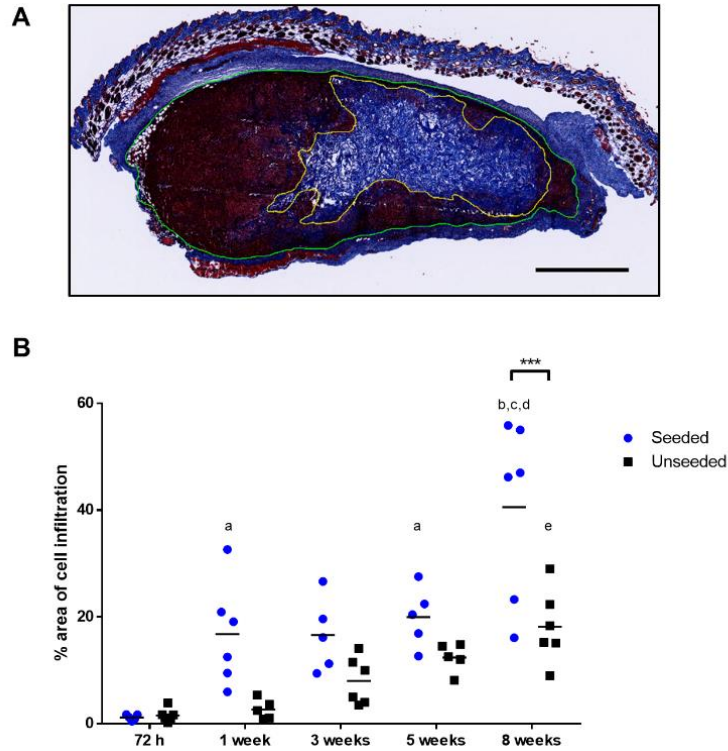


**Figure 4.8. ASC-seeding enhances cell recruitment within DAT scaffolds.** A) Sample implant cross-section illustrating the DAT scaffold region (contained within the area outlined by the green line) and the area of the scaffold infiltrated by cells (area between green and yellow lines). Scale bar: 1 mm. B) Quantitative measurements of the percentage area of cell infiltration revealed increased cell recruitment in the ASC-seeded scaffolds, with a delayed increase observed within the unseeded group. Two-way ANOVA, Tukey's post-hoc. \*\*\* $p < 0.001$  between groups indicated, <sup>a</sup> $p < 0.05$  vs 72 h seeded, <sup>b</sup> $p < 0.0001$  vs 72 h seeded, <sup>c</sup> $p < 0.001$  vs 1 wk and 3 wks seeded, <sup>d</sup> $p < 0.01$  vs 5 wks seeded, <sup>e</sup> $p < 0.05$  vs 72 h and 1 wk unseeded. N=5-6 implants/treatment group/time point.

### 4.3.3 Adipose tissue remodeling

Within Masson's trichrome stained tissue sections, quantitative analysis of adipose tissue remodeling revealed that a small amount of adipose tissue (<1% of the implant area) could be detected within the implant region as early as 1 week post-implantation (Table 4.1). Adipocytes were detected in a greater number of the ASC-seeded implants compared to unseeded controls at 1, 3, 5, and 8 weeks post-implantation. Moreover,

larger areas of remodeled adipose tissue were observed within the seeded group at the 3, 5, and 8 week time points compared to unseeded controls.

**Table 4.1. Adipose tissue remodeling in ASC-seeded and unseeded DAT implants.**

The number of implants containing adipocytes is displayed as a fraction of the total implants analyzed within each treatment group and time point. For groups in which adipocytes were observed, histological scoring of the percentage area of adipose tissue remodeling was performed and is indicated as a range by the number of ‘+’ symbols within brackets. <sup>+</sup><1% adipose tissue, <sup>++</sup>1-5%, <sup>+++</sup>5-10%.

	<b>Seeded</b>	<b>Unseeded</b>
<b>72 h</b>	0/6	0/6
<b>1 week</b>	4/6 (+)	1/6 (+)
<b>3 weeks</b>	2/6 (++ to +++)	0/6
<b>5 weeks</b>	2/6 (+ to +++)	0/5
<b>8 weeks</b>	4/6 (+ to +++)	3/6 (+)

#### 4.4 Histological detection and optical tracking of syngeneic donor dsRed<sup>+</sup> ASCs within implanted DAT scaffolds

In order to identify dsRed<sup>+</sup> donor cells within the implants, immunohistochemical analysis for dsRed was performed at 72 h, 1, 3, 5, and 8 weeks post-implantation. In addition, a trial was performed to investigate the feasibility of applying optical imaging techniques to quantitatively track the dsRed<sup>+</sup> ASCs within the implant region in living mice over time.

##### 4.4.1 Immunohistochemical detection of donor dsRed<sup>+</sup> cells

To assess dsRed<sup>+</sup> cell retention within the implants, immunohistochemical staining for dsRed was performed within ASC-seeded implants and unseeded controls, with follow-up quantitative analysis (N=4-6 implants/treatment group/time point). Positive staining for dsRed was detected within ASC-seeded implants at all time points examined (Figure 4.9, staining controls shown in Supplementary Figure 3), indicating that the syngeneic

donor cells were retained over the course of the study. The majority of positive staining appeared along the scaffold periphery; however, at 5 and 8 weeks post-implantation, a thin layer of infiltrating host cells was observed peripheral to the dsRed<sup>+</sup> cells within the scaffold. In implants in which adipose tissue formation was observed, the dsRed staining did not appear in association with the newly formed adipocytes, indicating that the tissues were host-derived. As expected, no positive staining for dsRed was observed within the unseeded scaffold controls at any of the time points examined (Figure 4.10).

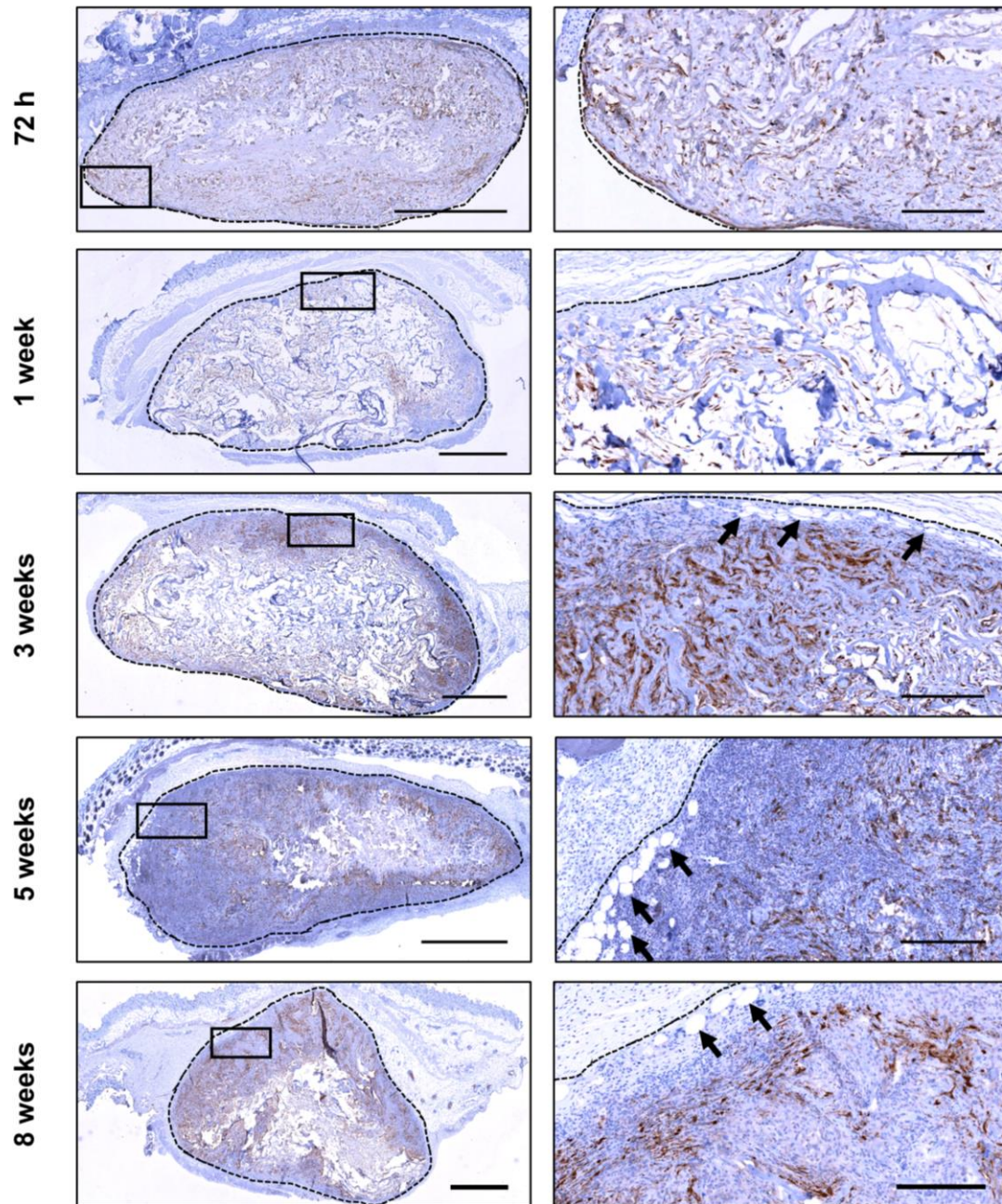


**Figure 4.9. Syngeneic dsRed<sup>+</sup> donor cells are observed in ASC-seeded DAT scaffolds up to 8 weeks post-implantation and are not localized to newly formed adipocytes.**

dsRed<sup>+</sup> cells were visualized through DAB staining along the scaffold periphery at each of the time points examined. Positive staining did not appear in association with adipocytes formed within the implant region. Insets in left panels are magnified in right panels. Dotted line: scaffold periphery; arrows: adipocytes within implant region; brown: positive staining for dsRed. Left panels scale: 1 mm, right panels scale: 200 μm.



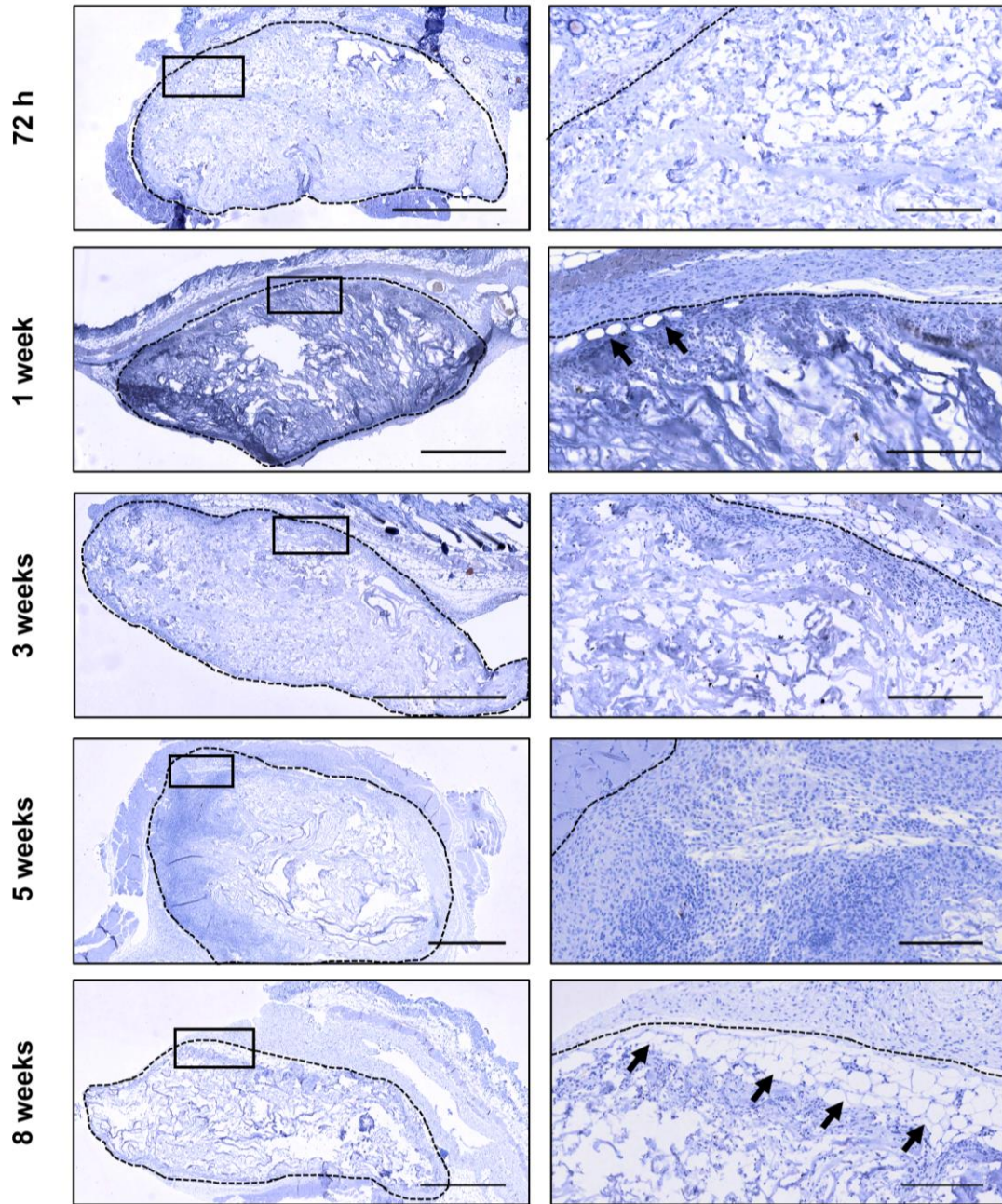


**Figure 4.10. dsRed<sup>+</sup> cells are not observed in unseeded DAT implant controls.** Insets in left panels are magnified in right panels. Dotted line: scaffold periphery; arrows: adipocytes within implant region; Brown: positive staining for dsRed. Left panels scale: 1 mm, right panels scale: 200  $\mu$ m.

Quantitative analysis of the fraction of dsRed<sup>+</sup> stained areas relative to the total implant area confirmed positive dsRed staining in the majority of the ASC-seeded implants (Figure 4.11). In contrast, there was no detectable staining for dsRed within the unseeded DAT controls. No significant differences were observed in terms of the percentage of positively stained area for dsRed within the ASC-seeded implants over time, supporting that the syngeneic donor ASCs were retained through the duration of the study. Variability in the percentage of positively stained areas was noted particularly at the 72 h and 3 week time points. This may be due to variations in the initial attachment of the ASCs to the DAT, or potentially due to cell migration or cell death in some cases.

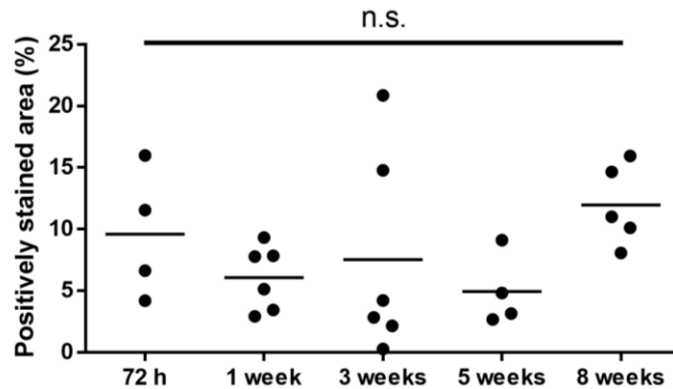


**Figure 4.11. Quantitative analysis of immunohistochemical staining confirmed positive dsRed staining within the ASC-seeded but not unseeded implants.**

Measurement of the percentage of area positively stained for dsRed confirmed positive staining in the ASC-seeded implants, with no significant changes in the percentage of positively stained area over time. In contrast, there was no detectable dsRed staining within the unseeded scaffold (not shown). One-way ANOVA, Tukey's post-hoc test. n.s.: non-significant.

#### 4.4.2 *In vitro* fluorescent detection of transgenic ASCs and macrophages seeded onto DAT scaffolds

To assess the feasibility of applying an optical imaging strategy to track donor dsRed<sup>+</sup> ASCs and infiltrating enhanced green fluorescent protein-positive (EGFP<sup>+</sup>) myeloid cells in the implants *in situ* within living animals, a pilot *in vitro* study was performed using

DAT scaffolds seeded with these transgenic cell populations (n=3 technical replicates, N=1 experiment). In scaffolds seeded with dsRed<sup>+</sup> ASCs at three different densities (2.0x10<sup>6</sup> cells/scaffold, 1.0x10<sup>6</sup> cells/scaffold, 0.5x10<sup>6</sup> cells/scaffold), greater levels of dsRed fluorescence were observed at higher seeding densities (Figure 4.12A).

Quantitative analysis of the radiant efficiency for dsRed confirmed higher levels of fluorescence in scaffolds seeded at 2x10<sup>6</sup> cells/scaffold relative to the other groups, with a decrease in the levels of fluorescence observed at the lower seeding densities (Figure 4.12B). The levels of dsRed fluorescence were greater within each of the seeded scaffolds compared to the unseeded controls even at the lowest seeding density examined.

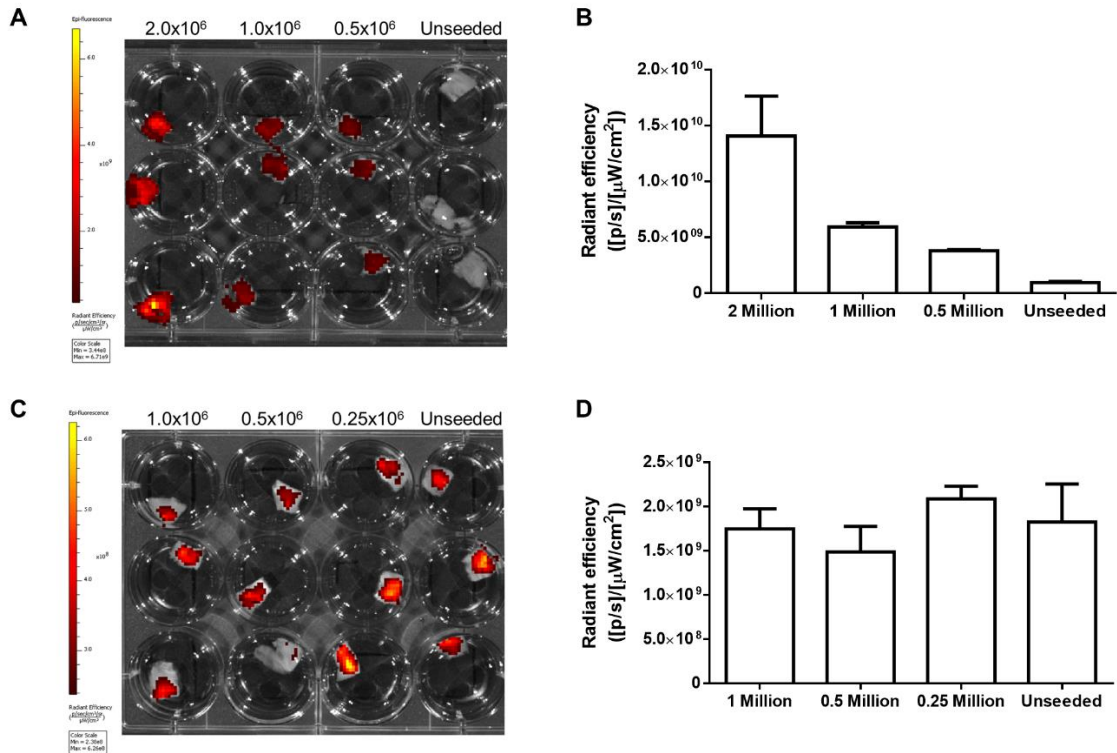


**Figure 4.12. dsRed<sup>+</sup> ASCs seeded onto DAT scaffolds *in vitro* can be detected by optical imaging.** A) Differences in dsRed fluorescence were observed between DAT scaffold groups seeded with variable numbers of murine dsRed<sup>+</sup> ASCs ( $2 \times 10^6$  ASCs/scaffold,  $1 \times 10^6$  ASCs/scaffold,  $0.5 \times 10^6$  ASCs/scaffold, or unseeded controls). B) Quantification of radiant efficiency revealed a decrease in fluorescence at lower seeding densities. C,D) No differences in GFP fluorescence or radiant efficiency were detected in DAT scaffolds seeded with variable numbers of EGFP<sup>+</sup> macrophages relative to the unseeded controls.

In contrast to the dsRed<sup>+</sup> ASCs, no differences in fluorescence were observed in scaffolds seeded with EGFP<sup>+</sup> macrophages derived from MacGreen mice relative to the unseeded controls (Figure 4.12C,D). Collagen is highly abundant in the DAT [21] and is known to autofluoresce at wavelengths that excite GFP [313], which may have interfered with the ability to detect the macrophages on the scaffolds. Thus, *in vivo* optical imaging was performed to track donor dsRed<sup>+</sup> ASCs but not infiltrating EGFP<sup>+</sup> myeloid cells in subsequent animal experiments using the MacGreen mouse model.

#### 4.4.3 *In vivo* tracking of dsRed<sup>+</sup> donor cells

A longitudinal *in vivo* optical imaging study was performed to track dsRed<sup>+</sup> donor cells in mice implanted with ASC-seeded and unseeded scaffolds. These results showed increased dsRed fluorescence in seeded versus unseeded scaffolds at 24 h, 72 h, 3, and 5 weeks post-implantation (N=3-8 mice imaged/time point; Figure 4.13A,B). In addition, dsRed fluorescence was significantly increased in the implant region of seeded scaffolds at 24 h, 72 h, 3, and 5 weeks post-implantation compared to baseline measurements taken of the skin at 24 h prior to implantation. At 1 and 8 weeks post-implantation, there was a significant decrease in dsRed fluorescence within the seeded implant regions of the mice relative to the 24 h and 72 h time points. Moreover, there were no statistical differences between the seeded implants at 1 and 8 weeks relative to the unseeded controls at the same time point, or relative to baseline measurements. This finding appears to contradict the immunohistochemical analysis of dsRed<sup>+</sup> cells within the implants, as dsRed<sup>+</sup> cells were noted at both of these time points. These differences may be attributed to darkening of the skin with changes in the hair growth cycle that were observed over time, which may have interfered with signaling acquisition. At the 8 week time point, histological analysis demonstrated that the seeded DAT implants appeared to be more contracted, and dsRed<sup>+</sup> cells were noted slightly more toward the interior of the scaffold, factors which may also have contributed to the decrease in dsRed fluorescence. Within the unseeded implant regions, there were no significant differences between time points or compared to baseline measurements, consistent with the immunohistochemical data.

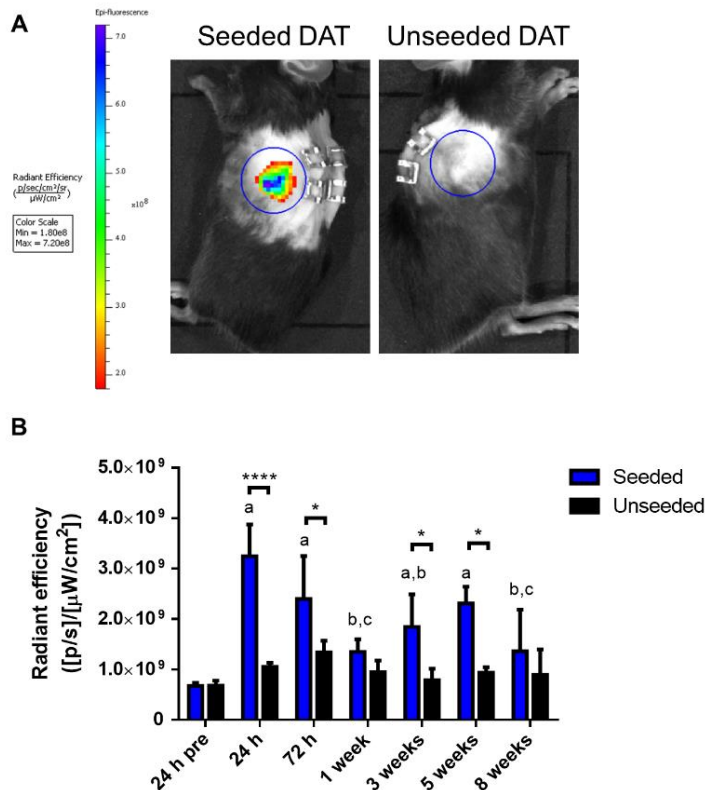


**Figure 4.13. Donor dsRed<sup>+</sup> cells are detected through optical imaging of ASC-seeded implant regions of mice at 24 h, 72 h, 3, and 5 weeks post-implantation.** A) dsRed fluorescence was observed within the implant region of the ASC-seeded DAT scaffold (left panel) but not the unseeded scaffold (right) of a mouse at 24 h post-implantation. Blue circle delineates implant region. B) Quantification of dsRed radiant efficiency revealed increased signal in seeded versus unseeded implants at 24 h, 72 h, 3, and 5 weeks, along with significantly higher levels of fluorescence relative to baseline at 24 h pre-implantation. A decrease in the signal within the seeded implant regions was observed at 1 and 8 weeks post-implantation relative to 24 h and 72 h, and was not significantly different from the unseeded controls or baseline controls at these time points. n=3-8 mice imaged/time point. \*p<0.05 between groups indicated, \*\*\*\*p<0.0001, <sup>a</sup>p<0.01 vs 24 h pre-implantation, <sup>b</sup>p<0.01 vs 24 h post-implantation, <sup>c</sup>p<0.05 vs 72 h post-implantation. Two-way ANOVA, Tukey's post-hoc.

## 4.5 Immunohistochemical analysis of infiltrating myeloid cells

### 4.5.1 Iba1<sup>+</sup> myeloid cell infiltration in DAT implants

In order to investigate immune cell infiltration into the implants, immunohistochemistry for Iba1, a marker expressed by monocytes and macrophages [314, 315], was performed in conjunction with staining for EGFP expressed by myeloid cells within the MacGreen mouse model [25]. EGFP<sup>+</sup>Iba1<sup>+</sup>DAPI<sup>+</sup> cells were observed in both seeded and unseeded implants at all time points examined, with peak levels observed at 3 weeks post-implantation within both groups (Figures 4.14 and 4.15; staining controls shown in Supplementary Figures 4 and 5). Follow-up quantitative analysis was performed to further assess differences.

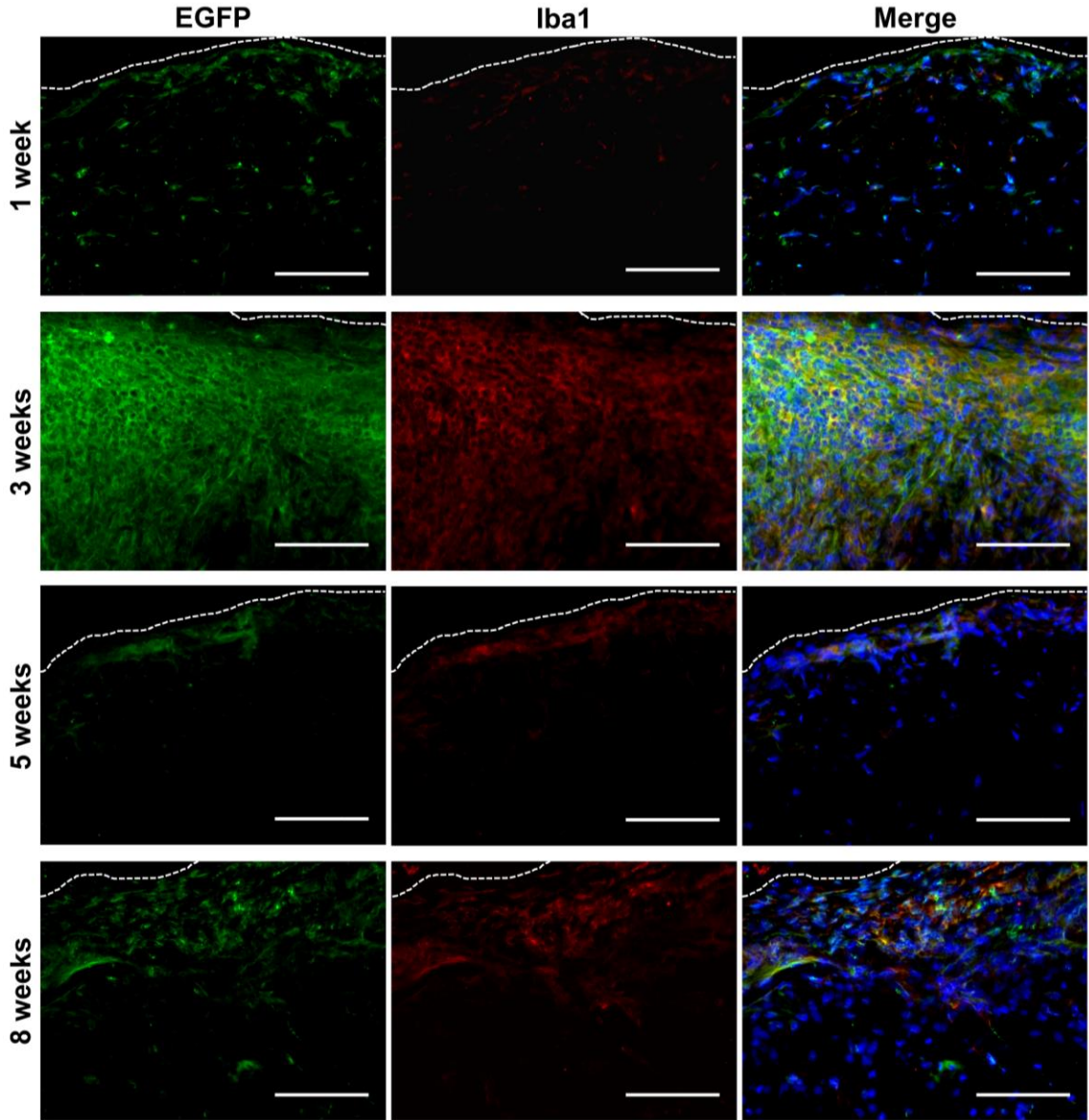


**Figure 4.14. Representative images of the scaffold periphery of EGFP and Iba1 co-staining in ASC-seeded DAT implants.** EGFP<sup>+</sup>Iba1<sup>+</sup>DAPI<sup>+</sup> cells were observed at 1, 3, 5, and 8 weeks post-implantation with peak infiltration at 3 weeks. Dotted line: scaffold periphery. Blue: cell nuclei, green: EGFP, red: Iba1. Scale: 100  $\mu$ m.



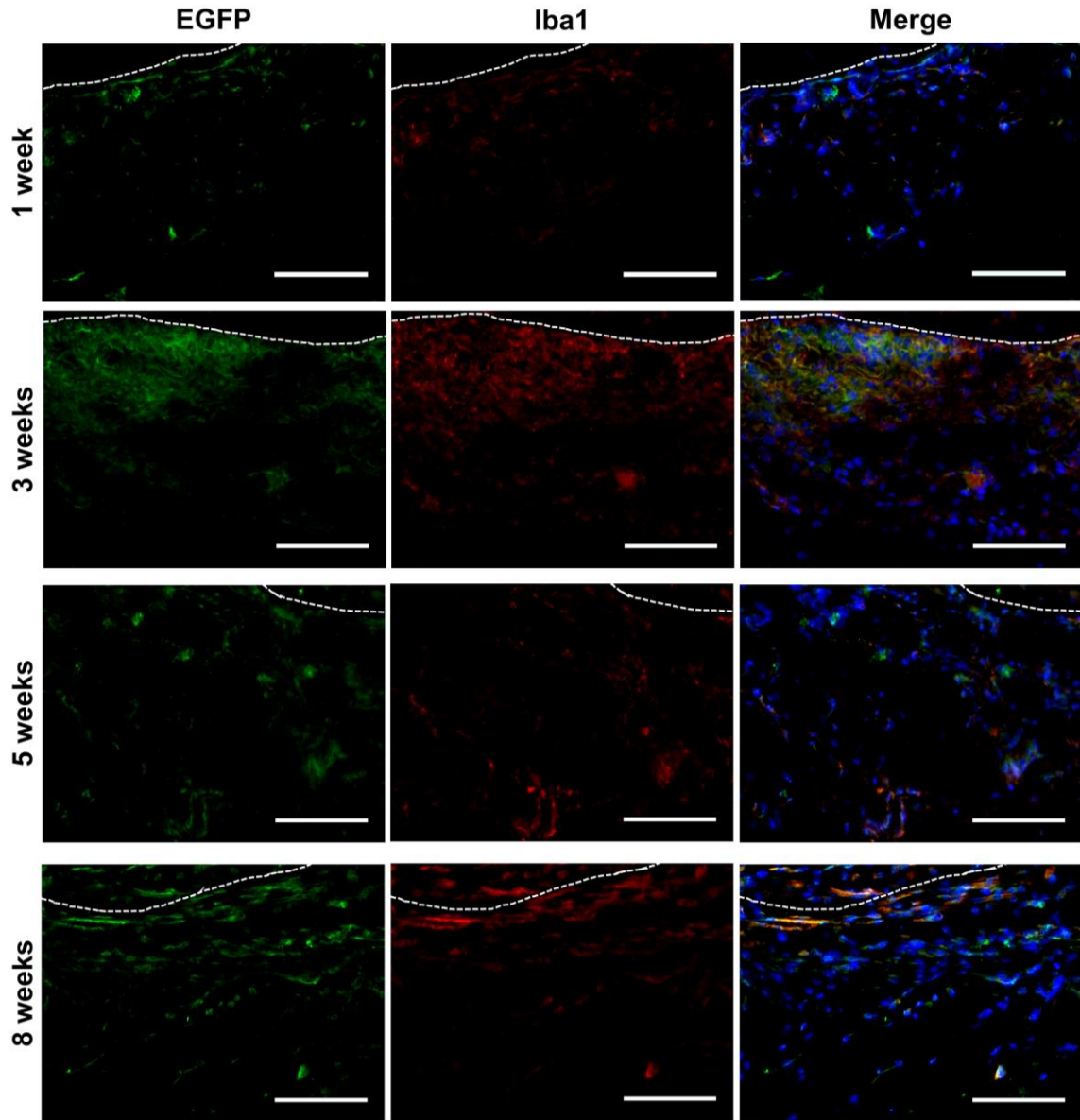


**Figure 4.15. Representative images of the scaffold periphery of EGFP and Iba1 co-staining in unseeded DAT implants.** EGFP<sup>+</sup>Iba1<sup>+</sup>DAPI<sup>+</sup> cells were observed at 1, 3, 5, and 8 weeks post-implantation with peak infiltration at 3 weeks. Dotted line: scaffold periphery. Blue: cell nuclei, green: EGFP, red: Iba1. Scale: 100  $\mu$ m.

Quantitative analysis of the EGFP and Iba1 staining was done by manual cell counting (Figure 4.16; N=5-6 implants/treatment group/time point; n=5-6 20X frames along the apical and basal borders of the scaffold). The analysis was performed using images captured on the implant periphery in order to control for the variable degrees of cell infiltration toward the scaffold interior, which was dependent on the implant group and the time point examined.

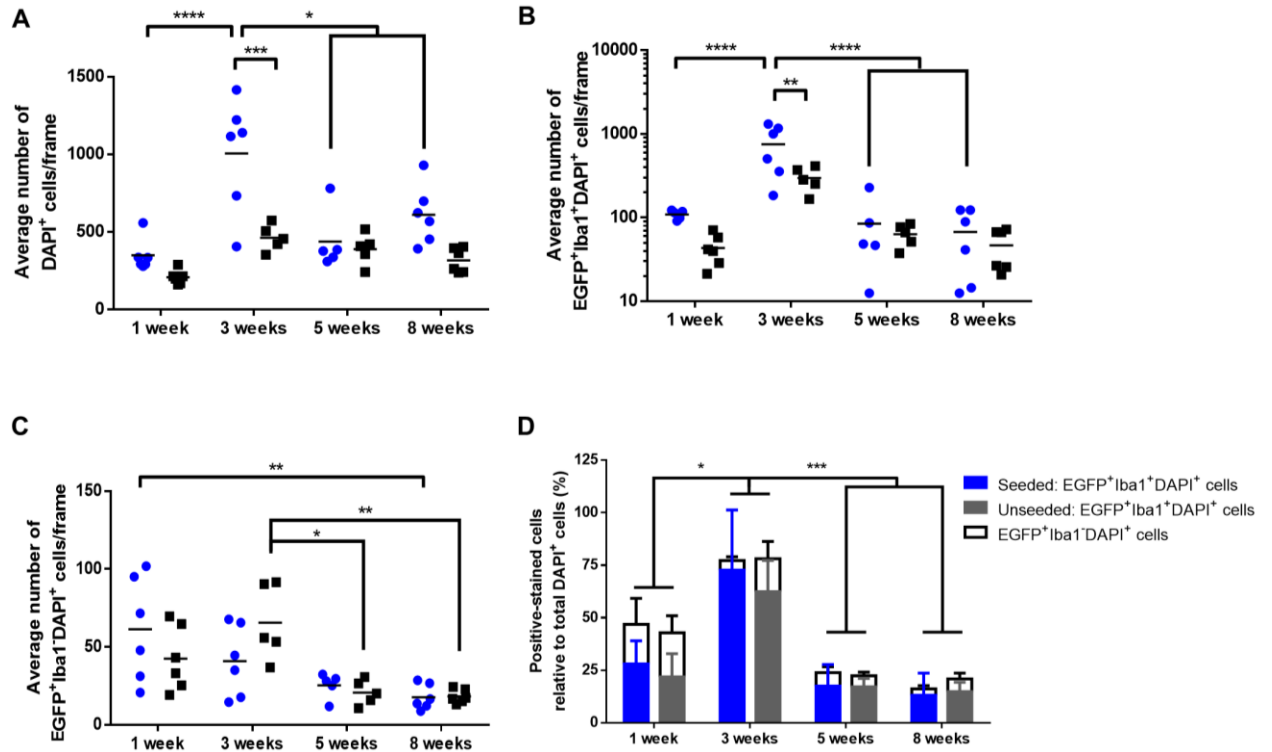


**Figure 4.16. Quantitative analysis of EGFP and Iba1 co-staining along the implant periphery.** A) Counting of DAPI<sup>+</sup> cell nuclei revealed a peak cell density within ASC-seeded implants (represented by blue circles) at 3 weeks relative to the unseeded controls (black squares) and the other time points. B) Numbers of EGFP<sup>+</sup>Iba1<sup>+</sup>DAPI<sup>+</sup> cells peaked within ASC-seeded implants (blue circles) at 3 weeks relative to the unseeded controls (black squares) and the other time points. C) Numbers of EGFP<sup>+</sup>Iba1<sup>-</sup>DAPI<sup>+</sup> cells gradually declined within ASC-seeded implants (blue circles), becoming significant at 8 weeks relative to 1 week. EGFP<sup>+</sup>Iba1<sup>-</sup>DAPI<sup>+</sup> cells persisted within unseeded scaffolds (black squares) up to 3 weeks followed by a significant decline at 5 and 8 weeks. D) The relative fraction of EGFP<sup>+</sup>Iba1<sup>+</sup>DAPI<sup>+</sup> cells (solid-filled bars) and total EGFP<sup>+</sup> myeloid cells (stacked column of solid-filled and unfilled bars) was significantly increased within both seeded and unseeded implants at 3 weeks relative to the other time points examined. Two-way ANOVA, Tukey's post-hoc test. \* $p < 0.05$  between groups indicated, \*\* $p < 0.01$ , \*\*\* $p < 0.001$ , \*\*\*\* $p < 0.0001$ .

In assessing the density of DAPI<sup>+</sup> cells along the scaffold periphery, peak cell densities were noted in the seeded DAT scaffold group at 3 weeks relative to the unseeded controls, as well as the other time points (Figure 4.16A). No significant changes in cell density were observed in the unseeded implants over time. Further, analysis of the numbers of EGFP<sup>+</sup>Iba1<sup>+</sup>DAPI<sup>+</sup> cells revealed similar trends to the total DAPI<sup>+</sup> cell counts, with significantly greater numbers of EGFP<sup>+</sup>Iba1<sup>+</sup>DAPI<sup>+</sup> cells within the seeded scaffold group at 3 weeks relative to the unseeded controls and the other time points examined (Figure 4.16B).

EGFP<sup>+</sup>Iba1<sup>-</sup>DAPI<sup>+</sup> cells were also observed at low levels within the implants, suggesting the presence of other myeloid cell populations such as neutrophils [316, 317].

Quantitative assessment of the numbers of EGFP<sup>+</sup>Iba1<sup>-</sup>DAPI<sup>+</sup> cells demonstrated that there were no differences between the seeded and unseeded scaffold groups at any of the time points examined (Figure 4.16D). However, within the seeded group, the number of EGFP<sup>+</sup>Iba1<sup>-</sup>DAPI<sup>+</sup> cells appeared to gradually decrease over time, with a significant difference observed between 1 and 8 weeks post-implantation. In the unseeded group, a small but non-significant increase in the EGFP<sup>+</sup>Iba1<sup>-</sup>DAPI<sup>+</sup> cell population was noted between 1 and 3 weeks, followed by a significant decline at 5 and 8 weeks relative to the 3 week time point. Variable numbers of EGFP<sup>+</sup>Iba1<sup>-</sup>DAPI<sup>+</sup> cells were observed at the 1 and 3 week time points suggesting that dynamic changes in this population may be occurring at these time points.

In order to account for the differences in cell densities observed along the implant periphery, the numbers of EGFP<sup>+</sup>Iba1<sup>+</sup>DAPI<sup>+</sup> cells and EGFP<sup>+</sup>Iba1<sup>-</sup>DAPI<sup>+</sup> cells were normalized to the total number of DAPI<sup>+</sup> cells counted within each region (Figure 4.16D). The relative fraction of EGFP<sup>+</sup>Iba1<sup>+</sup>DAPI<sup>+</sup> cells was significantly increased at 3 weeks compared to the other time points in both the seeded and unseeded implants, with the EGFP<sup>+</sup>Iba1<sup>+</sup>DAPI<sup>+</sup> cells representing >60% of the total cell population. These data suggest that the peak influx of EGFP<sup>+</sup>Iba1<sup>+</sup>DAPI<sup>+</sup> cells occurred at 3 weeks within the seeded and unseeded implants, with greater total cell recruitment in the ASC-seeded group. The EGFP<sup>+</sup>Iba1<sup>+</sup>DAPI<sup>+</sup> cell population then declined at 5 and 8 weeks. Analysis of the relative fraction of total EGFP<sup>+</sup>DAPI<sup>+</sup> cells (i.e. the pooled population of

EGFP<sup>+</sup>Iba1<sup>+</sup>DAPI<sup>+</sup> and EGFP<sup>+</sup>Iba1<sup>-</sup>DAPI<sup>+</sup> cells) showed a significant increase in this population within the seeded and unseeded implants at 3 weeks relative to the other time points, similar to that of the EGFP<sup>+</sup>Iba1<sup>+</sup>DAPI<sup>+</sup> cell population.

#### 4.5.2 Macrophage phenotypic markers in DAT scaffolds

To assess the potential for donor ASCs to modulate macrophage phenotype within DAT scaffolds, myeloid cell expression of the macrophage phenotypic markers inducible nitric oxide synthase (iNOS) and arginase-1 (Arg-1) were assessed within ASC-seeded and unseeded implants at 1, 3, 5, and 8 weeks post-implantation. iNOS is considered an M1 macrophage marker and is associated with the metabolism of arginine, forming nitric oxide (NO), which is used as a defense mechanism via oxidative/nitrosative damage [318]. M2-polarized macrophages are associated with the expression of Arg-1, an enzyme that indirectly limits arginine availability for NO production by hydrolyzing arginine, forming ornithine and urea [318]. Thus, iNOS and Arg-1 expression were examined in EGFP<sup>+</sup> myeloid cells within the ASC-seeded and unseeded implants using separate serial 5  $\mu$ m sections to co-stain EGFP with iNOS, and EGFP with Arg-1.

Expression of iNOS and Arg-1 were observed within EGFP<sup>+</sup> myeloid cells in both seeded and unseeded implants at all time points examined (N=5-6 implants/treatment group/time point; Figure 4.17 and 4.18, staining controls shown in Supplementary Figures 4 and 5; single channels shown in Supplementary Figures 6-9). Qualitatively, there did not appear to be major differences in the pattern of iNOS or Arg-1 expression within myeloid cells when comparing the seeded and unseeded groups at the time points investigated.

Expression of iNOS by EGFP<sup>+</sup> myeloid cells appeared to peak at 3 weeks relative to the other time points, and partially declined thereafter (Figure 4.17). Qualitative assessment of Arg-1 expression in myeloid cells within adjacent 5  $\mu$ m sections showed low levels of EGFP<sup>+</sup>Arg-1<sup>+</sup>DAPI<sup>+</sup> cells present at all time points investigated, with no major differences noted between time points (Figure 4.18).

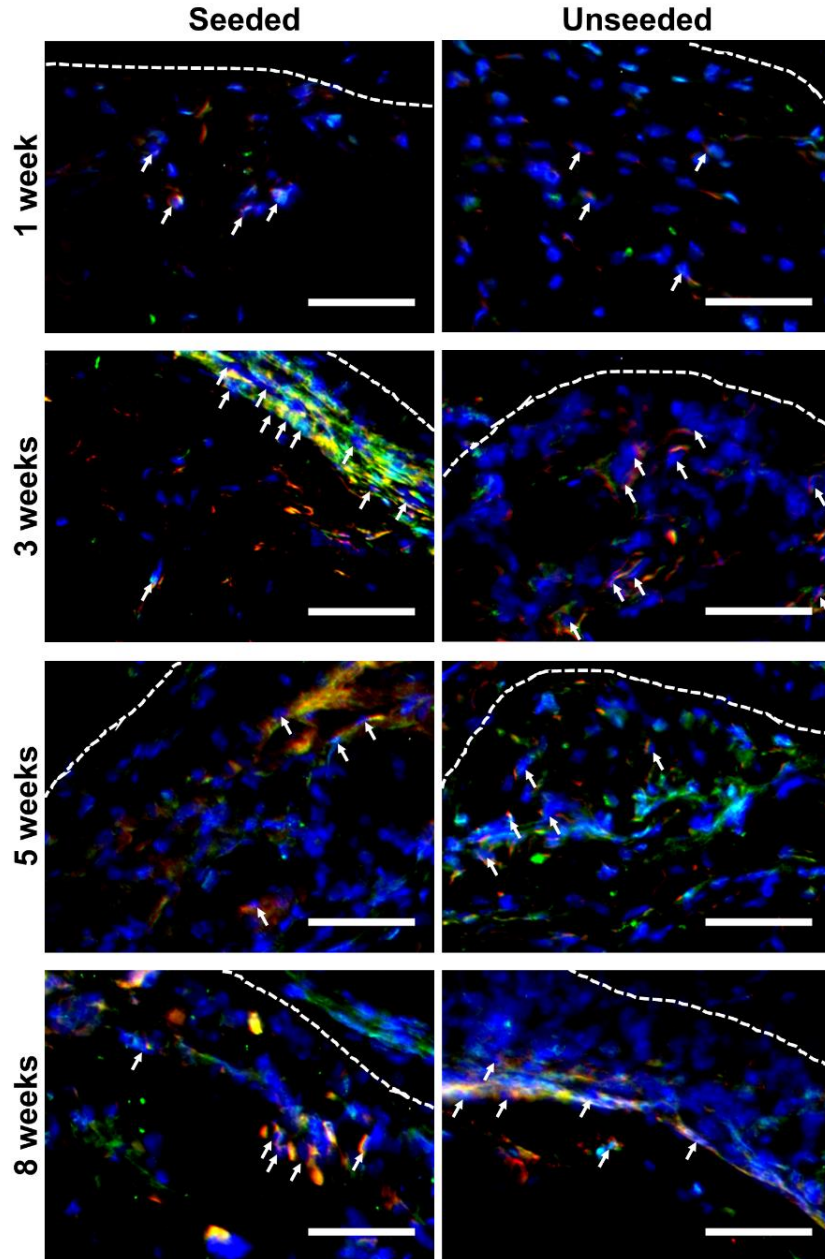


**Figure 4.17. Myeloid cell expression patterns of iNOS appear similar between seeded and unseeded DAT scaffolds.** EGFP<sup>+</sup> myeloid cells were observed to express iNOS at all time points in both seeded (left panels) and unseeded (right panels) implants. N=5-6 implants/scaffold group/time point. Dotted line: scaffold periphery. Blue: cell nuclei, green: EGFP, red: iNOS. Arrows: EGFP<sup>+</sup>iNOS<sup>+</sup>DAPI<sup>+</sup> cells. Scale: 50  $\mu$ m.

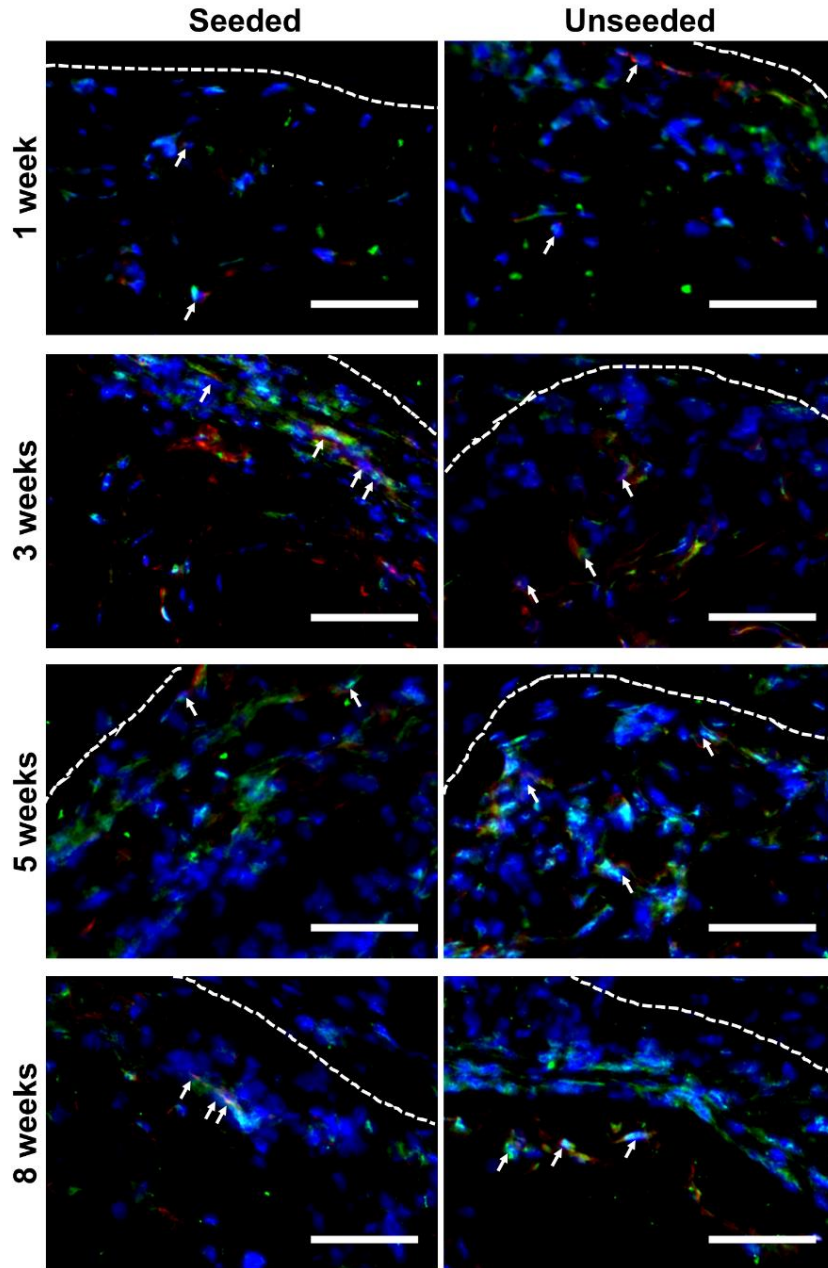


**Figure 4.18. Myeloid cell expression patterns of Arg-1 appear similar between seeded and unseeded DAT scaffolds.** EGFP<sup>+</sup> myeloid cells were observed to express Arg-1 at all time points in both seeded (left panels) and unseeded (right panels) implants. Dotted line: scaffold periphery. N=5-6 implants/scaffold group/time point. Blue: cell nuclei, green: EGFP, red: Arg-1. Arrows: EGFP<sup>+</sup>Arg-1<sup>+</sup>DAPI<sup>+</sup> cells. Scale: 50  $\mu$ m.

## Chapter 5

### 5 Discussion

Adipose-derived stem/stromal cells (ASCs) represent a clinically-translational cell source that can secrete beneficial paracrine factors with the capacity to promote tissue regeneration [126, 127]. Previous work from the Flynn laboratory has demonstrated that decellularized adipose tissue (DAT) scaffolds are a promising ASC delivery platform to promote *in vivo* adipose tissue regeneration for applications in plastic and reconstructive surgery [4]. However, a detailed understanding of the mechanisms of ASC-mediated tissue regeneration and the role of extracellular matrix (ECM)-derived scaffolds are critical for designing improved strategies that ensure stable and predictable regeneration. In the present work, dual transgenic reporter mouse models were applied to track and characterize syngeneic donor ASCs and infiltrating myeloid cell populations in tandem. The results demonstrated that the donor ASCs were retained over the course of the 8-week study and enhanced total cell recruitment and adipogenesis within the subcutaneously-implanted DAT scaffolds.

The first phase of this study involved developing protocols to isolate, culture, and characterize mouse ASCs, which had not been previously done in the Flynn laboratory. In contrast to human ASCs, mouse ASCs are much less well-characterized. In addition, methodological details for mouse ASC isolation and culture are often lacking in published studies, including the specific fat depots that are used. For the present work, initial emphasis was placed on isolating ASCs from the epididymal fat pad of the dsRed mice, which is a large depot that was used as the cell source in previous studies in the Wistar rat model [4, 182]. However, the mouse ASCs isolated from this depot did not expand well in culture, and cell death frequently occurred between passage 2 and passage 4. In an attempt to improve cell expansion and survival, a number of variables were explored, including different media formulations and flask coatings with Matrigel or fibronectin, but these appeared to have little impact on long-term cell viability and proliferation. Subsequently, the inguinal fat depot was explored as an alternative ASC source. The inguinal ASCs could be expanded more readily in culture, particularly by



using specially treated Primaria<sup>TM</sup> flasks to promote cell attachment for initial plating of the cells after isolation, as well as seeding flasks at relatively high cell densities (6,000-7,000 cells/cm<sup>2</sup>) when passaging. As such, the inguinal depot was selected for ASC isolations and was used in all experiments thereafter. Characterization of the inguinal depot-derived ASCs showed that these cells expressed mesenchymal cell surface markers, and could be induced to differentiate in culture along the adipogenic, osteogenic, and chondrogenic lineages, concordant with previous observations [105, 106, 319-323]. Further, protocols were established for dynamic seeding of the DAT scaffolds using ASCs sourced from the inguinal depot of the dsRed mice.

For the *in vivo* studies, DAT scaffolds seeded with dsRed<sup>+</sup> ASCs were subcutaneously implanted along with unseeded controls into syngeneic MacGreen mice. Histological assessment of the implants revealed a thin layer of fibrous connective tissue surrounding both the seeded and unseeded scaffolds. The fibrous layer may have formed due to an initial foreign body response or potentially due to movement of the implant within the subcutaneous space [324]. Qualitatively, the implant volume appeared to be relatively consistent over time, with the exception of the seeded scaffold group at 8 weeks. At this time point, the ASC-seeded scaffolds appeared to be slightly contracted, which may have been associated with increased cell infiltration and remodelling observed by Masson's trichrome staining. However, given that the DAT is highly hydrated, deformable, and can become remodeled and integrated with the surrounding tissues over time, long-term volume retention is difficult to measure quantitatively. Potentially, body composition analysis with cone beam volumetric  $\mu$ CT imaging could be applied in future work to perform longitudinal tracking of the implant volume [325].

In assessing total cell recruitment, ASC-seeding was shown to increase host cell infiltration into the DAT scaffolds relative to the low levels of infiltration observed in the unseeded controls. The low degree of cell infiltration within the unseeded DAT is in agreement with a previous study using a viscous DAT suspension prepared from human lipoaspirates, which showed similar low levels of cell infiltration at 7 weeks after subcutaneous injection in mice [175]. While both donor ASCs and myeloid cells were investigated in the present study, other cell types that may be present within the implants

include fibroblasts, pericytes, endothelial cells, host ASCs or MSCs, more committed adipogenic progenitors, and other leukocyte populations. The increase in total cell recruitment that was observed within the seeded scaffolds may be due to secretion of chemotactic factors by the ASCs, such as chemokine (C-C motif) ligand (CCL)-2,3,4,7 and -12 associated with leukocyte recruitment [12, 13]. In addition, chemokine (C-X-C) motif ligand 12 (CXCL-12), also termed stromal-derived factor-1, has been implicated as a chemokine involved in MSC homing to sites of injury [326]. Moreover, work by Stuermer *et al.* identified CXCL-12 as a key factor that induced ASC migration, with antibody neutralization of the CXCL-12 receptors C-X-C chemokine receptor (CXCR)-4 and CXCR7 significantly inhibiting the ASC migratory capacity [327]. While these studies suggest that leukocyte populations and MSCs may be recruited by ASCs to the DAT, further experiments are required in order to elucidate the different cell types present within the implants, and the mechanisms for recruitment.

ASC-seeding of ECM-derived scaffolds has been shown to enhance tissue regeneration for a number of applications, including for repair of cartilage defects and damaged myocardium, as well as for wound healing and adipose tissue regeneration [4, 276, 328-330]. A previous study from the Flynn laboratory demonstrated that seeding the DAT with allogeneic ASCs enhanced angiogenesis and adipogenesis within DAT scaffolds implanted subcutaneously in immunocompetent Wistar rats [4]. In the present study, while quantitative measurements showed that fat formation was also enhanced in the ASC-seeded group using the syngeneic transgenic mouse model, on average, greater fat formation was observed within the rat model at 8 weeks. These differences may be related to species variability in terms of the host response to the DAT as well as ASC function.

In order to investigate donor dsRed<sup>+</sup> ASC retention, immunohistochemical staining was performed to probe for dsRed within the implants. The staining results showed that the syngeneic ASCs appeared to be retained over the course of the 8 week study. Variable levels of dsRed staining were observed within the seeded implants, which may be due to donor ASC migration or cell death, or possible regional variations in ASC localization. Nonetheless, significant differences in the percentage area of dsRed staining were

observed in the seeded versus unseeded scaffolds at 8 weeks post-implantation, with the levels suggesting that the donor cells were retained within the implants over the duration of the study. Relatively few studies to date have quantitatively examined cell retention within decellularized scaffolds over time; however, these studies are important to both assess the efficacy of the delivery platform and the mechanisms of regeneration. The findings of the present work are consistent with a study by Sharma *et al.* who demonstrated the retention of autologous bone marrow-derived MSCs (bmMSCs) over 10 weeks within decellularized small intestinal submucosa (SIS) scaffolds in a baboon bladder regeneration model [202]. Overall, these results are promising, particularly given that poor retention of donor MSCs delivered in suspension has been identified as a key hurdle limiting the therapeutic efficacy of these cells [200, 201].

Immunohistochemical analysis of the dsRed<sup>+</sup> donor ASCs also revealed that newly formed adipocytes within the implants did not stain positive for dsRed, suggesting that these tissues were host-derived. In the previous study from our laboratory using the subcutaneous rat model, allogeneic donor ASCs were also shown to support fat formation through indirect mechanisms, as the donor cells qualitatively declined within the seeded implants at 4 and 8 weeks, becoming undetectable at 12 weeks [4]. Since syngeneic ASCs were used in the present work, the accelerated decline in the donor ASC population within the rat study may be related to a host response to the allogeneic cells. Work from other groups has also supported the indirect mechanisms of donor ASCs, since the subcutaneous delivery of human adipose-derived cell populations within ECM-derived hydrogels enhanced host-derived adipogenesis in immune-compromised mouse models [189, 331]. More specifically, staining for human-specific markers revealed that the human cells did not co-localize with newly formed adipocytes in these studies [189, 331]. Collectively, these results suggest that paracrine factor secretion may be a predominant mechanism through which ASCs promote adipogenesis within a tissue-engineering context.

As an additional method for donor cell tracking, *in vivo* optical imaging was performed to measure the levels of dsRed fluorescence within the implant regions over time, based on promising preliminary findings with *in vitro* cultured ASC-seeded DAT scaffolds. The *in*

*in vivo* experiments revealed differences in fluorescence between the seeded and unseeded scaffolds at 24 h, 72 h, 3, and 5 weeks post-implantation, but not at the 1 and 8 week time points. The failure of the optical imaging strategy to corroborate the immunohistochemical results may be related to changes in the hair growth cycle, resulting in darkening of the mouse skin pigment observed at some of the time points. Indeed, the optimal window for fluorescent detection using *in vivo* optical systems is between approximately 600 nm and 900 nm [332]. At wavelengths below 600 nm, light scattering and absorption by endogenous chromophores (such as melanin and haemoglobin) can impede signal acquisition [332]. The peak excitation and emission wavelengths for dsRed are 557 nm and 592 nm respectively, and thus do not fall within the range of the optimal window. As such, changes in skin colouring or hair growth may have negatively impacted signal acquisition. Moreover, at 8 weeks post-implantation, the seeded implants appeared partially contracted, and the donor dsRed<sup>+</sup> ASCs had migrated farther into the interior of the implant, which may have also contributed to the reduced signal at this time point. In future studies, bioluminescence imaging could be explored using ASCs genetically engineered to express luciferase, as this would likely give a more robust signal relative to fluorescent proteins [332].

In order to investigate the infiltration of myeloid cells into the DAT scaffolds, initial experiments focused on staining for enhanced green fluorescent protein (EGFP), expressed by myeloid cells in the MacGreen mouse model [25, 26], along with co-staining for Iba1, a marker expressed by monocytes and macrophages [314, 315]. ASC-seeding of the DAT was found to partially influence the infiltration of Iba1<sup>+</sup> myeloid cells as a significantly greater number of EGFP<sup>+</sup>Iba1<sup>+</sup> cells were detected along the implant periphery within the seeded versus unseeded implants at 3 weeks post-implantation. This suggests that the donor ASCs may have secreted chemotactic factors that increased myeloid cell infiltration. In support of this, Chen *et al.* demonstrated that the conditioned medium obtained from mouse bmMSCs cultured under hypoxic conditions significantly enhanced the *in vitro* migration of peripheral blood-derived CD14<sup>+</sup> human monocytes [333]. Additionally, the bmMSC medium contained high levels of CCL-3 and CCL-4, and subcutaneous injection of the conditioned media in a mouse excisional wound model

selectively increased infiltration of F4/80<sup>+</sup> macrophages, but not Gr1<sup>+</sup> (granulocyte marker) or CD3<sup>+</sup> (T cell marker) cells within the wounds relative to control medium or conditioned media obtained from fibroblast culture [333]. Macrophage recruitment by ASCs is an emerging area of interest, and the *in vivo* studies to date have focused primarily on assessing the effects of ASCs and MSCs on macrophage phenotype, rather than recruitment. In the previous study from our laboratory using the subcutaneous rat model, quantitative assessment of CD68<sup>+</sup> macrophages showed similar levels between ASC-seeded and unseeded DAT scaffolds and macrophage numbers remained relatively consistent between 1 and 12 weeks post-implantation, albeit changes in phenotype were noted [4]. In the current mouse study, the altered macrophage infiltration kinetics observed between time points and implant groups may also be related to species differences in terms of ASC function and the host response to the DAT. Importantly, the quantitative cell counting performed here was completed using 20X images taken along the implant periphery in order to control for the variable degrees of cell infiltration toward the interior of the implant. While further analysis could be performed on regions closer to the interior, in the majority of the implants, there was minimal or no cell infiltration beyond the border of the regions analyzed.

Analysis of the fraction of EGFP<sup>+</sup>Iba1<sup>+</sup> cells relative to the total cells counted along the implant periphery demonstrated a peak in this cell population within both the seeded and unseeded implants at 3 weeks. At this time point, EGFP<sup>+</sup>Iba1<sup>+</sup> cells represented >60% of the total nucleated cell population compared to approximately 10-20% at the 1, 5, and 8 week time points. Moreover, co-staining for EGFP with the M1 macrophage marker inducible nitric oxide synthase (iNOS) showed that qualitatively, the majority of infiltrating macrophages at 3 weeks were pro-inflammatory M1-like cells. Together these data suggest that the peak inflammatory response occurred at 3 weeks and had partially resolved by 5 and 8 weeks post-implantation, as the levels of macrophages declined within the implant region. Indeed, clearance of macrophages is crucial for the resolution of acute inflammation [334]; however, the mechanisms responsible for macrophage clearance are not clear. Some reports have suggested that macrophage efflux into neighbouring lymph nodes is a predominant mechanism by which macrophages decline

within a tissue [335, 336], while others have shown that local apoptosis may be the primary mechanism of clearance in the lung and peritoneum [337, 338]. As such, investigation into the apparent decline in the macrophage population between 3 and 5 weeks may present an interesting avenue of investigation for future studies.

The EGFP and Iba1 co-staining results also identified a small population of EGFP<sup>+</sup>Iba1<sup>-</sup> cells within the implants. Moreover, ASC-seeding appeared to accelerate the decline in this cell population relative to the unseeded controls. Given that EGFP expression is controlled by the macrophage colony-stimulating factor 1 receptor (*Csf1r*) promoter in the MacGreen model [26], the EGFP<sup>+</sup>Iba1<sup>-</sup> cells could represent a heterogeneous cell population. Notably, neutrophils express EGFP in the MacGreen model [25], and likely represent a fraction of the EGFP<sup>+</sup>Iba1<sup>-</sup> population as neutrophils do not express the Iba1 marker [316, 317]. In humans, neutrophils are typically cleared from injured or infected tissues within 3-5 days of the initial insult [261]. However, in mouse models, these cells can persist for longer periods of time [339]. For example, in mouse models of spinal cord injury, neutrophils are observed to persist at the injured site and a second peak of neutrophil infiltration can occur several weeks after injury during the process of tissue repair [340, 341]. Other cell types that may contribute to the EGFP<sup>+</sup>Iba1<sup>-</sup> cell population may include dendritic cells [26] and myeloid-derived suppressor cells [25], each of which have been shown to express low levels of EGFP within the MacGreen model [25, 26] and are involved in regulating the T cell response. Ultimately, further characterization studies would be required in order to elucidate the different myeloid cell types that may be involved and their potential roles in implant remodeling.

Finally, staining for EGFP in conjunction with either the M1 macrophage marker iNOS, or the M2 marker arginase-1 (Arg-1) was performed in adjacent tissue sections to examine macrophage phenotypes within the ASC-seeded and unseeded DAT implants. iNOS and Arg-1 staining were observed within EGFP<sup>+</sup> myeloid cells at all time points examined, and qualitatively, the expression patterns appeared similar between the seeded and unseeded groups. More specifically, a larger proportion of EGFP<sup>+</sup>iNOS<sup>+</sup> cells was observed, with low levels of EGFP<sup>+</sup>Arg-1<sup>+</sup> cells at all time points. The process of tissue repair and regeneration is associated with a shift from pro-inflammatory M1-polarized

macrophages to predominantly M2-polarized macrophages involved in regulating inflammation and tissue remodeling [342]. Moreover, ASCs have been shown to aid in this process by promoting an M2 macrophage phenotype [9, 11, 135]. Thus, the finding that EGFP<sup>+</sup>iNOS<sup>+</sup> cells appeared in greater numbers than EGFP<sup>+</sup>Arg-1<sup>+</sup> cells requires further study, particularly given that the robust infiltration of EGFP<sup>+</sup>Iba1<sup>+</sup> cells at 3 weeks appeared to diminish at 5 and 8 weeks post-implantation, suggesting that the pro-inflammatory response had partially resolved. Potentially, investigation into time points between 3 and 5 weeks would reveal an increase in M2-like macrophages that may have played a role in dampening the inflammatory response observed at the 3 week time point. Alternatively, M2-polarized macrophages may predominate at time points beyond 8 weeks post-implantation, as was found in the previous rat study from our laboratory [4]. These additional experiments would also help to determine whether ASCs influenced macrophage phenotype within the seeded implants.

## Chapter 6

### 6 Conclusions and Future Directions

#### 6.1 Summary of findings

In the first objective, methods were established to isolate adipose-derived stem/stromal cells (ASCs) from the inguinal fat pads of dsRed mice, and cell surface markers were characterized along with assessment of multilineage differentiation capacity. Flow cytometry results revealed that the ASCs expressed high levels of the stromal cell markers CD29, CD44, and CD90 as expected. In addition, the lack of positive staining for CD31 and CD45 precluded contamination by endothelial cells and leukocytes, respectively. Further, the mouse ASCs were shown to differentiate along the adipogenic, osteogenic, and chondrogenic lineages. Culture of ASCs in adipogenic differentiation media for 14 days showed increased intracellular lipid accumulation characteristic of developing adipocytes, as assessed through oil red O staining, relative to non-induced controls maintained in proliferation medium. The induced adipogenic cultures also displayed significantly increased activity of the lipogenic enzyme glycerol 3-phosphate dehydrogenase (GPDH) compared to controls. In terms of osteogenic differentiation, significantly increased activity of the enzyme alkaline phosphatase (ALP), an early marker of osteogenesis, was observed after 7 days of culture in osteogenic medium relative to non-induced controls. Moreover, small mineral deposits could be detected in the induced osteogenic cultures but not controls after 28 days of culture. Chondrogenic differentiation was performed by culturing the ASCs in 3D cell aggregates, and induced aggregate cultures were shown to express a qualitatively higher ratio of collagen II to collagen I relative to non-induced controls, indicative of chondrogenic differentiation. Finally, a pilot study was performed in order to verify the attachment of mouse ASCs to decellularized adipose tissue (DAT) scaffolds under dynamic seeding conditions. Qualitative visualization of ASC attachment at three different seeding densities ( $0.5 \times 10^6$  ASCs/scaffold,  $1 \times 10^6$  ASCs/scaffold, and  $2 \times 10^6$  ASCs/scaffold) showed greater levels of attachment at higher seeding densities. A seeding density of  $2 \times 10^6$  ASCs/scaffold was



selected for subsequent *in vivo* studies since this density provided a more homogenous ASC distribution along the scaffold periphery.

After initial characterization of the dsRed<sup>+</sup> mouse ASCs, experiments focused on assessing the *in vivo* response to ASC-seeded DAT scaffolds and unseeded controls implanted in syngeneic MacGreen mice at 72 h, 1, 3, 5, and 8 weeks post-implantation. For the second objective, Masson's trichrome staining was performed to assess total cell infiltration and tissue remodeling within the implants. Quantitative measurements of total cell recruitment revealed a significant increase in the fraction of the implant infiltrated by cells within the ASC-seeded versus unseeded implants at 8 weeks post-implantation. In addition, quantitative analysis of adipose tissue remodeling showed that adipocytes were present in a greater number of ASC-seeded implants at 1, 3, 5, and 8 weeks post-implantation relative to unseeded controls. The seeded implants also showed a greater percentage of adipose tissue remodeling at 3, 5, and 8 weeks compared to the unseeded group.

The third objective focused on assessing dsRed<sup>+</sup> donor cell retention in the DAT implants over time using immunohistochemistry and *in vivo* optical imaging.

Immunohistochemical staining at the 72 h, 1, 3, 5, and 8 week time points showed positive staining for dsRed in the seeded implants at all time points, with no positive staining in the unseeded controls. Quantitative measurements of the percentage of positively stained area confirmed that the syngeneic donor ASCs were retained in the majority of seeded implants over the course of the 8 week study. Using an optical imaging strategy to measure levels of dsRed fluorescence, an *in vitro* pilot study showed that differences in dsRed fluorescence could be observed in scaffolds seeded with varying densities of ASCs. However, when this strategy was applied *in vivo* to assess the levels of dsRed fluorescence within seeded and unseeded implant regions, the data only partially corroborated the immunohistochemical findings. More specifically, significant differences in the levels of dsRed fluorescence were obtained in comparing the ASC-seeded and unseeded implant regions at 24 h, 72 h, 3, and 5 weeks post-implantation, but a significant decline in fluorescence was observed at the 1 and 8 week time points. This inconsistency was likely due to darkening of the mouse skin that influenced light

scattering and absorption at 1 week, along with potential changes in the implant morphology at 8 weeks that may have impeded signal acquisition.

The final objective was to investigate the infiltrating enhanced green fluorescent protein (EGFP<sup>+</sup>) myeloid cell population within the ASC-seeded and unseeded DAT scaffolds at 1, 3, 5, and 8 weeks post-implantation in the MacGreen mouse model.

Immunohistochemical co-staining for EGFP and the monocyte/macrophage marker Iba1 suggested that macrophage infiltration peaked along the implant periphery within both the seeded and unseeded scaffolds at 3 weeks post-implantation. This population subsequently declined at the 5 and 8 week time points. Macrophage recruitment appeared to be augmented within the ASC-seeded implants relative to the unseeded controls at 3 weeks, as significantly greater numbers of EGFP<sup>+</sup>Iba1<sup>+</sup> cells were noted in the seeded group at this time point. Qualitative assessment of the pro-inflammatory M1 macrophage marker inducible nitric oxide synthase (iNOS) appeared to show relatively high levels of expression within EGFP<sup>+</sup> myeloid cells in both scaffold groups at each of the time points examined. Relative to iNOS, the M2 macrophage marker arginase-1 (Arg-1) was less frequently observed within the seeded and unseeded implants at each time point. There did not appear to be major differences in the levels of iNOS and Arg-1 expression when qualitatively comparing the ASC-seeded and unseeded implants.

## 6.2 Conclusions

Overall, these findings support the combined use of DAT and ASCs for adipose tissue engineering applications. Robust protocols were established to isolate and culture the mouse ASCs from the inguinal adipose tissue depot. A detailed characterization of the ASCs provided a more in-depth understanding of the cell population used to stimulate regeneration within the DAT scaffolds. ASC-seeding of the DAT scaffolds was shown to augment total cell recruitment and adipogenesis within the implants without contributing directly to the newly formed adipocytes. In addition, the syngeneic donor ASCs were retained within the DAT scaffolds over the course of the 8 week study, further supporting the use of DAT scaffolds as a cell delivery vehicle. The characterization of infiltrating myeloid cell populations requires further study, but suggests that donor ASCs may have

influenced myeloid cell infiltration kinetics. Taken together, these findings provide additional evidence supporting the use of DAT scaffolds for adipose tissue regeneration. The use of the dsRed and MacGreen transgenic mouse models facilitated tracking of the donor ASCs and infiltrating myeloid cells, and aids with investigation into regenerative mechanisms.

### 6.3 Future recommendations

In future work, the Masson's trichrome and immunohistochemical staining should be repeated using multiple sections throughout the implants in order to account for potential regional variations in tissue remodeling, total cell recruitment, ASC retention, and macrophage recruitment. In addition, it would be interesting to investigate other cell types that infiltrate the DAT scaffolds, such as adipogenic progenitors, which could be identified through co-staining for CD34<sup>+</sup>CD29<sup>+</sup>CD24<sup>+</sup> cells [343]. Angiogenesis could also be further explored by performing blood vessel counts within the Masson's trichrome stained sections, or by staining for markers such as CD31 and vascular endothelial growth factor (VEGF).

In assessing the host response to the ASC-seeded and unseeded DAT scaffolds, future work should focus on identifying other populations of immune cells that may be present within the DAT. In particular, experiments should be performed to examine the EGFP<sup>+</sup>Iba1<sup>-</sup> cells to identify more specifically the myeloid cell types within this population. More specifically, immunohistochemical staining for neutrophil markers (such as Ly6G or neutrophil elastase) could be performed with EGFP co-staining. As T cells have also been shown to mediate remodeling of extracellular matrix (ECM)-derived scaffolds [277], staining for innate  $\gamma\delta$  T cells and adaptive CD3<sup>+</sup>CD4<sup>+</sup> T helper cells and CD3<sup>+</sup>CD8<sup>+</sup> cytotoxic T cells could be performed, along with co-staining for CD4<sup>+</sup>CD25<sup>+</sup>FOXP3<sup>+</sup> for regulatory T cells [344]. These additional experiments would aid in furthering the understanding of the potential immunomodulatory role of the donor ASCs. To supplement immunohistochemical staining experiments, western blotting could be performed to assess protein levels of pro- and anti-inflammatory cytokines, such as tumour necrosis factor-alpha (TNF $\alpha$ ) and interleukin (IL)-10, within the ASC-seeded and

unseeded implants. In addition, flow cytometry could be performed in future work using collagenase-digested implants in order to more quantitatively assess the abundance of different cell types that may be present within the scaffolds. Alternatively, laser capture microdissection could be applied in order to extract dsRed<sup>+</sup> donor ASCs and EGFP<sup>+</sup> myeloid cells from the implants for further characterization with reverse transcription quantitative PCR [345].

Given that significant differences were observed between the ASC-seeded and unseeded implants in terms of total cell recruitment, as well as macrophage recruitment, further immunohistochemical staining could be performed to examine the expression of chemotactic factors. This could be done by staining for dsRed to identify the donor ASCs, along with co-staining for chemotactic factors such as chemokine C-X-C motif ligand 12 (CXCL-12), which has been implicated in the recruitment of leukocyte and MSC populations [12, 13, 326].

With respect to studies that could be performed in the long-term, methods to further enhance fat formation within the DAT scaffolds should be explored using the mouse models applied in this study. This may allow for more apparent differences between the seeded and unseeded implants in terms of adipose tissue remodeling and the host response. For example, DAT scaffolds could be implanted into the inguinal region of the mouse since the scaffold would be adjacent to the femoral and epigastric arteries, which may allow for enhanced recruitment of progenitor cell populations and immune cells. Further, this is also the location from which the donor ASCs are obtained, and this may influence recruitment of progenitors and other cell types from neighbouring tissues since the donor ASCs would be in close proximity to their native fat depot. Alternatively, Kelly *et al.* have developed an *in vivo* model for engineered adipogenesis by using the superficial epigastric artery as a vascular pedicle within a silicone-encased Matrigel chamber [346]. A similar technique could be applied by surgically implanting the DAT scaffolds to encircle the epigastric artery.

Besides investigating alternative implantation sites, strategies could be explored to alter donor ASC function as a potential means to augment adipose tissue regeneration. For

example, ASC-seeded DAT scaffolds could be cultured in adipogenic differentiation medium to pre-differentiate the syngeneic ASCs prior to implantation. This technique was explored in a study by Cho *et al.*, in which human ASC-seeded fibrin scaffolds were implanted subcutaneously into athymic mice, showing enhanced adipogenesis in the pre-differentiated versus undifferentiated groups [347]. Alternatively, ASC-seeded DAT scaffolds could be cultured under hypoxic conditions prior to implantation. While hypoxic exposure has been shown to inhibit adipogenic differentiation of ASCs [348], there are studies to suggest that hypoxia can enhance the secretion of angiogenic and immunomodulatory factors [349, 350]. Since the current study suggests that the donor ASCs did not contribute directly to newly formed adipocytes, augmented paracrine factor secretion through hypoxic pre-conditioning could be an interesting avenue of exploration.

Additional strategies to enhance fat formation could include the addition of growth factors to the DAT prior to implantation. In particular, incorporating basic fibroblast growth factor (bFGF) into collagen [351, 352] or gelatin-based [353] scaffolds has been shown to augment adipogenesis after subcutaneous implantation in mice. bFGF is a potent mitogen and chemoattractant, and has been shown to promote angiogenesis and adipogenesis *in vivo* [352, 354]. Co-delivery of bFGF and ASCs within the DAT may have an additive effect in promoting adipogenesis, as was reported using bFGF-loaded fibrin scaffolds pre-seeded with ASCs and implanted subcutaneously into mice [347]. As an alternative approach, mouse ASCs could be genetically engineered to overexpress bFGF prior to delivery. Genetically engineered ASCs could allow for more stable growth factor delivery over time given that the syngeneic ASCs appeared to be well-retained within the DAT over the course of the present study.

In addition to investigating methods to enhance fat formation, a cell type control could be included as an additional experimental group in order to further elucidate the effects of the donor ASCs relative to another cell type. For example, the DAT scaffolds could be seeded with syngeneic dermal fibroblasts, since these cells function primarily to secrete ECM, and are much more limited in terms of their ability to secrete immunomodulatory and angiogenic factors [355, 356]. Alternatively, a comparison study could be performed

in order to assess the effects of MSCs isolated from different tissue sources (such as adipose, bone marrow, and cord blood) on tissue regeneration within the DAT implants.

## References

1. Patrick CW, Jr. Adipose tissue engineering: the future of breast and soft tissue reconstruction following tumor resection. *Semin Surg Oncol*. 2000;19(3):302-11.
2. Patrick CW, Jr. Tissue engineering strategies for adipose tissue repair. *Anat Rec*. 2001;263(4):361-6.
3. Flynn L, Woodhouse KA. Adipose tissue engineering with cells in engineered matrices. *Organogenesis*. 2008;4(4):228-35.
4. Han TT, Toutounji S, Amsden BG, Flynn LE. Adipose-derived stromal cells mediate in vivo adipogenesis, angiogenesis and inflammation in decellularized adipose tissue bioscaffolds. *Biomaterials*. 2015;72:125-37.
5. Flynn LE. The use of decellularized adipose tissue to provide an inductive microenvironment for the adipogenic differentiation of human adipose-derived stem cells. *Biomaterials*. 2010;31(17):4715-24.
6. Gonzalez-Rey E, Gonzalez MA, Varela N, O'Valle F, Hernandez-Cortes P, Rico L, et al. Human adipose-derived mesenchymal stem cells reduce inflammatory and T cell responses and induce regulatory T cells in vitro in rheumatoid arthritis. *Ann Rheum Dis*. 2010;69(1):241-8.
7. Manning CN, Martel C, Sakiyama-Elbert SE, Silva MJ, Shah S, Gelberman RH, et al. Adipose-derived mesenchymal stromal cells modulate tendon fibroblast responses to macrophage-induced inflammation in vitro. *Stem Cell Res Ther*. 2015;6(1):74.
8. Adutler-Lieber S, Ben-Mordechai T, Naftali-Shani N, Asher E, Loberman D, Raanani E, et al. Human Macrophage Regulation Via Interaction With Cardiac Adipose Tissue-Derived Mesenchymal Stromal Cells. *J Cardiovasc Pharmacol Ther*. 2012;18(1):78-86.
9. Rybalko V, Hsieh PL, Ricles LM, Chung E, Farrar RP, Suggs LJ. Therapeutic potential of adipose-derived stem cells and macrophages for ischemic skeletal muscle repair. *Regen Med*. 2017;12(2):153-67.
10. Manferdini C, Paoletta F, Gabusi E, Gambari L, Piacentini A, Filardo G, et al. Adipose stromal cells mediated switching of the pro-inflammatory profile of M1-like macrophages is facilitated by PGE2: in vitro evaluation. *Osteoarthritis Cartilage*. 2017;25(7):1161-71.
11. Dong Z, Peng Z, Chang Q, Lu F. The survival condition and immunoregulatory function of adipose stromal vascular fraction (SVF) in the early stage of nonvascularized adipose transplantation. *PLoS One*. 2013;8(11):e80364.

12. Ren G, Zhao X, Wang Y, Zhang X, Chen X, Xu C, et al. CCR2-dependent recruitment of macrophages by tumor-educated mesenchymal stromal cells promotes tumor development and is mimicked by TNFalpha. *Cell Stem Cell*. 2012;11(6):812-24.
13. Chen L, Tredget EE, Wu PY, Wu Y. Paracrine factors of mesenchymal stem cells recruit macrophages and endothelial lineage cells and enhance wound healing. *PLoS One*. 2008;3(4):e1886.
14. Thomas GP, Hemmrich K, Abberton KM, McCombe D, Penington AJ, Thompson EW, et al. Zymosan-induced inflammation stimulates neo-adipogenesis. *Int J Obes (Lond)*. 2008;32(2):239-48.
15. Lilja HE, Morrison WA, Han XL, Palmer J, Taylor C, Tee R, et al. An adipoinductive role of inflammation in adipose tissue engineering: key factors in the early development of engineered soft tissues. *Stem Cells Dev*. 2013;22(10):1602-13.
16. Debels H, Galea L, Han XL, Palmer J, van Rooijen N, Morrison W, et al. Macrophages play a key role in angiogenesis and adipogenesis in a mouse tissue engineering model. *Tissue Eng Part A*. 2013;19(23-24):2615-25.
17. Weisberg SP, McCann D, Desai M, Rosenbaum M, Leibel RL, Ferrante AW, Jr. Obesity is associated with macrophage accumulation in adipose tissue. *J Clin Invest*. 2003;112(12):1796-808.
18. Lumeng CN, Bodzin JL, Saltiel AR. Obesity induces a phenotypic switch in adipose tissue macrophage polarization. *J Clin Invest*. 2007;117(1):175-84.
19. Greenberg AS, Obin MS. Obesity and the role of adipose tissue in inflammation and metabolism. *Am J Clin Nutr*. 2006;83(2):461s-5s.
20. Ouchi N, Parker JL, Lugus JJ, Walsh K. Adipokines in inflammation and metabolic disease. *Nat Rev Immunol*. 2011;11(2):85-97.
21. Kuljanin M, Brown CFC, Raleigh MJ, Lajoie GA, Flynn LE. Collagenase treatment enhances proteomic coverage of low-abundance proteins in decellularized matrix bioscaffolds. *Biomaterials*. 2017;144:130-43.
22. Omid E, Fuetterer L, Reza Mousavi S, Armstrong RC, Flynn LE, Samani A. Characterization and assessment of hyperelastic and elastic properties of decellularized human adipose tissues. *J Biomech*. 2014;47(15):3657-63.
23. Haddad SM, Omid E, Flynn LE, Samani A. Comparative biomechanical study of using decellularized human adipose tissues for post-mastectomy and post-lumpectomy breast reconstruction. *Journal of the mechanical behavior of biomedical materials*. 2016;57:235-45.



24. Vintersten K, Monetti C, Gertsenstein M, Zhang P, Laszlo L, Biechele S, et al. Mouse in red: red fluorescent protein expression in mouse ES cells, embryos, and adult animals. *Genesis (New York, NY : 2000)*. 2004;40(4):241-6.
25. Mooney JE, Summers KM, Gongora M, Grimmond SM, Campbell JH, Hume DA, et al. Transcriptional switching in macrophages associated with the peritoneal foreign body response. *Immunol Cell Biol*. 2014;92(6):518-26.
26. Sasmono RT, Oceandy D, Pollard JW, Tong W, Pavli P, Wainwright BJ, et al. A macrophage colony-stimulating factor receptor-green fluorescent protein transgene is expressed throughout the mononuclear phagocyte system of the mouse. *Blood*. 2003;101(3):1155-63.
27. Wronska A, Kmiec Z. Structural and biochemical characteristics of various white adipose tissue depots. *Acta Physiol (Oxf)*. 2012;205(2):194-208.
28. Esteve Rafols M. Adipose tissue: cell heterogeneity and functional diversity. *Endocrinologia y nutricion : organo de la Sociedad Espanola de Endocrinologia y Nutricion*. 2014;61(2):100-12.
29. Himms-Hagen J. Nonshivering thermogenesis. *Brain Res Bull*. 1984;12(2):151-60.
30. Hansen JB, Kristiansen K. Regulatory circuits controlling white versus brown adipocyte differentiation. *Biochem J*. 2006;398(2):153-68.
31. van Marken Lichtenbelt WD, Vanhomerig JW, Smulders NM, Drossaerts JM, Kemerink GJ, Bouvy ND, et al. Cold-activated brown adipose tissue in healthy men. *N Engl J Med*. 2009;360(15):1500-8.
32. Frayn KN, Karpe F, Fielding BA, Macdonald IA, Coppack SW. Integrative physiology of human adipose tissue. *Int J Obes Relat Metab Disord*. 2003;27(8):875-88.
33. Lass A, Zimmermann R, Oberer M, Zechner R. Lipolysis - a highly regulated multi-enzyme complex mediates the catabolism of cellular fat stores. *Prog Lipid Res*. 2011;50(1):14-27.
34. Brown BN, Freund JM, Han L, Rubin JP, Reing JE, Jeffries EM, et al. Comparison of three methods for the derivation of a biologic scaffold composed of adipose tissue extracellular matrix. *Tissue Eng Part C Methods*. 2011;17(4):411-21.
35. Bunnell BA, Flaat M, Gagliardi C, Patel B, Ripoll C. Adipose-derived stem cells: isolation, expansion and differentiation. *Methods*. 2008;45(2):115-20.
36. Baker GL. Human adipose tissue composition and age. *Am J Clin Nutr*. 1969;22(7):829-35.

37. Cinti S. Transdifferentiation properties of adipocytes in the adipose organ. *Am J Physiol Endocrinol Metab.* 2009;297(5):E977-86.
38. Gregoire FM, Smas CM, Sul HS. Understanding adipocyte differentiation. *Physiol Rev.* 1998;78(3):783-809.
39. Crandall DL, Hausman GJ, Kral JG. A review of the microcirculation of adipose tissue: anatomic, metabolic, and angiogenic perspectives. *Microcirculation.* 1997;4(2):211-32.
40. Romijn JA, Fliers E. Sympathetic and parasympathetic innervation of adipose tissue: metabolic implications. *Curr Opin Clin Nutr Metab Care.* 2005;8(4):440-4.
41. Trayhurn P. Adipocyte biology. *Obes Rev.* 2007;8 Suppl 1:41-4.
42. Trayhurn P, Beattie JH. Physiological role of adipose tissue: white adipose tissue as an endocrine and secretory organ. *Proc Nutr Soc.* 2001;60(3):329-39.
43. Fonseca-Alaniz MH, Takada J, Alonso-Vale MI, Lima FB. Adipose tissue as an endocrine organ: from theory to practice. *J Pediatr (Rio J).* 2007;83(5 Suppl):S192-203.
44. Park HK, Ahima RS. Physiology of leptin: energy homeostasis, neuroendocrine function and metabolism. *Metabolism.* 2015;64(1):24-34.
45. Yamauchi T, Kadowaki T. Physiological and pathophysiological roles of adiponectin and adiponectin receptors in the integrated regulation of metabolic and cardiovascular diseases. *Int J Obes (Lond).* 2008;32 Suppl 7:S13-8.
46. Ouchi N, Walsh K. Adiponectin as an anti-inflammatory factor. *Clinica chimica acta; international journal of clinical chemistry.* 2007;380(1-2):24-30.
47. Kaji H. Adipose Tissue-Derived Plasminogen Activator Inhibitor-1 Function and Regulation. *Comprehensive Physiology.* 2016;6(4):1873-96.
48. Trayhurn P, Wood IS. Adipokines: inflammation and the pleiotropic role of white adipose tissue. *Br J Nutr.* 2004;92(3):347-55.
49. Choi JH, Gimble JM, Lee K, Marra KG, Rubin JP, Yoo JJ, et al. Adipose tissue engineering for soft tissue regeneration. *Tissue Eng Part B Rev.* 2010;16(4):413-26.
50. Bauer-Kreisel P, Goepferich A, Blunk T. Cell-delivery therapeutics for adipose tissue regeneration. *Advanced drug delivery reviews.* 2010;62(7-8):798-813.
51. 2016 Plastic Surgery Statistics Report. American Society of Plastic Surgeons.
52. Young DA, Christman KL. Injectable biomaterials for adipose tissue engineering. *Biomed Mater.* 2012;7(2):024104.

53. Billings E, Jr., May JW, Jr. Historical review and present status of free fat graft autotransplantation in plastic and reconstructive surgery. *Plast Reconstr Surg.* 1989;83(2):368-81.
54. Kaufman MR, Miller TA, Huang C, Roostaeian J, Wasson KL, Ashley RK, et al. Autologous fat transfer for facial recontouring: is there science behind the art? *Plast Reconstr Surg.* 2007;119(7):2287-96.
55. Haneke E. Adverse effects of fillers and their histopathology. *Facial Plast Surg.* 2014;30(6):599-614.
56. El-Khalawany M, Fawzy S, Saied A, Al Said M, Amer A, Eassa B. Dermal filler complications: a clinicopathologic study with a spectrum of histologic reaction patterns. *Ann Diagn Pathol.* 2015;19(1):10-5.
57. Beahm EK, Walton RL, Patrick CW, Jr. Progress in adipose tissue construct development. *Clin Plast Surg.* 2003;30(4):547-58, viii.
58. Patrick CW, Jr., Zheng B, Johnston C, Reece GP. Long-term implantation of preadipocyte-seeded PLGA scaffolds. *Tissue Eng.* 2002;8(2):283-93.
59. Kang SW, Seo SW, Choi CY, Kim BS. Porous poly(lactic-co-glycolic acid) microsphere as cell culture substrate and cell transplantation vehicle for adipose tissue engineering. *Tissue Eng Part C Methods.* 2008;14(1):25-34.
60. Discher DE, Mooney DJ, Zandstra PW. Growth factors, matrices, and forces combine and control stem cells. *Science.* 2009;324(5935):1673-7.
61. Lin SD, Wang KH, Kao AP. Engineered adipose tissue of predefined shape and dimensions from human adipose-derived mesenchymal stem cells. *Tissue Eng Part A.* 2008;14(5):571-81.
62. Weiser B, Prantl L, Schubert TE, Zellner J, Fischbach-Teschl C, Spruss T, et al. In vivo development and long-term survival of engineered adipose tissue depend on in vitro precultivation strategy. *Tissue Eng Part A.* 2008;14(2):275-84.
63. Place ES, Evans ND, Stevens MM. Complexity in biomaterials for tissue engineering. *Nat Mater.* 2009;8(6):457-70.
64. von Heimburg D, Zachariah S, Heschel I, Kuhling H, Schoof H, Hafemann B, et al. Human preadipocytes seeded on freeze-dried collagen scaffolds investigated in vitro and in vivo. *Biomaterials.* 2001;22(5):429-38.
65. Itoi Y, Takatori M, Hyakusoku H, Mizuno H. Comparison of readily available scaffolds for adipose tissue engineering using adipose-derived stem cells. *J Plast Reconstr Aesthet Surg.* 2010;63(5):858-64.

66. Bellas E, Panilaitis BJ, Glettig DL, Kirker-Head CA, Yoo JJ, Marra KG, et al. Sustained volume retention in vivo with adipocyte and lipoaspirate seeded silk scaffolds. *Biomaterials*. 2013;34(12):2960-8.
67. Jaikumar D, Sajesh KM, Soumya S, Nimal TR, Chennazhi KP, Nair SV, et al. Injectable alginate-O-carboxymethyl chitosan/nano fibrin composite hydrogels for adipose tissue engineering. *Int J Biol Macromol*. 2015;74:318-26.
68. Halberstadt C, Austin C, Rowley J, Culberson C, Loeb sack A, Wyatt S, et al. A hydrogel material for plastic and reconstructive applications injected into the subcutaneous space of a sheep. *Tissue Eng*. 2002;8(2):309-19.
69. Robb KP, Shridhar A, Flynn LE. Decellularized matrices as cell-instructive scaffolds to guide tissue-specific regeneration. *ACS Biomaterials Science & Engineering*. 2017.
70. Friedenstein AJ, Piatetzky S, II, Petrakova KV. Osteogenesis in transplants of bone marrow cells. *J Embryol Exp Morphol*. 1966;16(3):381-90.
71. Friedenstein AJ, Petrakova KV, Kurolesova AI, Frolova GP. Heterotopic of bone marrow. Analysis of precursor cells for osteogenic and hematopoietic tissues. *Transplantation*. 1968;6(2):230-47.
72. Zuk PA, Zhu M, Ashjian P, De Ugarte DA, Huang JI, Mizuno H, et al. Human adipose tissue is a source of multipotent stem cells. *Mol Biol Cell*. 2002;13(12):4279-95.
73. Griffiths MJ, Bonnet D, Janes SM. Stem cells of the alveolar epithelium. *Lancet*. 2005;366(9481):249-60.
74. Beltrami AP, Barlucchi L, Torella D, Baker M, Limana F, Chimenti S, et al. Adult cardiac stem cells are multipotent and support myocardial regeneration. *Cell*. 2003;114(6):763-76.
75. Chong PP, Selvaratnam L, Abbas AA, Kamarul T. Human peripheral blood derived mesenchymal stem cells demonstrate similar characteristics and chondrogenic differentiation potential to bone marrow derived mesenchymal stem cells. *J Orthop Res*. 2012;30(4):634-42.
76. Toma JG, Akhavan M, Fernandes KJ, Barnabe-Heider F, Sadikot A, Kaplan DR, et al. Isolation of multipotent adult stem cells from the dermis of mammalian skin. *Nat Cell Biol*. 2001;3(9):778-84.
77. Strem BM, Hicok KC, Zhu M, Wulur I, Alfonso Z, Schreiber RE, et al. Multipotential differentiation of adipose tissue-derived stem cells. *Keio J Med*. 2005;54(3):132-41.
78. Corselli M, Chen CW, Crisan M, Lazzari L, Peault B. Perivascular ancestors of adult multipotent stem cells. *Arterioscler Thromb Vasc Biol*. 2010;30(6):1104-9.

79. Lin G, Garcia M, Ning H, Banie L, Guo YL, Lue TF, et al. Defining stem and progenitor cells within adipose tissue. *Stem Cells Dev.* 2008;17(6):1053-63.
80. Wright JT, Hausman GJ. Monoclonal antibodies against cell surface antigens expressed during porcine adipocyte differentiation. *Int J Obes.* 1990;14(5):395-409.
81. Bourin P, Bunnell BA, Casteilla L, Dominici M, Katz AJ, March KL, et al. Stromal cells from the adipose tissue-derived stromal vascular fraction and culture expanded adipose tissue-derived stromal/stem cells: a joint statement of the International Federation for Adipose Therapeutics and Science (IFATS) and the International Society for Cellular Therapy (ISCT). *Cytotherapy.* 2013;15(6):641-8.
82. Yu G, Wu X, Dietrich MA, Polk P, Scott LK, Ptitsyn AA, et al. Yield and characterization of subcutaneous human adipose-derived stem cells by flow cytometric and adipogenic mRNA analyzes. *Cytotherapy.* 2010;12(4):538-46.
83. Zhu M, Heydarkhan-Hagvall S, Hedrick M, Benhaim P, Zuk P. Manual Isolation of Adipose-derived Stem Cells from Human Lipoaspirates. *Journal of Visualized Experiments : JoVE.* 2013(79):50585.
84. Locke M, Windsor J, Dunbar PR. Human adipose-derived stem cells: isolation, characterization and applications in surgery. *ANZ J Surg.* 2009;79(4):235-44.
85. Gimble JM, Bunnell BA, Chiu ES, Guilak F. Concise review: Adipose-derived stromal vascular fraction cells and stem cells: let's not get lost in translation. *Stem Cells.* 2011;29(5):749-54.
86. Peterson B, Zhang J, Iglesias R, Kabo M, Hedrick M, Benhaim P, et al. Healing of critically sized femoral defects, using genetically modified mesenchymal stem cells from human adipose tissue. *Tissue Eng.* 2005;11(1-2):120-9.
87. Wagner W, Ho AD. Mesenchymal stem cell preparations--comparing apples and oranges. *Stem cell reviews.* 2007;3(4):239-48.
88. Haasters F, Prall WC, Anz D, Bourquin C, Pautke C, Endres S, et al. Morphological and immunocytochemical characteristics indicate the yield of early progenitors and represent a quality control for human mesenchymal stem cell culturing. *J Anat.* 2009;214(5):759-67.
89. Baer PC, Geiger H. Adipose-derived mesenchymal stromal/stem cells: tissue localization, characterization, and heterogeneity. *Stem Cells Int.* 2012;2012:812693.
90. Guilak F, Lott KE, Awad HA, Cao Q, Hicok KC, Fermor B, et al. Clonal analysis of the differentiation potential of human adipose-derived adult stem cells. *J Cell Physiol.* 2006;206(1):229-37.
91. Oedayrajsingh-Varma MJ, van Ham SM, Knippenberg M, Helder MN, Klein-Nulend J, Schouten TE, et al. Adipose tissue-derived mesenchymal stem cell yield and

growth characteristics are affected by the tissue-harvesting procedure. *Cytherapy*. 2006;8(2):166-77.

92. Schaffler A, Buchler C. Concise review: adipose tissue-derived stromal cells--basic and clinical implications for novel cell-based therapies. *Stem Cells*. 2007;25(4):818-27.

93. Shah FS, Li J, Dietrich M, Wu X, Hausmann MG, LeBlanc KA, et al. Comparison of Stromal/Stem Cells Isolated from Human Omental and Subcutaneous Adipose Depots: Differentiation and Immunophenotypic Characterization. *Cells Tissues Organs*. 2014;200(3-4):204-11.

94. Aksu AE, Rubin JP, Dudas JR, Marra KG. Role of gender and anatomical region on induction of osteogenic differentiation of human adipose-derived stem cells. *Ann Plast Surg*. 2008;60(3):306-22.

95. Russo V, Yu C, Belliveau P, Hamilton A, Flynn LE. Comparison of Human Adipose-Derived Stem Cells Isolated from Subcutaneous, Omental, and Intrathoracic Adipose Tissue Depots for Regenerative Applications. *Stem Cells Transl Med*. 2014;3(2):206-17.

96. Schipper BM, Marra KG, Zhang W, Donnenberg AD, Rubin JP. Regional anatomic and age effects on cell function of human adipose-derived stem cells. *Ann Plast Surg*. 2008;60(5):538-44.

97. Choudhery MS, Badowski M, Muise A, Pierce J, Harris DT. Donor age negatively impacts adipose tissue-derived mesenchymal stem cell expansion and differentiation. *J Transl Med*. 2014;12:8.

98. Frazier TP, Gimble JM, Devay JW, Tucker HA, Chiu ES, Rowan BG. Body mass index affects proliferation and osteogenic differentiation of human subcutaneous adipose tissue-derived stem cells. *BMC Cell Biol*. 2013;14:34.

99. van Harmelen V, Skurk T, Rohrig K, Lee YM, Halbleib M, Aprath-Husmann I, et al. Effect of BMI and age on adipose tissue cellularity and differentiation capacity in women. *Int J Obes Relat Metab Disord*. 2003;27(8):889-95.

100. Mojallal A, Lequeux C, Shipkov C, Duclos A, Braye F, Rohrich R, et al. Influence of age and body mass index on the yield and proliferation capacity of adipose-derived stem cells. *Aesthetic Plast Surg*. 2011;35(6):1097-105.

101. Yu G, Wu X, Kilroy G, Halvorsen YD, Gimble JM, Floyd ZE. Isolation of murine adipose-derived stem cells. *Methods Mol Biol*. 2011;702:29-36.

102. Zheng B, Cao B, Li G, Huard J. Mouse adipose-derived stem cells undergo multilineage differentiation in vitro but primarily osteogenic and chondrogenic differentiation in vivo. *Tissue Eng*. 2006;12(7):1891-901.

103. Taha MF, Hedayati V. Isolation, identification and multipotential differentiation of mouse adipose tissue-derived stem cells. *Tissue Cell*. 2010;42(4):211-6.
104. Ogawa R, Mizuno H, Watanabe A, Migita M, Shimada T, Hyakusoku H. Osteogenic and chondrogenic differentiation by adipose-derived stem cells harvested from GFP transgenic mice. *Biochem Biophys Res Commun*. 2004;313(4):871-7.
105. Malladi P, Xu Y, Chiou M, Giaccia AJ, Longaker MT. Effect of reduced oxygen tension on chondrogenesis and osteogenesis in adipose-derived mesenchymal cells. *Am J Physiol Cell Physiol*. 2006;290(4):C1139-46.
106. Yamamoto N, Akamatsu H, Hasegawa S, Yamada T, Nakata S, Ohkuma M, et al. Isolation of multipotent stem cells from mouse adipose tissue. *J Dermatol Sci*. 2007;48(1):43-52.
107. McIntosh K, Zvonic S, Garrett S, Mitchell JB, Floyd ZE, Hammill L, et al. The immunogenicity of human adipose-derived cells: temporal changes in vitro. *Stem Cells*. 2006;24(5):1246-53.
108. Gronthos S, Franklin DM, Leddy HA, Robey PG, Storms RW, Gimble JM. Surface protein characterization of human adipose tissue-derived stromal cells. *J Cell Physiol*. 2001;189(1):54-63.
109. Gehmert S, Wenzel C, Loibl M, Brockhoff G, Huber M, Krutsch W, et al. Adipose tissue-derived stem cell secreted IGF-1 protects myoblasts from the negative effect of myostatin. *Biomed Res Int*. 2014;2014:129048.
110. Liu HY, Chiou JF, Wu AT, Tsai CY, Leu JD, Ting LL, et al. The effect of diminished osteogenic signals on reduced osteoporosis recovery in aged mice and the potential therapeutic use of adipose-derived stem cells. *Biomaterials*. 2012;33(26):6105-12.
111. Luna AC, Madeira ME, Conceicao TO, Moreira JA, Laiso RA, Maria DA. Characterization of adipose-derived stem cells of anatomical region from mice. *BMC Res Notes*. 2014;7:552.
112. MacDougald OA, Mandrup S. Adipogenesis: forces that tip the scales. *Trends Endocrinol Metab*. 2002;13(1):5-11.
113. Loftus TM, Lane MD. Modulating the transcriptional control of adipogenesis. *Curr Opin Genet Dev*. 1997;7(5):603-8.
114. Tang QQ, Lane MD. Role of C/EBP homologous protein (CHOP-10) in the programmed activation of CCAAT/enhancer-binding protein-beta during adipogenesis. *Proc Natl Acad Sci U S A*. 2000;97(23):12446-50.
115. Rosen ED, Walkey CJ, Puigserver P, Spiegelman BM. Transcriptional regulation of adipogenesis. *Genes Dev*. 2000;14(11):1293-307.

116. Rieusset J, Touri F, Michalik L, Escher P, Desvergne B, Niesor E, et al. A new selective peroxisome proliferator-activated receptor gamma antagonist with antiobesity and antidiabetic activity. *Mol Endocrinol.* 2002;16(11):2628-44.
117. Tyagi S, Gupta P, Saini AS, Kaushal C, Sharma S. The peroxisome proliferator-activated receptor: A family of nuclear receptors role in various diseases. *J Adv Pharm Technol Res.* 2011;2(4):236-40.
118. Niemeyer P, Kornacker M, Mehlhorn A, Seckinger A, Vohrer J, Schmal H, et al. Comparison of immunological properties of bone marrow stromal cells and adipose tissue-derived stem cells before and after osteogenic differentiation in vitro. *Tissue Eng.* 2007;13(1):111-21.
119. Grottkau BE, Lin Y. Osteogenesis of Adipose-Derived Stem Cells. *Bone research.* 2013;1(2):133-45.
120. Honda Y, Ding X, Mussano F, Wiberg A, Ho CM, Nishimura I. Guiding the osteogenic fate of mouse and human mesenchymal stem cells through feedback system control. *Sci Rep.* 2013;3:3420.
121. Phimphilai M, Zhao Z, Boules H, Roca H, Franceschi RT. BMP signaling is required for RUNX2-dependent induction of the osteoblast phenotype. *J Bone Miner Res.* 2006;21(4):637-46.
122. Goldring MB, Tsuchimochi K, Ijiri K. The control of chondrogenesis. *J Cell Biochem.* 2006;97(1):33-44.
123. Estes BT, Diekman BO, Guilak F. Monolayer cell expansion conditions affect the chondrogenic potential of adipose-derived stem cells. *Biotechnol Bioeng.* 2008;99(4):986-95.
124. Frith J, Genever P. Transcriptional control of mesenchymal stem cell differentiation. *Transfus Med Hemother.* 2008;35(3):216-27.
125. Komori T. Regulation of skeletal development by the Runx family of transcription factors. *J Cell Biochem.* 2005;95(3):445-53.
126. Baraniak PR, McDevitt TC. Stem cell paracrine actions and tissue regeneration. *Regen Med.* 2010;5(1):121-43.
127. Liang X, Ding Y, Zhang Y, Tse HF, Lian Q. Paracrine mechanisms of mesenchymal stem cell-based therapy: current status and perspectives. *Cell Transplant.* 2014;23(9):1045-59.
128. Yoo KH, Jang IK, Lee MW, Kim HE, Yang MS, Eom Y, et al. Comparison of immunomodulatory properties of mesenchymal stem cells derived from adult human tissues. *Cell Immunol.* 2009;259(2):150-6.



129. Russell KA, Chow NHC, Dukoff D, Gibson TWG, LaMarre J, Betts DH, et al. Characterization and Immunomodulatory Effects of Canine Adipose Tissue- and Bone Marrow-Derived Mesenchymal Stromal Cells. *PLoS One*. 2016;11(12):e0167442.
130. Ock S-A, Baregundi Subbarao R, Lee Y-M, Lee J-H, Jeon R-H, Lee S-L, et al. Comparison of Immunomodulation Properties of Porcine Mesenchymal Stromal/Stem Cells Derived from the Bone Marrow, Adipose Tissue, and Dermal Skin Tissue. *Stem Cells Int*. 2016;2016:9581350.
131. Puissant B, Barreau C, Bourin P, Clavel C, Corre J, Bousquet C, et al. Immunomodulatory effect of human adipose tissue-derived adult stem cells: comparison with bone marrow mesenchymal stem cells. *Br J Haematol*. 2005;129(1):118-29.
132. Leto Barone AA, Khalifian S, Lee WP, Brandacher G. Immunomodulatory effects of adipose-derived stem cells: fact or fiction? *Biomed Res Int*. 2013;2013:383685.
133. Blaber SP, Webster RA, Hill CJ, Breen EJ, Kuah D, Vesey G, et al. Analysis of in vitro secretion profiles from adipose-derived cell populations. *J Transl Med*. 2012;10:172.
134. Mosser DM, Edwards JP. Exploring the full spectrum of macrophage activation. *Nat Rev Immunol*. 2008;8(12):958-69.
135. Jiang D, Qi Y, Walker NG, Sindrilaru A, Hainzl A, Wlaschek M, et al. The effect of adipose tissue derived MSCs delivered by a chemically defined carrier on full-thickness cutaneous wound healing. *Biomaterials*. 2013;34(10):2501-15.
136. Wang X, Gu H, Qin D, Yang L, Huang W, Essandoh K, et al. Exosomal miR-223 Contributes to Mesenchymal Stem Cell-Elicited Cardioprotection in Polymicrobial Sepsis. *Sci Rep*. 2015;5:13721.
137. Aggarwal S, Pittenger MF. Human mesenchymal stem cells modulate allogeneic immune cell responses. *Blood*. 2005;105(4):1815-22.
138. Krampera M, Cosmi L, Angeli R, Pasini A, Liotta F, Andreini A, et al. Role for interferon-gamma in the immunomodulatory activity of human bone marrow mesenchymal stem cells. *Stem Cells*. 2006;24(2):386-98.
139. DelaRosa O, Lombardo E, Beraza A, Mancheno-Corvo P, Ramirez C, Menta R, et al. Requirement of IFN-gamma-mediated indoleamine 2,3-dioxygenase expression in the modulation of lymphocyte proliferation by human adipose-derived stem cells. *Tissue Eng Part A*. 2009;15(10):2795-806.
140. Cui L, Yin S, Liu W, Li N, Zhang W, Cao Y. Expanded adipose-derived stem cells suppress mixed lymphocyte reaction by secretion of prostaglandin E2. *Tissue Eng*. 2007;13(6):1185-95.

141. Lin CS, Lin G, Lue TF. Allogeneic and xenogeneic transplantation of adipose-derived stem cells in immunocompetent recipients without immunosuppressants. *Stem Cells Dev.* 2012;21(15):2770-8.
142. Fang B, Song Y, Liao L, Zhang Y, Zhao RC. Favorable response to human adipose tissue-derived mesenchymal stem cells in steroid-refractory acute graft-versus-host disease. *Transplant Proc.* 2007;39(10):3358-62.
143. Fang B, Song Y, Lin Q, Zhang Y, Cao Y, Zhao RC, et al. Human adipose tissue-derived mesenchymal stromal cells as salvage therapy for treatment of severe refractory acute graft-vs.-host disease in two children. *Pediatr Transplant.* 2007;11(7):814-7.
144. Fang B, Song Y, Zhao RC, Han Q, Lin Q. Using human adipose tissue-derived mesenchymal stem cells as salvage therapy for hepatic graft-versus-host disease resembling acute hepatitis. *Transplant Proc.* 2007;39(5):1710-3.
145. Lai K, Zeng K, Zeng F, Wei J, Tan G. Allogeneic adipose-derived stem cells suppress Th17 lymphocytes in patients with active lupus in vitro. *Acta biochimica et biophysica Sinica.* 2011;43(10):805-12.
146. Rehman J, Traktuev D, Li J, Merfeld-Clauss S, Temm-Grove CJ, Bovenkerk JE, et al. Secretion of angiogenic and antiapoptotic factors by human adipose stromal cells. *Circulation.* 2004;109(10):1292-8.
147. Blaber SP, Webster RA, Hill CJ, Breen EJ, Kuah D, Vesey G, et al. Analysis of in vitro secretion profiles from adipose-derived cell populations. *J Transl Med.* 2012;10:172-.
148. Moon MH, Kim SY, Kim YJ, Kim SJ, Lee JB, Bae YC, et al. Human adipose tissue-derived mesenchymal stem cells improve postnatal neovascularization in a mouse model of hindlimb ischemia. *Cell Physiol Biochem.* 2006;17(5-6):279-90.
149. Fan W, Sun D, Liu J, Liang D, Wang Y, Narsinh KH, et al. Adipose stromal cells amplify angiogenic signaling via the VEGF/mTOR/Akt pathway in a murine hindlimb ischemia model: a 3D multimodality imaging study. *PLoS One.* 2012;7(9):e45621.
150. Vu NB, Le HT, Dao TT, Phi LT, Phan NK, Ta VT. Allogeneic Adipose-Derived Mesenchymal Stem Cell Transplantation Enhances the Expression of Angiogenic Factors in a Mouse Acute Hindlimb Ischemic Model. *Adv Exp Med Biol.* 2017.
151. Suga H, Glotzbach JP, Sorkin M, Longaker MT, Gurtner GC. Paracrine mechanism of angiogenesis in adipose-derived stem cell transplantation. *Ann Plast Surg.* 2014;72(2):234-41.
152. Zhao L, Johnson T, Liu D. Therapeutic angiogenesis of adipose-derived stem cells for ischemic diseases. *Stem Cell Res Ther.* 2017;8(1):125.

153. Cai L, Johnstone BH, Cook TG, Liang Z, Traktuev D, Cornetta K, et al. Suppression of hepatocyte growth factor production impairs the ability of adipose-derived stem cells to promote ischemic tissue revascularization. *Stem Cells*. 2007;25(12):3234-43.
154. Frantz C, Stewart KM, Weaver VM. The extracellular matrix at a glance. *J Cell Sci*. 2010;123(24):4195-200.
155. LeBleu VS, Macdonald B, Kalluri R. Structure and function of basement membranes. *Exp Biol Med (Maywood)*. 2007;232(9):1121-9.
156. Hubmacher D, Apte SS. The biology of the extracellular matrix: novel insights. *Curr Opin Rheumatol*. 2013;25(1):65-70.
157. Gordon MK, Hahn RA. Collagens. *Cell Tissue Res*. 2010;339(1):247-57.
158. Blackstone Neil W. *Molecular Biology of the Cell*. Fourth Edition. By Bruce Alberts, Alexander Johnson, Julian Lewis, Martin Raff, Keith Roberts , and Peter Walter. *The Quarterly Review of Biology*. 2003;78(1):91-2.
159. Uzman A. *Molecular Cell Biology (4th edition)* Harvey Lodish, Arnold Berk, S. Lawrence Zipursky, Paul Matsudaira, David Baltimore and James Darnell; Freeman & Co., New York, NY, 2000, 1084 pp., list price \$102.25, ISBN 0-7167-3136-3. *Biochem Mol Biol Educ*. 2001;29(3):126-8.
160. Yanagishita M. Function of proteoglycans in the extracellular matrix. *Acta Pathol Jpn*. 1993;43(6):283-93.
161. Bissell MJ, Aggeler J. Dynamic reciprocity: how do extracellular matrix and hormones direct gene expression? *Prog Clin Biol Res*. 1987;249:251-62.
162. Schultz GS, Davidson JM, Kirsner RS, Bornstein P, Herman IM. Dynamic reciprocity in the wound microenvironment. *Wound Repair Regen*. 2011;19(2):134-48.
163. Xu R, Boudreau A, Bissell MJ. Tissue architecture and function: dynamic reciprocity via extra- and intra-cellular matrices. *Cancer Metastasis Rev*. 2009;28(1-2):167-76.
164. Jackson HW, Defamie V, Waterhouse P, Khokha R. TIMPs: versatile extracellular regulators in cancer. *Nat Rev Cancer*. 2017;17(1):38-53.
165. Lu P, Weaver VM, Werb Z. The extracellular matrix: A dynamic niche in cancer progression. *The Journal of Cell Biology*. 2012;196(4):395.
166. Cox TR, Ertler JT. Remodeling and homeostasis of the extracellular matrix: implications for fibrotic diseases and cancer. *Dis Model Mech*. 2011;4(2):165-78.

167. Ventre M, Netti PA. Engineering Cell Instructive Materials To Control Cell Fate and Functions through Material Cues and Surface Patterning. *ACS Appl Mater Interfaces*. 2016;8(24):14896-908.
168. Custodio CA, Reis RL, Mano JF. Engineering biomolecular microenvironments for cell instructive biomaterials. *Adv Healthc Mater*. 2014;3(6):797-810.
169. Shafiq M, Jung Y, Kim SH. Insight on stem cell preconditioning and instructive biomaterials to enhance cell adhesion, retention, and engraftment for tissue repair. *Biomaterials*. 2016;90:85-115.
170. Zhang Z, Gupte MJ, Ma PX. Biomaterials and Stem Cells for Tissue Engineering. *Expert Opin Biol Ther*. 2013;13(4):527-40.
171. Kornmuller A, Brown CFC, Yu C, Flynn LE. Fabrication of Extracellular Matrix-derived Foams and Microcarriers as Tissue-specific Cell Culture and Delivery Platforms. *J Vis Exp*. 2017(122).
172. DeQuach JA, Yuan SH, Goldstein LS, Christman KL. Decellularized porcine brain matrix for cell culture and tissue engineering scaffolds. *Tissue Eng Part A*. 2011;17(21-22):2583-92.
173. Swinehart IT, Badylak SF. Extracellular matrix bioscaffolds in tissue remodeling and morphogenesis. *Dev Dyn*. 2016;245(3):351-60.
174. Wang L, Johnson JA, Zhang Q, Beahm EK. Combining decellularized human adipose tissue extracellular matrix and adipose-derived stem cells for adipose tissue engineering. *Acta Biomater*. 2013;9(11):8921-31.
175. Choi JS, Kim BS, Kim JY, Kim JD, Choi YC, Yang HJ, et al. Decellularized extracellular matrix derived from human adipose tissue as a potential scaffold for allograft tissue engineering. *Journal of biomedical materials research Part A*. 2011;97(3):292-9.
176. Wu I, Nahas Z, Kimmerling KA, Rosson GD, Elisseff JH. An injectable adipose matrix for soft-tissue reconstruction. *Plast Reconstr Surg*. 2012;129(6):1247-57.
177. Young DA, Ibrahim DO, Hu D, Christman KL. Injectable hydrogel scaffold from decellularized human lipoaspirate. *Acta Biomater*. 2011;7(3):1040-9.
178. Roosens A, Somers P, De Somer F, Carriel V, Van Nooten G, Cornelissen R. Impact of Detergent-Based Decellularization Methods on Porcine Tissues for Heart Valve Engineering. *Ann Biomed Eng*. 2016.
179. Faulk DM, Carruthers CA, Warner HJ, Kramer CR, Reing JE, Zhang L, et al. The effect of detergents on the basement membrane complex of a biologic scaffold material. *Acta Biomater*. 2014;10(1):183-93.

180. Reing JE, Brown BN, Daly KA, Freund JM, Gilbert TW, Hsiong SX, et al. The effects of processing methods upon mechanical and biologic properties of porcine dermal extracellular matrix scaffolds. *Biomaterials*. 2010;31(33):8626-33.
181. Flynn LE. The use of decellularized adipose tissue to provide an inductive microenvironment for the adipogenic differentiation of human adipose-derived stem cells. *Biomaterials*. 2010;31(17):4715-24.
182. Yu C, Bianco J, Brown C, Fuetterer L, Watkins JF, Samani A, et al. Porous decellularized adipose tissue foams for soft tissue regeneration. *Biomaterials*. 2013;34(13):3290-302.
183. Yu C, Kornmuller A, Brown C, Hoare T, Flynn LE. Decellularized adipose tissue microcarriers as a dynamic culture platform for human adipose-derived stem/stromal cell expansion. *Biomaterials*. 2017;120:66-80.
184. Turner AE, Yu C, Bianco J, Watkins JF, Flynn LE. The performance of decellularized adipose tissue microcarriers as an inductive substrate for human adipose-derived stem cells. *Biomaterials*. 2012;33(18):4490-9.
185. Turner AE, Flynn LE. Design and characterization of tissue-specific extracellular matrix-derived microcarriers. *Tissue Eng Part C Methods*. 2012;18(3):186-97.
186. Shridhar A, Gillies E, Amsden BG, Flynn LE. Composite Bioscaffolds Incorporating Decellularized ECM as a Cell-Instructive Component Within Hydrogels as In Vitro Models and Cell Delivery Systems. *Methods Mol Biol*. 2017.
187. Brown CF, Yan J, Han TT, Marecak DM, Amsden BG, Flynn LE. Effect of decellularized adipose tissue particle size and cell density on adipose-derived stem cell proliferation and adipogenic differentiation in composite methacrylated chondroitin sulphate hydrogels. *Biomed Mater*. 2015;10(4):045010.
188. Cheung HK, Han TT, Marecak DM, Watkins JF, Amsden BG, Flynn LE. Composite hydrogel scaffolds incorporating decellularized adipose tissue for soft tissue engineering with adipose-derived stem cells. *Biomaterials*. 2014;35(6):1914-23.
189. Adam Young D, Bajaj V, Christman KL. Award winner for outstanding research in the PhD category, 2014 Society for Biomaterials annual meeting and exposition, Denver, Colorado, April 16-19, 2014: Decellularized adipose matrix hydrogels stimulate in vivo neovascularization and adipose formation. *Journal of biomedical materials research Part A*. 2014;102(6):1641-51.
190. Kayabolen A, Keskin D, Aykan A, Karslioglu Y, Zor F, Tezcaner A. Native extracellular matrix/fibroin hydrogels for adipose tissue engineering with enhanced vascularization. *Biomed Mater*. 2017;12(3):035007.
191. Li L, Chen X, Wang WE, Zeng C. How to Improve the Survival of Transplanted Mesenchymal Stem Cell in Ischemic Heart? *Stem Cells Int*. 2016;2016:9682757.

192. Li X, Tamama K, Xie X, Guan J. Improving Cell Engraftment in Cardiac Stem Cell Therapy. *Stem Cells Int.* 2016;2016:7168797.
193. Ho SS, Murphy KC, Binder BY, Vissers CB, Leach JK. Increased Survival and Function of Mesenchymal Stem Cell Spheroids Entrapped in Instructive Alginate Hydrogels. *Stem Cells Transl Med.* 2016;5(6):773-81.
194. Wang S, Qu X, Zhao RC. Clinical applications of mesenchymal stem cells. *J Hematol Oncol.* 2012;5:19.
195. Paterson YZ, Rash N, Garvican ER, Paillot R, Guest DJ. Equine mesenchymal stromal cells and embryo-derived stem cells are immune privileged in vitro. *Stem Cell Res Ther.* 2014;5(4):90.
196. Petrie Aronin CE, Tuan RS. Therapeutic potential of the immunomodulatory activities of adult mesenchymal stem cells. *Birth Defects Res C Embryo Today.* 2010;90(1):67-74.
197. Krampera M, Glennie S, Dyson J, Scott D, Laylor R, Simpson E, et al. Bone marrow mesenchymal stem cells inhibit the response of naive and memory antigen-specific T cells to their cognate peptide. *Blood.* 2003;101(9):3722-9.
198. Scarritt ME, Pashos NC, Bunnell BA. A Review of Cellularization Strategies for Tissue Engineering of Whole Organs. *Frontiers in Bioengineering and Biotechnology.* 2015;3:43.
199. Badylak SF, Taylor D, Uygun K. Whole-organ tissue engineering: decellularization and recellularization of three-dimensional matrix scaffolds. *Annu Rev Biomed Eng.* 2011;13:27-53.
200. Chang W, Song B-W, Hwang K-C. Mesenchymal Stem Cell Survival in Infarcted Myocardium: Adhesion and Anti-death Signals. In: Hayat MA, editor. *Stem Cells and Cancer Stem Cells, Volume 10: Therapeutic Applications in Disease and Injury.* Dordrecht: Springer Netherlands; 2013. p. 35-43.
201. Lee S, Choi E, Cha MJ, Hwang KC. Cell adhesion and long-term survival of transplanted mesenchymal stem cells: a prerequisite for cell therapy. *Oxid Med Cell Longev.* 2015;2015:632902.
202. Sharma AK, Bury MI, Marks AJ, Fuller NJ, Meisner JW, Tapaskar N, et al. A nonhuman primate model for urinary bladder regeneration using autologous sources of bone marrow-derived mesenchymal stem cells. *Stem Cells.* 2011;29(2):241-50.
203. Lam MT, Nauta A, Meyer NP, Wu JC, Longaker MT. Effective delivery of stem cells using an extracellular matrix patch results in increased cell survival and proliferation and reduced scarring in skin wound healing. *Tissue Eng Part A.* 2013;19(5-6):738-47.

204. Zhang Y, He Y, Bharadwaj S, Hammam N, Carnagey K, Myers R, et al. Tissue-specific extracellular matrix coatings for the promotion of cell proliferation and maintenance of cell phenotype. *Biomaterials*. 2009;30(23-24):4021-8.
205. Higuchi S, Lin Q, Wang J, Lim TK, Joshi SB, Anand GS, et al. Heart extracellular matrix supports cardiomyocyte differentiation of mouse embryonic stem cells. *J Biosci Bioeng*. 2013;115(3):320-5.
206. Nakayama KH, Lee CC, Batchelder CA, Tarantal AF. Tissue specificity of decellularized rhesus monkey kidney and lung scaffolds. *PLoS One*. 2013;8(5):e64134.
207. O'Neill JD, Freytes DO, Anandappa AJ, Oliver JA, Vunjak-Novakovic GV. The regulation of growth and metabolism of kidney stem cells with regional specificity using extracellular matrix derived from kidney. *Biomaterials*. 2013;34(38):9830-41.
208. Pokrywczynska M, Jundzill A, Bodnar M, Adamowicz J, Tworkiewicz J, Szyberg L, et al. Do mesenchymal stem cells modulate the milieu of reconstructed bladder wall? *Arch Immunol Ther Exp (Warsz)*. 2013;61(6):483-93.
209. Chang CW, Petrie T, Clark A, Lin X, Sondergaard CS, Griffiths LG. Mesenchymal Stem Cell Seeding of Porcine Small Intestinal Submucosal Extracellular Matrix for Cardiovascular Applications. *PLoS One*. 2016;11(4):e0153412.
210. Wang YH, Chen J, Zhou J, Nong F, Lv JH, Liu J. Reduced inflammatory cell recruitment and tissue damage in spinal cord injury by acellular spinal cord scaffold seeded with mesenchymal stem cells. *Exp Ther Med*. 2017;13(1):203-7.
211. Nie C, Zhang G, Yang D, Liu T, Liu D, Xu J, et al. Targeted delivery of adipose-derived stem cells via acellular dermal matrix enhances wound repair in diabetic rats. *J Tissue Eng Regen Med*. 2015;9(3):224-35.
212. Adam Young D, Bajaj V, Christman KL. Decellularized adipose matrix hydrogels stimulate in vivo neovascularization and adipose formation. *J Biomed Mater Res Part A*. 2014;102(6):1641-51.
213. Merritt EK, Cannon MV, Hammers DW, Le LN, Gokhale R, Sarathy A, et al. Repair of traumatic skeletal muscle injury with bone-marrow-derived mesenchymal stem cells seeded on extracellular matrix. *Tissue Eng Part A*. 2010;16(9):2871-81.
214. Godier-Furnémont AFG, Martens TP, Koeckert MS, Wan L, Parks J, Arai K, et al. Composite scaffold provides a cell delivery platform for cardiovascular repair. *Proc Natl Acad Sci U S A*. 2011;108(19):7974-9.
215. Chang Y, Lai PH, Wei HJ, Lin WW, Chen CH, Hwang SM, et al. Tissue regeneration observed in a basic fibroblast growth factor-loaded porous acellular bovine pericardium populated with mesenchymal stem cells. *J Thorac Cardiovasc Surg*. 2007;134(1):65-73, .e1-4.

216. Brown BN, Badylak SF. Extracellular matrix as an inductive scaffold for functional tissue reconstruction. *Transl Res.* 2014;163(4):268-85.
217. Gattazzo F, Urciuolo A, Bonaldo P. Extracellular matrix: a dynamic microenvironment for stem cell niche. *Biochim Biophys Acta.* 2014;1840(8):2506-19.
218. Klaas M, Kangur T, Viil J, Maemets-Allas K, Minajeva A, Vadi K, et al. The alterations in the extracellular matrix composition guide the repair of damaged liver tissue. *Sci Rep.* 2016;6:27398.
219. Lu P, Weaver VM, Werb Z. The extracellular matrix: a dynamic niche in cancer progression. *J Cell Biol.* 2012;196(4):395-406.
220. Li Q, Uygun BE, Geerts S, Ozer S, Scalf M, Gilpin SE, et al. Proteomic Analysis of Naturally-Sourced Biological Scaffolds. *Biomaterials.* 2016;75:37-46.
221. Welham NV, Chang Z, Smith LM, Frey BL. Proteomic analysis of a decellularized human vocal fold mucosa scaffold using 2D electrophoresis and high-resolution mass spectrometry. *Biomaterials.* 2013;34(3):669-76.
222. Aamodt JM, Grainger DW. Extracellular matrix-based biomaterial scaffolds and the host response. *Biomaterials.* 2016;86:68-82.
223. Hoganson DM, O'Doherty EM, Owens GE, Harilal DO, Goldman SM, Bowley CM, et al. The retention of extracellular matrix proteins and angiogenic and mitogenic cytokines in a decellularized porcine dermis. *Biomaterials.* 2010;31(26):6730-7.
224. Ricard-Blum S, Salza R. Matricryptins and matrikines: biologically active fragments of the extracellular matrix. *Exp Dermatol.* 2014;23(7):457-63.
225. Mauney J, Olsen BR, Volloch V. Matrix remodeling as stem cell recruitment event: a novel in vitro model for homing of human bone marrow stromal cells to the site of injury shows crucial role of extracellular collagen matrix. *Matrix Biol.* 2010;29(8):657-63.
226. Agrawal V, Johnson SA, Reing J, Zhang L, Tottey S, Wang G, et al. Epimorphic regeneration approach to tissue replacement in adult mammals. *Proc Natl Acad Sci U S A.* 2010;107(8):3351-5.
227. Davis GE, Bayless KJ, Davis MJ, Meininger GA. Regulation of tissue injury responses by the exposure of matricryptic sites within extracellular matrix molecules. *Am J Pathol.* 2000;156(5):1489-98.
228. Maquart FX, Pasco S, Ramont L, Hornebeck W, Monboisse JC. An introduction to matrikines: extracellular matrix-derived peptides which regulate cell activity. Implication in tumor invasion. *Crit Rev Oncol Hematol.* 2004;49(3):199-202.



229. Briones MPP, Kamisato S, Maeda I, Takami N, Okamoto K. Macrophage Chemotactic Response to Elastin-Derived VGVAPG and VGVPG Permutations: A Structure-Activity Relationship and Receptor Binding Assay. In: Lebl M, Houghten RA, editors. *Peptides: The Wave of the Future: Proceedings of the Second International and the Seventeenth American Peptide Symposium, June 9–14, 2001, San Diego, California, USA*. Dordrecht: Springer Netherlands; 2001. p. 807-8.
230. Adair-Kirk TL, Senior RM. Fragments of Extracellular Matrix as Mediators of Inflammation. *Int J Biochem Cell Biol*. 2008;40(6-7):1101-10.
231. Hynes RO. The extracellular matrix: not just pretty fibrils. *Science*. 2009;326(5957):1216-9.
232. Muiznieks LD, Keeley FW. Molecular assembly and mechanical properties of the extracellular matrix: A fibrous protein perspective. *BBA Mol Basis Dis*. 2013;1832(7):866-75.
233. Li D, Zhou J, Chowdhury F, Cheng J, Wang N, Wang F. Role of mechanical factors in fate decisions of stem cells. *Regen Med*. 2011;6(2):229-40.
234. Luo T, Mohan K, Iglesias PA, Robinson DN. Molecular mechanisms of cellular mechanosensing. *Nat Mater*. 2013;12(11):1064-71.
235. Legate KR, Wickstrom SA, Fassler R. Genetic and cell biological analysis of integrin outside-in signaling. *Genes Dev*. 2009;23(4):397-418.
236. Buitenhuis M. The role of PI3K/protein kinase B (PKB/c-akt) in migration and homing of hematopoietic stem and progenitor cells. *Curr Opin Hematol*. 2011;18(4):226-30.
237. Engler AJ, Sen S, Sweeney HL, Discher DE. Matrix Elasticity Directs Stem Cell Lineage Specification. *Cell*. 2006;126(4):677-89.
238. Brown BN, Barnes CA, Kasick RT, Michel R, Gilbert TW, Beer-Stolz D, et al. Surface Characterization of Extracellular Matrix Scaffolds. *Biomaterials*. 2010;31(3):428-37.
239. Brown B, Lindberg K, Reing J, Stolz DB, Badylak SF. The basement membrane component of biologic scaffolds derived from extracellular matrix. *Tissue Eng*. 2006;12(3):519-26.
240. Loh QL, Choong C. Three-Dimensional Scaffolds for Tissue Engineering Applications: Role of Porosity and Pore Size. *Tissue Eng Part B Rev*. 2013;19(6):485-502.
241. Murphy CM, Haugh MG, O'Brien FJ. The effect of mean pore size on cell attachment, proliferation and migration in collagen-glycosaminoglycan scaffolds for bone tissue engineering. *Biomaterials*. 2010;31(3):461-6.

242. McBeath R, Pirone DM, Nelson CM, Bhadriraju K, Chen CS. Cell shape, cytoskeletal tension, and RhoA regulate stem cell lineage commitment. *Dev Cell*. 2004;6(4):483-95.
243. Navarro M, Michiardi A, Castaño O, Planell JA. Biomaterials in orthopaedics. *Journal of the Royal Society Interface*. 2008;5(27):1137-58.
244. Sridharan R, Cameron AR, Kelly DJ, Kearney CJ, O'Brien FJ. Biomaterial based modulation of macrophage polarization: a review and suggested design principles. *Materials Today*. 2015;18(6):313-25.
245. Rungsiyakull C, Li Q, Sun G, Li W, Swain MV. Surface morphology optimization for osseointegration of coated implants. *Biomaterials*. 2010;31(27):7196-204.
246. Albrektsson T, Branemark PI, Hansson HA, Lindstrom J. Osseointegrated titanium implants. Requirements for ensuring a long-lasting, direct bone-to-implant anchorage in man. *Acta Orthop Scand*. 1981;52(2):155-70.
247. Franz S, Rammelt S, Scharnweber D, Simon JC. Immune responses to implants - a review of the implications for the design of immunomodulatory biomaterials. *Biomaterials*. 2011;32(28):6692-709.
248. Sperling C, Fischer M, Maitz MF, Werner C. Blood coagulation on biomaterials requires the combination of distinct activation processes. *Biomaterials*. 2009;30(27):4447-56.
249. Heemskerk JW, Bevers EM, Lindhout T. Platelet activation and blood coagulation. *Thromb Haemost*. 2002;88(2):186-93.
250. Gorbet MB, Sefton MV. Biomaterial-associated thrombosis: roles of coagulation factors, complement, platelets and leukocytes. *Biomaterials*. 2004;25(26):5681-703.
251. Nilsson B, Ekdahl KN, Mollnes TE, Lambris JD. The role of complement in biomaterial-induced inflammation. *Mol Immunol*. 2007;44(1-3):82-94.
252. Hed J, Johansson M, Lindroth M. Complement activation according to the alternate pathway by glass and plastic surfaces and its role in neutrophil adhesion. *Immunol Lett*. 1984;8(6):295-9.
253. Fischer M, Sperling C, Tengvall P, Werner C. The ability of surface characteristics of materials to trigger leukocyte tissue factor expression. *Biomaterials*. 2010;31(9):2498-507.
254. Bianchi ME. DAMPs, PAMPs and alarmins: all we need to know about danger. *J Leukoc Biol*. 2007;81(1):1-5.

255. Grandjean-Laquerriere A, Tabary O, Jacquot J, Richard D, Frayssinet P, Guenounou M, et al. Involvement of toll-like receptor 4 in the inflammatory reaction induced by hydroxyapatite particles. *Biomaterials*. 2007;28(3):400-4.
256. Pakianathan DR. Extracellular matrix proteins and leukocyte function. *J Leukoc Biol*. 1995;57(5):699-702.
257. Uzarski JS, Van De Walle AB, McFetridge PS. Preimplantation processing of ex vivo-derived vascular biomaterials: effects on peripheral cell adhesion. *Journal of biomedical materials research Part A*. 2013;101(1):123-31.
258. Anderson JM, Rodriguez A, Chang DT. FOREIGN BODY REACTION TO BIOMATERIALS. *Semin Immunol*. 2008;20(2):86-100.
259. Kobayashi SD, Voyich JM, Burlak C, DeLeo FR. Neutrophils in the innate immune response. *Arch Immunol Ther Exp (Warsz)*. 2005;53(6):505-17.
260. Delgado-Rizo V, Martínez-Guzmán MA, Iñiguez-Gutierrez L, García-Orozco A, Alvarado-Navarro A, Fafutis-Morris M. Neutrophil Extracellular Traps and Its Implications in Inflammation: An Overview. *Front Immunol*. 2017;8:81.
261. Fox S, Leitch AE, Duffin R, Haslett C, Rossi AG. Neutrophil apoptosis: relevance to the innate immune response and inflammatory disease. *J Innate Immun*. 2010;2(3):216-27.
262. Trivedi A, Olivas AD, Noble-Haesslein LJ. Inflammation and Spinal Cord Injury: Infiltrating Leukocytes as Determinants of Injury and Repair Processes. *Clin Neurosci Res*. 2006;6(5):283-92.
263. Perobelli SM, Galvani RG, Goncalves-Silva T, Xavier CR, Nobrega A, Bonomo A. Plasticity of neutrophils reveals modulatory capacity. *Braz J Med Biol Res*. 2015;48(8):665-75.
264. Tsuda Y, Takahashi H, Kobayashi M, Hanafusa T, Herndon DN, Suzuki F. Three different neutrophil subsets exhibited in mice with different susceptibilities to infection by methicillin-resistant *Staphylococcus aureus*. *Immunity*. 2004;21(2):215-26.
265. Mencacci A, Cenci E, Spaccapelo R, Tonnetti L, del Sero G, d'Ostiani CF, et al. Neutrophils producing interleukin-10 antagonize the effect of interleukin-12 in mice with candidiasis. *Ann N Y Acad Sci*. 1996;795:394-6.
266. De Santo C, Arscott R, Booth S, Karydis I, Jones M, Asher R, et al. Invariant NKT cells modulate the suppressive activity of IL-10-secreting neutrophils differentiated with serum amyloid A. *Nat Immunol*. 2010;11(11):1039-46.
267. Balderramas HA, Penitenti M, Rodrigues DR, Bachiega TF, Fernandes RK, Ikoma MR, et al. Human neutrophils produce IL-12, IL-10, PGE2 and LTB4 in response

to *Paracoccidioides brasiliensis*. Involvement of TLR2, mannose receptor and dectin-1. *Cytokine*. 2014;67(1):36-43.

268. Schmielau J, Finn OJ. Activated granulocytes and granulocyte-derived hydrogen peroxide are the underlying mechanism of suppression of t-cell function in advanced cancer patients. *Cancer Res*. 2001;61(12):4756-60.

269. Munder M, Schneider H, Luckner C, Giese T, Langhans CD, Fuentes JM, et al. Suppression of T-cell functions by human granulocyte arginase. *Blood*. 2006;108(5):1627-34.

270. Muller I, Munder M, Kropf P, Hansch GM. Polymorphonuclear neutrophils and T lymphocytes: strange bedfellows or brothers in arms? *Trends Immunol*. 2009;30(11):522-30.

271. Jhunjhunwala S. Neutrophils at the Biological–Material Interface. *ACS Biomaterials Science & Engineering*. 2017.

272. Thevenot PT, Baker DW, Weng H, Sun MW, Tang L. The pivotal role of fibrocytes and mast cells in mediating fibrotic reactions to biomaterials. *Biomaterials*. 2011;32(33):8394-403.

273. Avula MN, Rao AN, McGill LD, Grainger DW, Solzbacher F. Foreign body response to subcutaneous biomaterial implants in a mast cell-deficient Kit(w-Sh) murine model. *Acta Biomater*. 2014;10(5):1856-63.

274. Zdolsek J, Eaton JW, Tang L. Histamine release and fibrinogen adsorption mediate acute inflammatory responses to biomaterial implants in humans. *J Transl Med*. 2007;5:31.

275. Tang L, Jennings TA, Eaton JW. Mast cells mediate acute inflammatory responses to implanted biomaterials. *Proc Natl Acad Sci U S A*. 1998;95(15):8841-6.

276. Galvez-Monton C, Bragos R, Soler-Botija C, Diaz-Guemes I, Prat-Vidal C, Crisostomo V, et al. Noninvasive Assessment of an Engineered Bioactive Graft in Myocardial Infarction: Impact on Cardiac Function and Scar Healing. *Stem Cells Transl Med*. 2017;6(2):647-55.

277. Wang RM, Johnson TD, He J, Rong Z, Wong M, Nigam V, et al. Humanized mouse model for assessing the human immune response to xenogeneic and allogeneic decellularized biomaterials. *Biomaterials*. 2017;129:98-110.

278. Lutz MB, Schuler G. Immature, semi-mature and fully mature dendritic cells: which signals induce tolerance or immunity? *Trends Immunol*. 2002;23(9):445-9.

279. Babensee JE. Interaction of dendritic cells with biomaterials. *Semin Immunol*. 2008;20(2):101-8.

280. Yoshida M, Babensee JE. Differential effects of agarose and poly(lactic-co-glycolic acid) on dendritic cell maturation. *Journal of biomedical materials research Part A*. 2006;79(2):393-408.
281. Gabrilovich DI, Nagaraj S. Myeloid-derived-suppressor cells as regulators of the immune system. *Nature reviews Immunology*. 2009;9(3):162-74.
282. Saiwai H, Kumamaru H, Ohkawa Y, Kubota K, Kobayakawa K, Yamada H, et al. Ly6C<sup>+</sup> Ly6G<sup>-</sup> Myeloid-derived suppressor cells play a critical role in the resolution of acute inflammation and the subsequent tissue repair process after spinal cord injury. *J Neurochem*. 2013;125(1):74-88.
283. Melero-Jerez C, Ortega MC, Moliné-Velázquez V, Clemente D. Myeloid derived suppressor cells in inflammatory conditions of the central nervous system. *BBA Mol Basis Dis*. 2016;1862(3):368-80.
284. Shepard JL, Zon LI. Developmental derivation of embryonic and adult macrophages. *Curr Opin Hematol*. 2000;7(1):3-8.
285. Epelman S, Lavine KJ, Randolph GJ. Origin and functions of tissue macrophages. *Immunity*. 2014;41(1):21-35.
286. Ferrante CJ, Leibovich SJ. Regulation of Macrophage Polarization and Wound Healing. *Adv Wound Care (New Rochelle)*. 2012;1(1):10-6.
287. Mantovani A, Sica A, Sozzani S, Allavena P, Vecchi A, Locati M. The chemokine system in diverse forms of macrophage activation and polarization. *Trends Immunol*. 2004;25(12):677-86.
288. Martinez FO, Gordon S. The M1 and M2 paradigm of macrophage activation: time for reassessment. *F1000Prime Reports*. 2014;6:13.
289. Avdic S, Cao JZ, McSharry BP, Clancy LE, Brown R, Steain M, et al. Human cytomegalovirus interleukin-10 polarizes monocytes toward a deactivated M2c phenotype to repress host immune responses. *J Virol*. 2013;87(18):10273-82.
290. Porcheray F, Viaud S, Rimaniol AC, Leone C, Samah B, Dereuddre-Bosquet N, et al. Macrophage activation switching: an asset for the resolution of inflammation. *Clin Exp Immunol*. 2005;142(3):481-9.
291. Stout RD, Jiang C, Matta B, Tietzel I, Watkins SK, Suttles J. Macrophages sequentially change their functional phenotype in response to changes in microenvironmental influences. *J Immunol*. 2005;175(1):342-9.
292. Stout RD, Watkins SK, Suttles J. Functional plasticity of macrophages: in situ reprogramming of tumor-associated macrophages. *J Leukoc Biol*. 2009;86(5):1105-9.

293. Arnold L, Henry A, Poron F, Baba-Amer Y, van Rooijen N, Plonquet A, et al. Inflammatory monocytes recruited after skeletal muscle injury switch into antiinflammatory macrophages to support myogenesis. *J Exp Med*. 2007;204(5):1057-69.
294. Crane MJ, Daley JM, van Houtte O, Brancato SK, Henry WL, Jr., Albina JE. The monocyte to macrophage transition in the murine sterile wound. *PLoS One*. 2014;9(1):e86660.
295. Gundra UM, Girgis NM, Ruckerl D, Jenkins S, Ward LN, Kurtz ZD, et al. Alternatively activated macrophages derived from monocytes and tissue macrophages are phenotypically and functionally distinct. *Blood*. 2014;123(20):e110-22.
296. Auffray C, Fogg D, Garfa M, Elain G, Join-Lambert O, Kayal S, et al. Monitoring of blood vessels and tissues by a population of monocytes with patrolling behavior. *Science*. 2007;317(5838):666-70.
297. Nahrendorf M, Swirski FK, Aikawa E, Stangenberg L, Wurdinger T, Figueiredo JL, et al. The healing myocardium sequentially mobilizes two monocyte subsets with divergent and complementary functions. *J Exp Med*. 2007;204(12):3037-47.
298. Novak ML, Koh TJ. Macrophage phenotypes during tissue repair. *J Leukoc Biol*. 2013;93(6):875-81.
299. Deonaraine K, Panelli MC, Stashower ME, Jin P, Smith K, Slade HB, et al. Gene expression profiling of cutaneous wound healing. *J Transl Med*. 2007;5:11.
300. Spiller KL, Anfang RR, Spiller KJ, Ng J, Nakazawa KR, Daulton JW, et al. The role of macrophage phenotype in vascularization of tissue engineering scaffolds. *Biomaterials*. 2014;35(15):4477-88.
301. Anderson JM, Rodriguez A, Chang DT. Foreign body reaction to biomaterials. *Semin Immunol*. 2008;20(2):86-100.
302. Brown BN, Valentin JE, Stewart-Akers AM, McCabe GP, Badylak SF. Macrophage phenotype and remodeling outcomes in response to biologic scaffolds with and without a cellular component. *Biomaterials*. 2009;30(8):1482-91.
303. Fishman JM, Lowdell MW, Urbani L, Ansari T, Burns AJ, Turmaine M, et al. Immunomodulatory effect of a decellularized skeletal muscle scaffold in a discordant xenotransplantation model. *Proc Natl Acad Sci U S A*. 2013;110(35):14360-5.
304. Badylak SF, Valentin JE, Ravindra AK, McCabe GP, Stewart-Akers AM. Macrophage phenotype as a determinant of biologic scaffold remodeling. *Tissue Eng Part A*. 2008;14(11):1835-42.
305. Brown BN, Londono R, Tottey S, Zhang L, Kukla KA, Wolf MT, et al. Macrophage phenotype as a predictor of constructive remodeling following the

- implantation of biologically derived surgical mesh materials. *Acta Biomater.* 2012;8(3):978-87.
306. Sicari BM, Dziki JL, Siu BF, Medberry CJ, Dearth CL, Badylak SF. The promotion of a constructive macrophage phenotype by solubilized extracellular matrix. *Biomaterials.* 2014;35(30):8605-12.
307. Londono R, Dziki JL, Haljasmaa E, Turner NJ, Leifer CA, Badylak SF. The effect of cell debris within biologic scaffolds upon the macrophage response. *Journal of biomedical materials research Part A.* 2017;105(8):2109-18.
308. Yu G, Wu X, Kilroy G, Halvorsen Y-DC, Gimble JM, Floyd ZE. Isolation of Murine Adipose-Derived Stem Cells. In: Gimble JM, Bunnell BA, editors. *Adipose-Derived Stem Cells: Methods and Protocols.* Totowa, NJ: Humana Press; 2011. p. 29-36.
309. Zhao Y, Waldman SD, Flynn LE. The effect of serial passaging on the proliferation and differentiation of bovine adipose-derived stem cells. *Cells Tissues Organs.* 2012;195(5):414-27.
310. Schindelin J, Arganda-Carreras I, Frise E, Kaynig V, Longair M, Pietzsch T, et al. Fiji: an open-source platform for biological-image analysis. *Nature methods.* 2012;9(7):676-82.
311. Taha MF, Hedayati V. Isolation, identification and multipotential differentiation of mouse adipose tissue-derived stem cells. *Tissue Cell.* 2010;42(4):211-6.
312. Diekman BO, Rowland CR, Lennon DP, Caplan AI, Guilak F. Chondrogenesis of adult stem cells from adipose tissue and bone marrow: induction by growth factors and cartilage-derived matrix. *Tissue Eng Part A.* 2010;16(2):523-33.
313. Croce AC, Bottiroli G. Autofluorescence spectroscopy and imaging: a tool for biomedical research and diagnosis. *Eur J Histochem.* 2014;58(4):2461.
314. Tanaka R, Komine-Kobayashi M, Mochizuki H, Yamada M, Furuya T, Migita M, et al. Migration of enhanced green fluorescent protein expressing bone marrow-derived microglia/macrophage into the mouse brain following permanent focal ischemia. *Neuroscience.* 2003;117(3):531-9.
315. Imai Y, Iбата I, Ito D, Ohsawa K, Kohsaka S. A novel gene *iba1* in the major histocompatibility complex class III region encoding an EF hand protein expressed in a monocytic lineage. *Biochem Biophys Res Commun.* 1996;224(3):855-62.
316. Ji KA, Yang MS, Jeong HK, Min KJ, Kang SH, Jou I, et al. Resident microglia die and infiltrated neutrophils and monocytes become major inflammatory cells in lipopolysaccharide-injected brain. *Glia.* 2007;55(15):1577-88.
317. Jeong H-K, Ji K, Min K, Joe E-H. Brain Inflammation and Microglia: Facts and Misconceptions. *Exp Neurobiol.* 2013;22(2):59-67.

318. Rath M, Muller I, Kropf P, Closs EI, Munder M. Metabolism via Arginase or Nitric Oxide Synthase: Two Competing Arginine Pathways in Macrophages. *Front Immunol.* 2014;5:532.
319. Yamamoto M, Nakata H, Hao J, Chou J, Kasugai S, Kuroda S. Osteogenic Potential of Mouse Adipose-Derived Stem Cells Sorted for CD90 and CD105 In Vitro. *Stem Cells Int.* 2014;2014:576358.
320. Al-Salleeh F, Beatty MW, Reinhardt RA, Petro TM, Crouch L. Human osteogenic protein-1 induces osteogenic differentiation of adipose-derived stem cells harvested from mice. *Arch Oral Biol.* 2008;53(10):928-36.
321. Chiou M, Xu Y, Longaker MT. Mitogenic and chondrogenic effects of fibroblast growth factor-2 in adipose-derived mesenchymal cells. *Biochem Biophys Res Commun.* 2006;343(2):644-52.
322. Lin Y, Tian W, Chen X, Yan Z, Li Z, Qiao J, et al. Expression of exogenous or endogenous green fluorescent protein in adipose tissue-derived stromal cells during chondrogenic differentiation. *Mol Cell Biochem.* 2005;277(1-2):181-90.
323. Choi KM, Seo YK, Yoon HH, Song KY, Kwon SY, Lee HS, et al. Effect of ascorbic acid on bone marrow-derived mesenchymal stem cell proliferation and differentiation. *J Biosci Bioeng.* 2008;105(6):586-94.
324. Hench L. *An Introduction to Bioceramics.* Second ed: Imperial College Press; 2013.
325. Granton PV, Norley CJ, Umoh J, Turley EA, Frier BC, Noble EG, et al. Rapid in vivo whole body composition of rats using cone beam muCT. *Journal of applied physiology (Bethesda, Md : 1985).* 2010;109(4):1162-9.
326. Hocking AM. The Role of Chemokines in Mesenchymal Stem Cell Homing to Wounds. *Adv Wound Care.* 2015;4(11):623-30.
327. Stuermer EK, Lipenksy A, Thamm O, Neugebauer E, Schaefer N, Fuchs P, et al. The role of SDF-1 in homing of human adipose-derived stem cells. *Wound Repair Regen.* 2015;23(1):82-9.
328. Kang H, Peng J, Lu S, Liu S, Zhang L, Huang J, et al. In vivo cartilage repair using adipose-derived stem cell-loaded decellularized cartilage ECM scaffolds. *J Tissue Eng Regen Med.* 2014;8(6):442-53.
329. Huang SP, Hsu CC, Chang SC, Wang CH, Deng SC, Dai NT, et al. Adipose-derived stem cells seeded on acellular dermal matrix grafts enhance wound healing in a murine model of a full-thickness defect. *Ann Plast Surg.* 2012;69(6):656-62.



330. Liu S, Zhang H, Zhang X, Lu W, Huang X, Xie H, et al. Synergistic angiogenesis promoting effects of extracellular matrix scaffolds and adipose-derived stem cells during wound repair. *Tissue Eng Part A*. 2011;17(5-6):725-39.
331. Stillaert F, Findlay M, Palmer J, Idrizi R, Cheang S, Messina A, et al. Host rather than graft origin of Matrigel-induced adipose tissue in the murine tissue-engineering chamber. *Tissue Eng*. 2007;13(9):2291-300.
332. Cool SK, Breyne K, Meyer E, De Smedt SC, Sanders NN. Comparison of in vivo optical systems for bioluminescence and fluorescence imaging. *J Fluoresc*. 2013;23(5):909-20.
333. Chen L, Tredget EE, Wu PYG, Wu Y. Paracrine Factors of Mesenchymal Stem Cells Recruit Macrophages and Endothelial Lineage Cells and Enhance Wound Healing. *PLoS One*. 2008;3(4):e1886.
334. Serhan CN, Brain SD, Buckley CD, Gilroy DW, Haslett C, O'Neill LA, et al. Resolution of inflammation: state of the art, definitions and terms. *FASEB J*. 2007;21(2):325-32.
335. Bellingan GJ, Caldwell H, Howie SE, Dransfield I, Haslett C. In vivo fate of the inflammatory macrophage during the resolution of inflammation: inflammatory macrophages do not die locally, but emigrate to the draining lymph nodes. *J Immunol*. 1996;157(6):2577-85.
336. Cao C, Lawrence DA, Strickland DK, Zhang L. A specific role of integrin Mac-1 in accelerated macrophage efflux to the lymphatics. *Blood*. 2005;106(9):3234-41.
337. Gautier EL, Ivanov S, Lesnik P, Randolph GJ. Local apoptosis mediates clearance of macrophages from resolving inflammation in mice. *Blood*. 2013;122(15):2714-22.
338. Janssen WJ, Barthel L, Muldrow A, Oberley-Deegan RE, Kearns MT, Jakubzick C, et al. Fas determines differential fates of resident and recruited macrophages during resolution of acute lung injury. *Am J Respir Crit Care Med*. 2011;184(5):547-60.
339. Eruslanov EB, Lyadova IV, Kondratieva TK, Majorov KB, Scheglov IV, Orlova MO, et al. Neutrophil Responses to Mycobacterium tuberculosis Infection in Genetically Susceptible and Resistant Mice. *Infect Immun*. 2005;73(3):1744-53.
340. Kigerl KA, McGaughy VM, Popovich PG. Comparative analysis of lesion development and intraspinal inflammation in four strains of mice following spinal contusion injury. *J Comp Neurol*. 2006;494(4):578-94.
341. Trivedi A, Olivas AD, Noble-Haesslein LJ. Inflammation and Spinal Cord Injury: Infiltrating Leukocytes as Determinants of Injury and Repair Processes. *Clin Neurosci Res*. 2006;6(5):283-92.

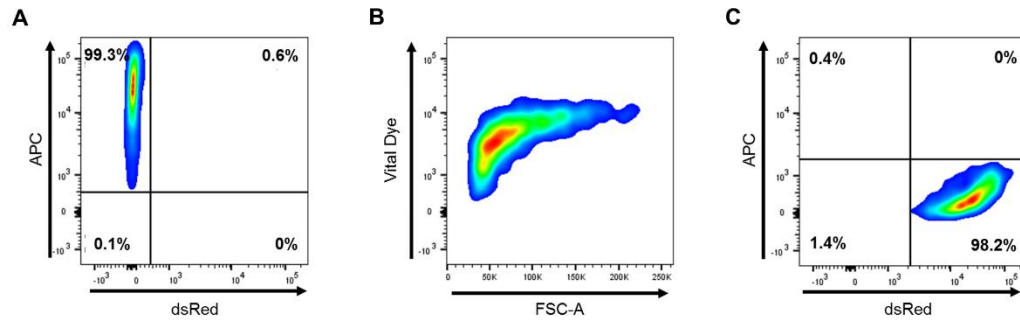
342. Ortega-Gómez A, Perretti M, Soehnlein O. Resolution of inflammation: an integrated view. *EMBO Mol Med*. 2013;5(5):661-74.
343. Berry R, Rodeheffer MS. Characterization of the adipocyte cellular lineage in vivo. *Nat Cell Biol*. 2013;15(3):302-8.
344. de Boer OJ, van der Loos CM, Teeling P, van der Wal AC, Teunissen MB. Immunohistochemical analysis of regulatory T cell markers FOXP3 and GITR on CD4+CD25+ T cells in normal skin and inflammatory dermatoses. *J Histochem Cytochem*. 2007;55(9):891-8.
345. Paulsen SJ, Larsen LK. Laser capture microdissection and quantitative-PCR analysis. *Methods Mol Biol*. 2011;789:127-35.
346. Kelly JL, Findlay MW, Knight KR, Penington A, Thompson EW, Messina A, et al. Contact with existing adipose tissue is inductive for adipogenesis in matrigel. *Tissue Eng*. 2006;12(7):2041-7.
347. Cho SW, Kim I, Kim SH, Rhie JW, Choi CY, Kim BS. Enhancement of adipose tissue formation by implantation of adipogenic-differentiated preadipocytes. *Biochem Biophys Res Commun*. 2006;345(2):588-94.
348. Choi JR, Pinguan-Murphy B, Wan Abas WA, Noor Azmi MA, Omar SZ, Chua KH, et al. Impact of low oxygen tension on stemness, proliferation and differentiation potential of human adipose-derived stem cells. *Biochem Biophys Res Commun*. 2014;448(2):218-24.
349. He J, Cai Y, Luo LM, Liu HB. Hypoxic adipose mesenchymal stem cells derived conditioned medium protects myocardial infarct in rat. *Eur Rev Med Pharmacol Sci*. 2015;19(22):4397-406.
350. Xu L, Wang X, Wang J, Liu D, Wang Y, Huang Z, et al. Hypoxia-induced secretion of IL-10 from adipose-derived mesenchymal stem cell promotes growth and cancer stem cell properties of Burkitt lymphoma. *Tumour Biol*. 2016;37(6):7835-42.
351. Kimura Y, Ozeki M, Inamoto T, Tabata Y. Adipose tissue engineering based on human preadipocytes combined with gelatin microspheres containing basic fibroblast growth factor. *Biomaterials*. 2003;24(14):2513-21.
352. Ito R, Morimoto N, Liem PH, Nakamura Y, Kawai K, Taira T, et al. Adipogenesis using human adipose tissue-derived stromal cells combined with a collagen/gelatin sponge sustaining release of basic fibroblast growth factor. *J Tissue Eng Regen Med*. 2014;8(12):1000-8.
353. Kimura Y, Ozeki M, Inamoto T, Tabata Y. Adipose tissue engineering based on human preadipocytes combined with gelatin microspheres containing basic fibroblast growth factor. *Biomaterials*. 2003;24(14):2513-21.

354. Mignatti P, Rifkin DB. Release of basic fibroblast growth factor, an angiogenic factor devoid of secretory signal sequence: a trivial phenomenon or a novel secretion mechanism? *J Cell Biochem.* 1991;47(3):201-7.

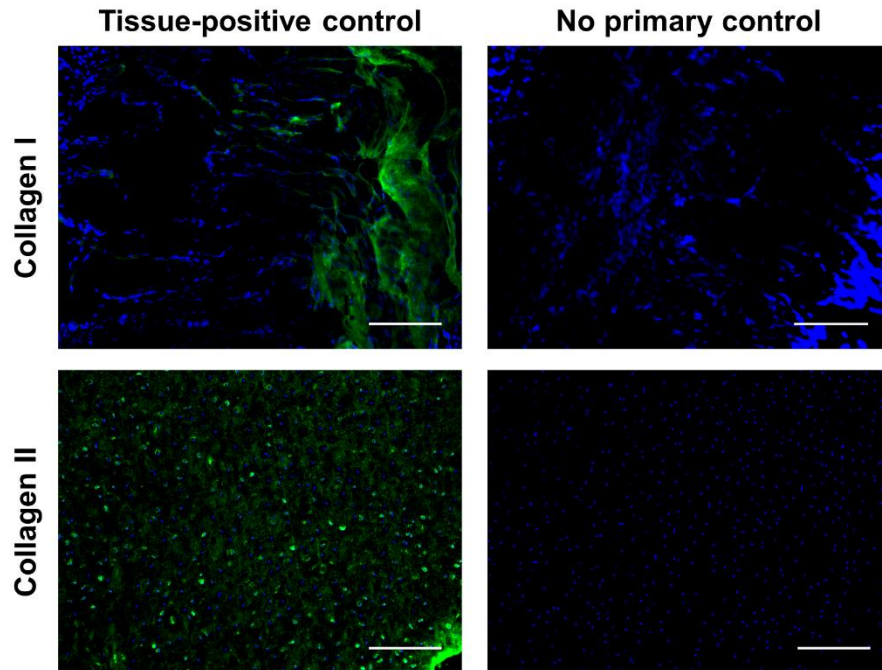
355. Wojtowicz AM, Oliveira S, Carlson MW, Zawadzka A, Rousseau CF, Baksh D. The importance of both fibroblasts and keratinocytes in a bilayered living cellular construct used in wound healing. *Wound Repair Regen.* 2014;22(2):246-55.

356. Williams IR. Fibroblasts A2 - Delves, Peter J. *Encyclopedia of Immunology* (Second Edition). Oxford: Elsevier; 1998. p. 905-9.

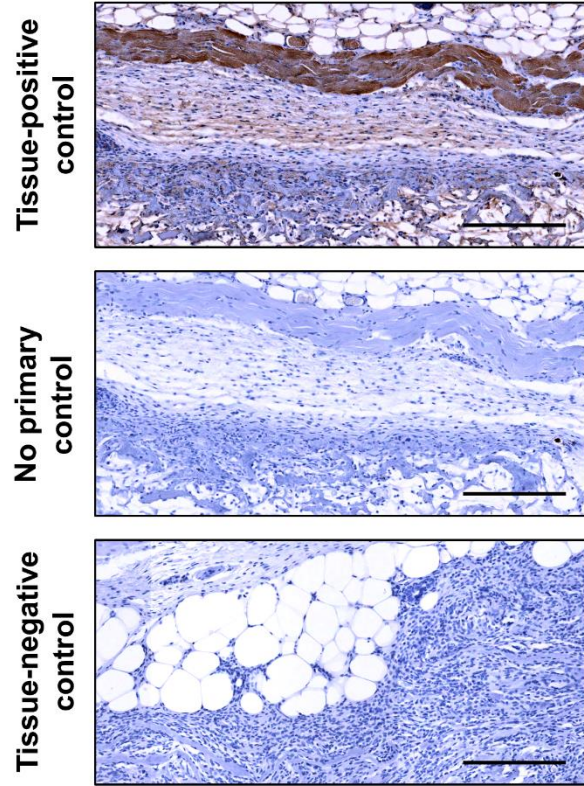
## Appendix 1



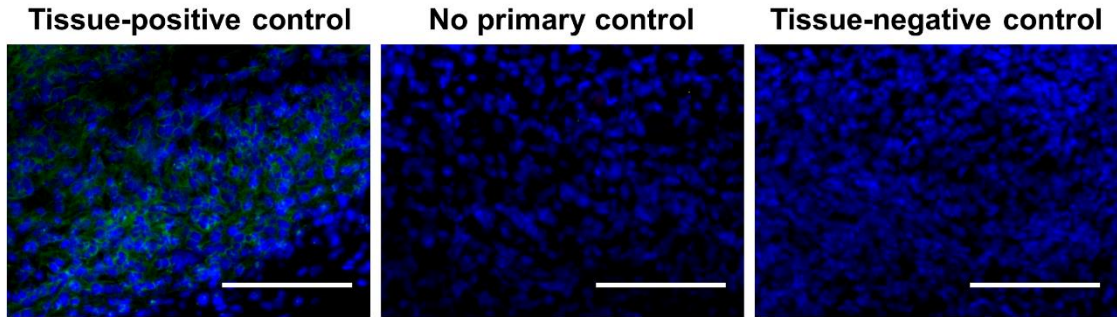
**Supplementary Figure 1. Representative scatter plots depicting fluorescence minus one (FMO) flow cytometry controls.** A) dsRed FMO demonstrating gating of wild-type ASCs positively stained with an APC-conjugated antibody. B) Viability dye FMO showing gating of APC-stained dsRed<sup>+</sup> ASCs not stained with viability dye. C) APC FMO demonstrating gating of viability dye-stained dsRed<sup>+</sup> ASCs without antibody staining.



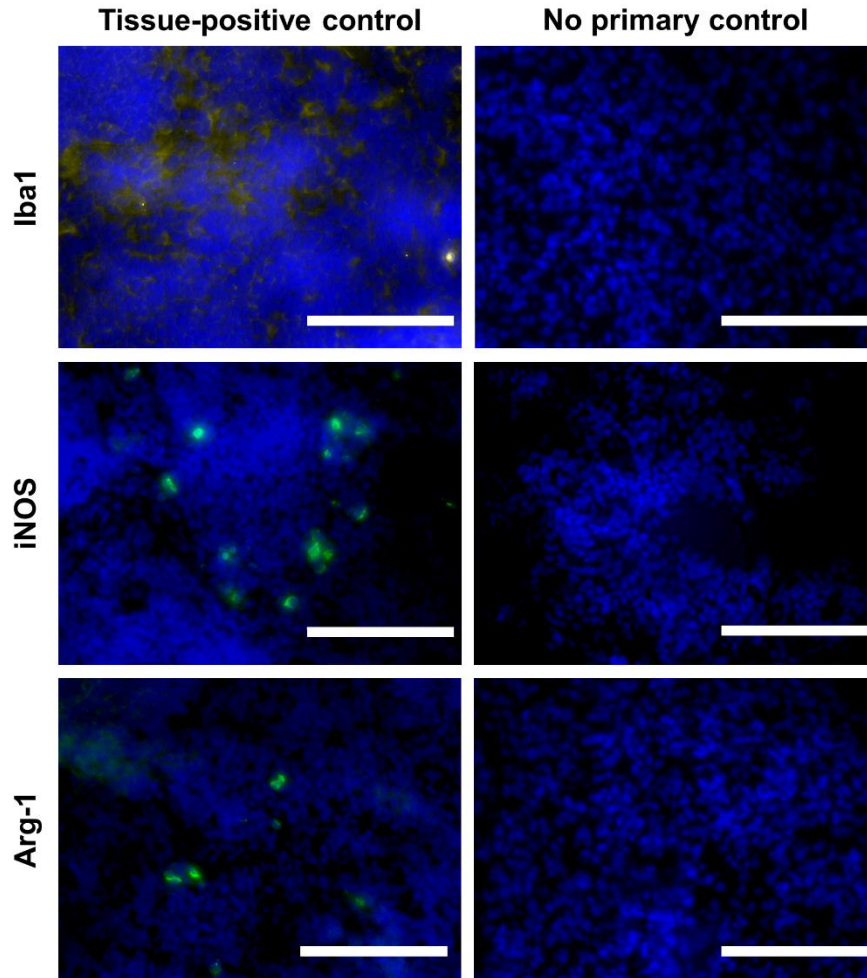
**Supplementary Figure 2. Immunohistochemistry of tissue-positive (left panels) and no primary (right panels) controls for collagen I (top panels) and collagen II (bottom panels).** Porcine auricular cartilage samples with surrounding skin showed positive expression of collagen I in the skin and collagen II expression within the cartilage. Green: positive staining for collagen I or collagen II (as indicated), blue: cell nuclei. Scale: 200  $\mu\text{m}$ .



**Supplementary Figure 3. Immunohistochemistry of tissue-positive, no primary, and tissue-negative controls for dsRed staining.** Representative images of the scaffold periphery in dsRed-stained tissue sections of DAT scaffolds implanted in dsRed mice (tissue-positive control; top panel), or in MacGreen mice with no dsRed<sup>+</sup> ASCs administered (tissue-negative control; bottom panel). A representative no primary control is also shown (middle panel). Brown: positive staining for dsRed. Scale: 200  $\mu$ m.

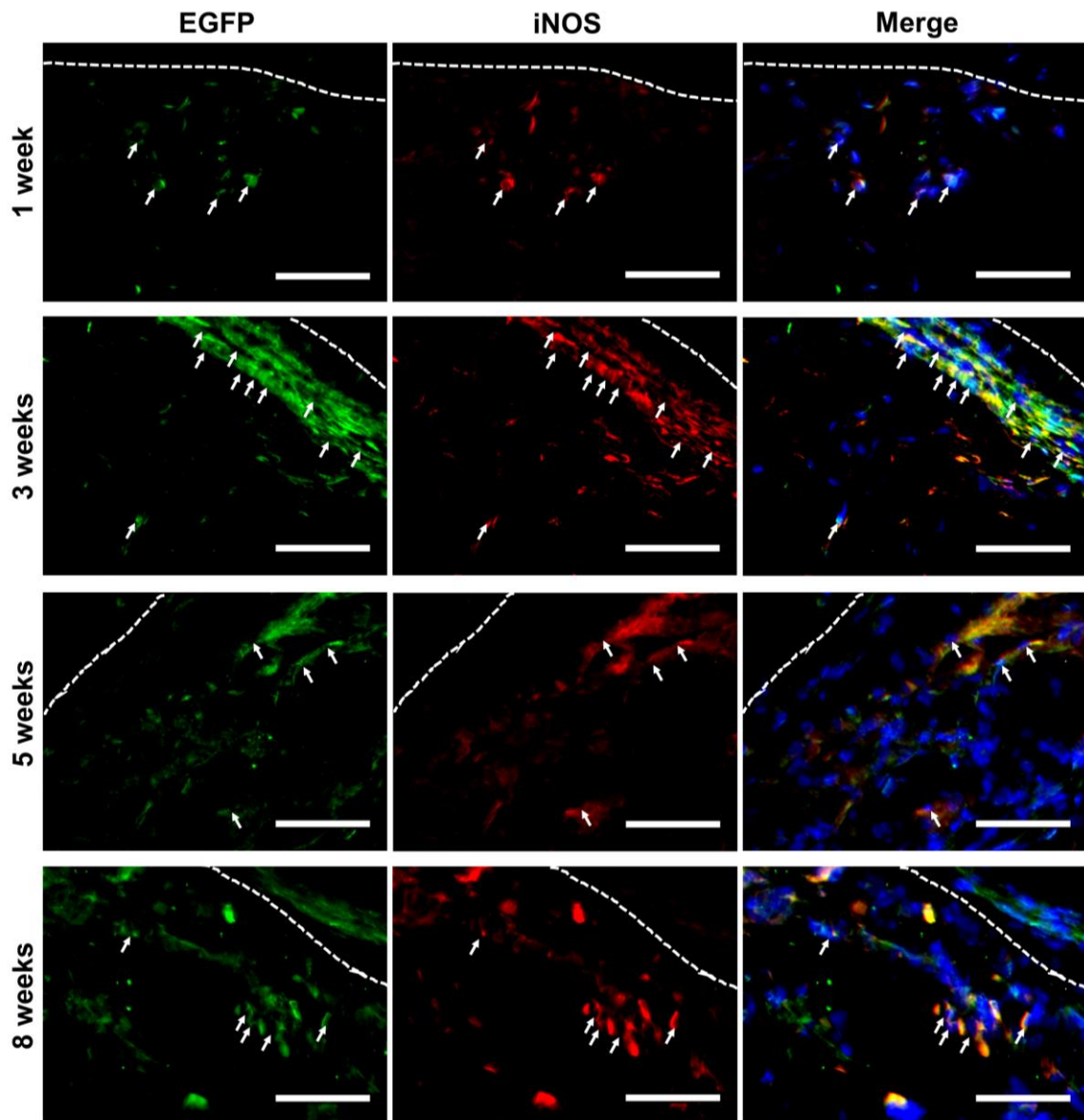


**Supplementary Figure 4. Immunohistochemistry of mouse spleen tissue-positive, no primary, and tissue-negative controls for EGFP staining.** Representative images of EGFP-stained mouse spleens from MacGreen mice (tissue-positive control; left panel), and wild-type mice (tissue-negative control; right panel). A representative no primary control is also shown (middle panel). Green: positive staining, blue: cell nuclei. Scale: 100  $\mu\text{m}$ .

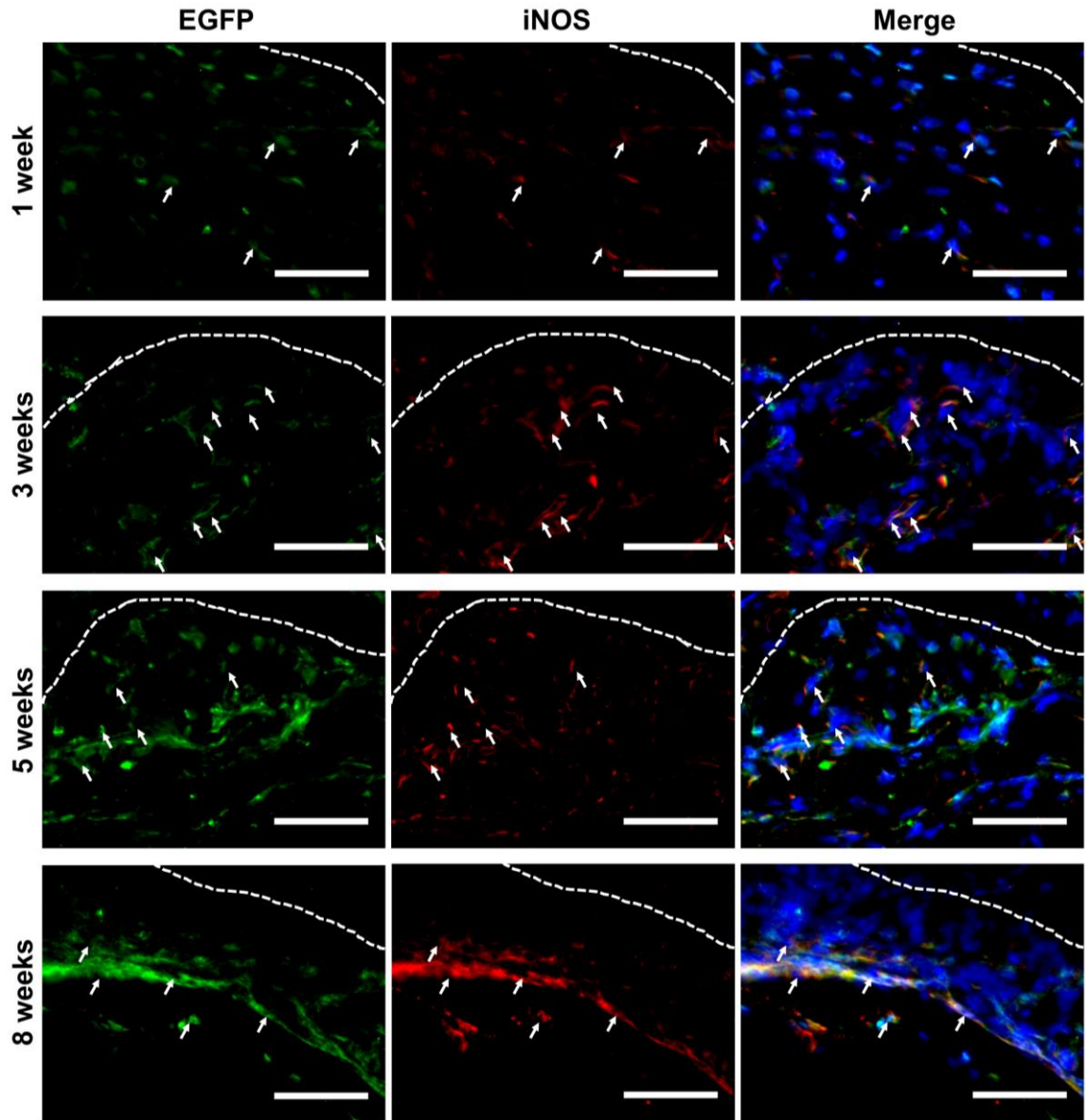


**Supplementary Figure 5. Immunohistochemistry of mouse spleen tissue-positive (left panels) and no primary (right panels) controls for Iba1 (top panels), iNOS (middle panels), and Arg-1 (bottom panels). Yellow (for Iba1) or green (for iNOS and Arg-1): positive staining, blue: cell nuclei. Scale: 100  $\mu$ m.**

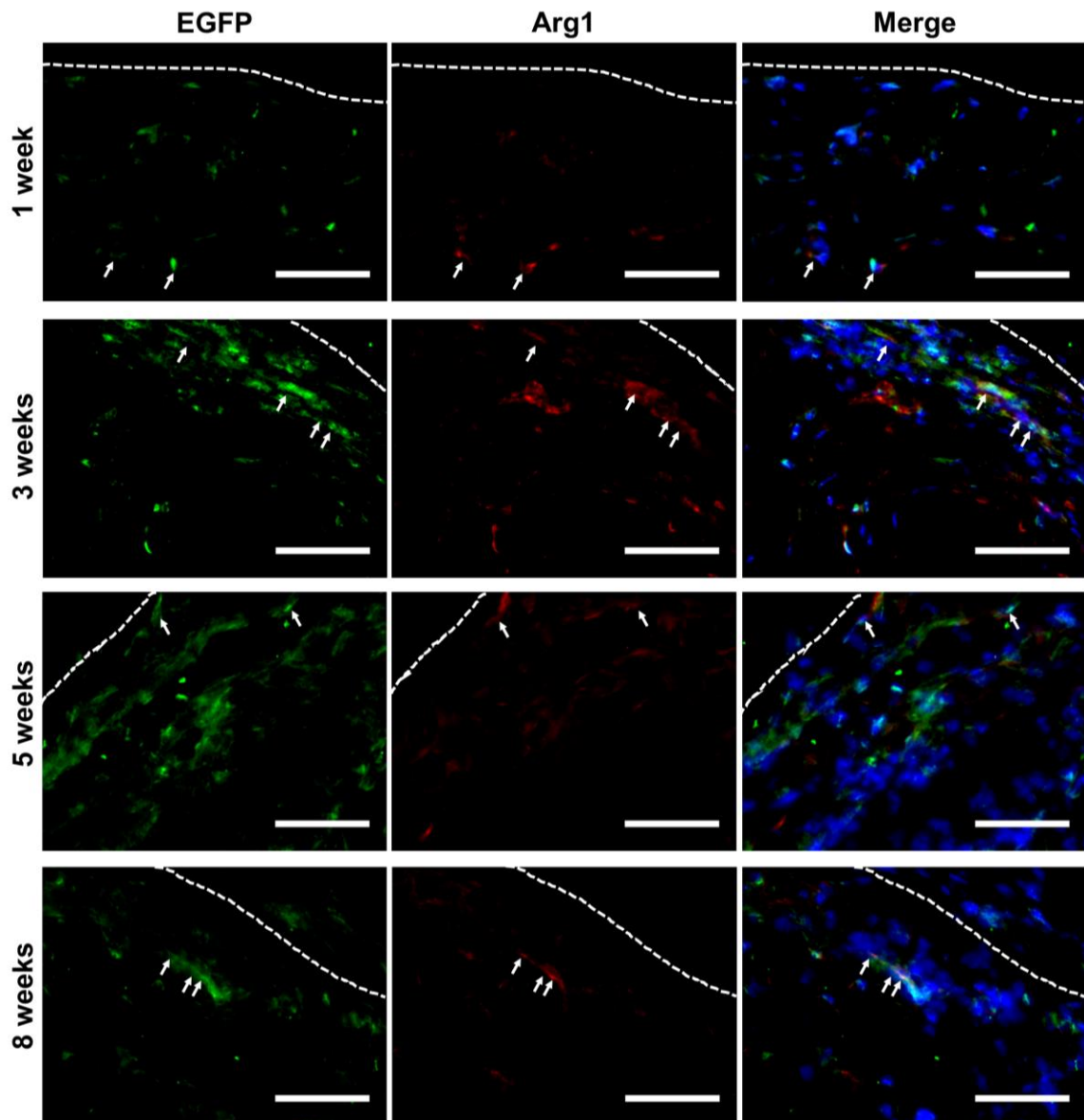




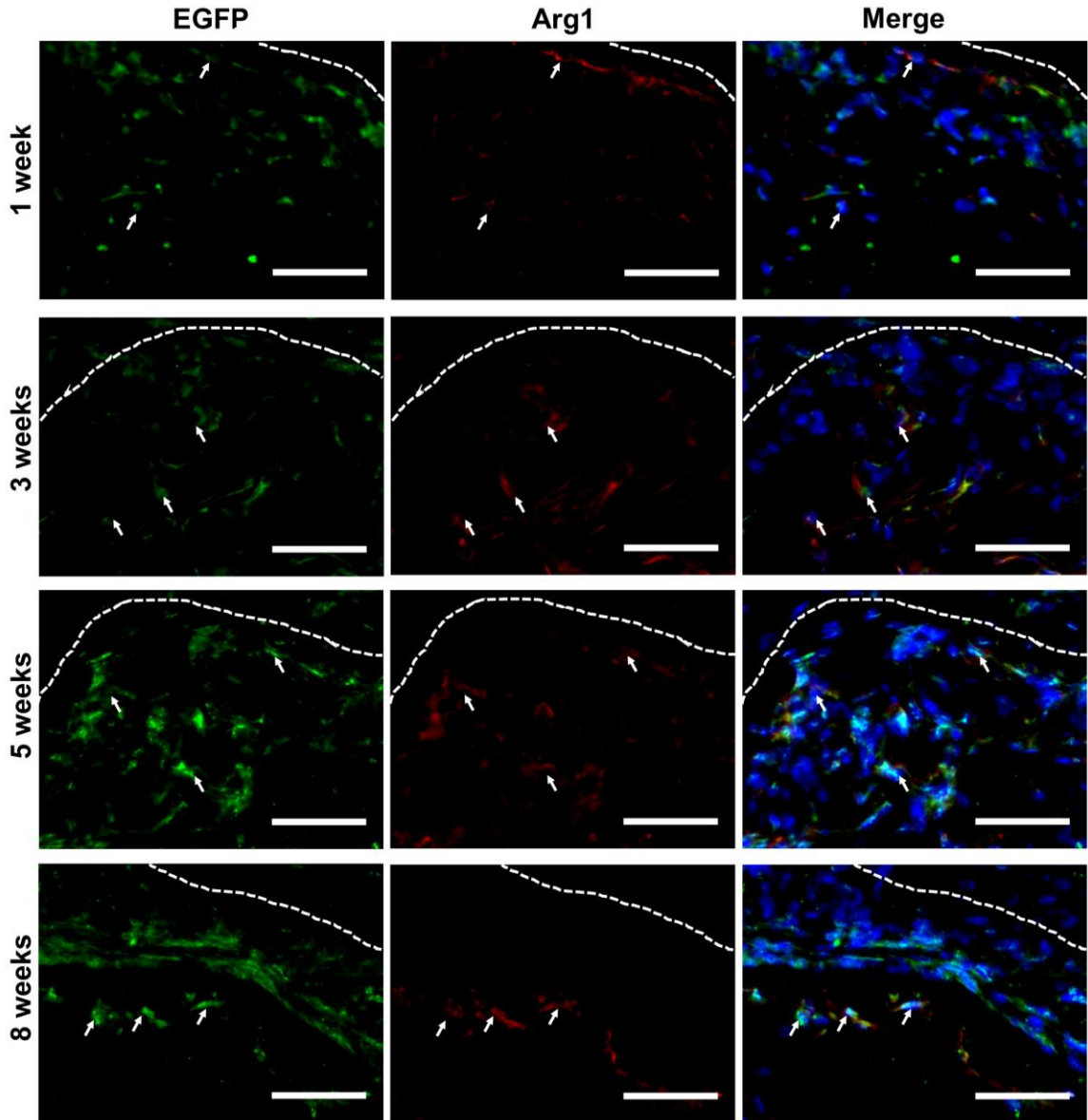
**Supplementary Figure 6. Single channel and merged images of ASC-seeded DAT scaffolds co-stained for EGFP and iNOS. Arrows: EGFP<sup>+</sup>iNOS<sup>+</sup>DAPI<sup>+</sup> cells. Dotted line: scaffold periphery. Green: EGFP, red: iNOS, blue: cell nuclei. Scale: 50  $\mu$ m.**



**Supplementary Figure 7. Single channel and merged images of unseeded DAT scaffolds co-stained for EGFP and iNOS.** Arrows: EGFP<sup>+</sup>iNOS<sup>+</sup>DAPI<sup>+</sup> cells. Dotted line: scaffold periphery. Green: EGFP, red: iNOS, blue: cell nuclei. Scale: 50  $\mu$ m.



**Supplementary Figure 8. Single channel and merged images of ASC-seeded DAT scaffolds co-stained for EGFP and Arg-1. Arrows: EGFP<sup>+</sup>Arg1<sup>+</sup>DAPI<sup>+</sup> cells. Dotted line: scaffold periphery. Green: EGFP, red: Arg-1, blue: cell nuclei. Scale: 50  $\mu$ m.**



**Supplementary Figure 9. Single channel and merged images of unseeded DAT scaffolds co-stained for EGFP and Arg-1. Arrows: EGFP<sup>+</sup>Arg1<sup>+</sup>DAPI<sup>+</sup> cells. Dotted line: scaffold periphery. Green: EGFP, red: Arg-1, blue: cell nuclei. Scale: 50  $\mu$ m.**

# Appendix 2

## Animal care committee approval

Subject: eSirius3G Notification -- 2015-049 Annual Renewal Approved  
From: eSirius3GWebServer <esirius3g@uwo.ca>  
Date: 2017-11-01, 10:13 AM  
To: lauren.fynn@uwo.ca, aspc@uwo.ca



2015-049:2:

**AUP Number:** 2015-049  
**AUP Title:** Characterization of Soft Tissue Regeneration with Bioscaffolds and Adipose-derived Stem/Stromal Cells (ASCs)  
**Yearly Renewal Date:** 11/01/2018

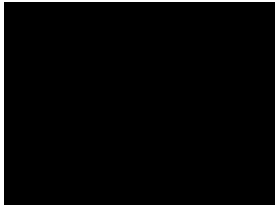
**The YEARLY RENEWAL to Animal Use Protocol (AUP) 2015-049 has been approved by the Animal Care Committee (ACC), and will be approved through to the above review date.**

Please at this time review your AUP with your research team to ensure full understanding by everyone listed within this AUP.

As per your declaration within this approved AUP, you are obligated to ensure that:

- 1) Animals used in this research project will be cared for in alignment with:
  - a) Western's Senate MAPs 7.12, 7.10, and 7.15  
[http://www.uwo.ca/univsec/policies\\_procedures/research.html](http://www.uwo.ca/univsec/policies_procedures/research.html)
  - b) University Council on Animal Care Policies and related Animal Care Committee procedures  
[http://uwo.ca/research/services/animalethics/animal\\_care\\_and\\_use\\_policies.html](http://uwo.ca/research/services/animalethics/animal_care_and_use_policies.html)
- 2) As per UCAC's Animal Use Protocols Policy,
  - a) this AUP accurately represents intended animal use;
  - b) external approvals associated with this AUP, including permits and scientific/departmental peer approvals, are complete and accurate;
  - c) any divergence from this AUP will not be undertaken until the related Protocol Modification is approved by the ACC; and
  - d) AUP form submissions - Annual Protocol Renewals and Full AUP Renewals - will be submitted and attended to within timeframes outlined by the ACC. [http://uwo.ca/research/services/animalethics/animal\\_use\\_protocols.html](http://uwo.ca/research/services/animalethics/animal_use_protocols.html)
- 3) As per MAPP 7.10 all individuals listed within this AUP as having any hands-on animal contact will
  - a) be made familiar with and have direct access to this AUP;
  - b) complete all required CCAC mandatory training ([training@uwo.ca](mailto:training@uwo.ca)); and
  - c) be overseen by me to ensure appropriate care and use of animals.
- 4) As per MAPP 7.15,
  - a) Practice will align with approved AUP elements;
  - b) Unrestricted access to all animal areas will be given to ACVS Veterinarians and ACC Leaders;
  - c) UCAC policies and related ACC procedures will be followed, including but not limited to:
    - i) Research Animal Procurement
    - ii) Animal Care and Use Records
    - iii) Sick Animal Response
    - iv) Continuing Care Visits
- 5) As per institutional OH&S policies, all individuals listed within this AUP who will be using or potentially exposed to hazardous materials will have completed in advance the appropriate institutional OH&S training, facility-level training, and reviewed related (M)SDS Sheets, <http://www.uwo.ca/hr/learn/required/index.html>

Submitted by: Copeman, Laura  
on behalf of the Animal Care Committee  
University Council on Animal Care



The University of Western Ontario  
Animal Care Committee / University Council on Animal Care  
London, Ontario Canada N6A 5C1  
519-661-2111 x 88792 Fax 519-661-2028  
[aspc@uwo.ca](mailto:aspc@uwo.ca) / <http://www.uwo.ca/research/services/animalethics/index.html>

\*\*\* THIS IS AN EMAIL NOTIFICATION ONLY. PLEASE DO NOT REPLY \*\*\*

# Research ethics board approval



Western  
Research

Research Ethics

## Western University Health Science Research Ethics Board HSREB Delegated Initial Approval Notice

**Principal Investigator:** Dr. Lauren Flynn

**Department & Institution:** Schulich School of Medicine and Dentistry/Anatomy & Cell Biology, Western University

**HSREB File Number:** 105426

**Study Title:** Tissue Engineering with Adipose-derived Stem Cells

**Sponsor:** Canadian Institutes of Health Research

**HSREB Initial Approval Date:** August 13, 2014

**HSREB Expiry Date:** August 31, 2019

### Documents Approved and/or Received for Information:

Document Name	Comments	Version Date
Other	Letter for OR and Clinic Staff to Introduce the Study (received June 2/14)	
Western University Protocol		2014/07/23
Letter of Information & Consent		2014/07/23

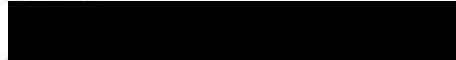
The Western University Health Science Research Ethics Board (HSREB) has reviewed and approved the above named study, as of the HSREB Initial Approval Date noted above.

HSREB approval for this study remains valid until the HSREB Expiry Date noted above, conditional to timely submission and acceptance of HSREB Continuing Ethics Review. If an Updated Approval Notice is required prior to the HSREB Expiry Date, the Principal Investigator is responsible for completing and submitting an HSREB Updated Approval Form in a timely fashion.

The Western University HSREB operates in compliance with the Tri-Council Policy Statement Ethical Conduct for Research Involving Humans (TCPS2), the International Conference on Harmonization of Technical Requirements for Registration of Pharmaceuticals for Human Use Guideline for Good Clinical Practice Practices (ICH E6 R1), the Ontario Personal Health Information Protection Act (PHIPA, 2004), Part 4 of the Natural Health Product Regulations, Health Canada Medical Device Regulations and Part C, Division 5, of the Food and Drug Regulations of Health Canada.

Members of the HSREB who are named as Investigators in research studies do not participate in discussions related to, nor vote on such studies when they are presented to the REB.

The HSREB is registered with the U.S. Department of Health & Human Services under the IRB registration number IRB 0000940.



Ethics Officer, on behalf of Dr. Joseph Gilbert, HSREB Chair

### Ethics Officer to Contact for Further Information

Erika Basile ebasile@uwo.ca	Grace Kelly grace.kelly@uwo.ca	Miss Mekhaal mmekhaal@uwo.ca	Vikki Tran vikki.tran@uwo.ca
--------------------------------	-----------------------------------	---------------------------------	---------------------------------

*This is an official document. Please retain the original in your files.*

# Curriculum Vitae

**Name:** Kevin P. Robb

**Post-secondary Education and Degrees:** McGill University  
Montréal, Québec, Canada  
2011-2015 B.Sc. Honours Physiology

The University of Western Ontario  
London, Ontario, Canada  
2015-present M.E.Sc. Candidate

**Honours and Awards:** Western Graduate Scholarship  
Biomedical Engineering Graduate Program  
2015-present

First Class Honours  
McGill University  
2015

J.W. McConnell Scholarship  
McGill University  
2011-2014

**Related Work Experience** Teaching Assistant  
The University of Western Ontario  
2015-2016

## Publications:

- 1) Robb KP, Shridhar A, Flynn LE. Decellularized matrices as cell-instructive scaffolds to guide tissue-specific regeneration. *ACS Biomaterials Science & Engineering*. Accepted Nov. 13, 2017. DOI: 10.1021/acsbmaterials.7b00619
- 2) Robb KP, Cotechini T, Allaire C, Sperou A, Graham CH. Inflammation-induced fetal growth restriction in rats is associated with increased placental HIF-1 $\alpha$  accumulation. *PloS one*. 2017;12(4):e0175805.
- 3) Han TTY, Shridhar A, Robb K, Kornmuller A, Brown CFC, Flynn LE. CHAPTER 6 Natural Materials as Smart Scaffolds for Tissue Engineering. *Smart Materials for Tissue Engineering: Fundamental Principles: The Royal Society of Chemistry*; 2017. p. 124-62.